12-2023

Static and Dynamic State Estimation Applications in Power Systems Protection and Control Engineering

Ibukunoluwa Olayemi Korede
University of Tennessee, Knoxville, ikorede@vols.utk.edu

To the Graduate Council:

I am submitting herewith a dissertation written by Ibukunoluwa Olayemi Korede entitled "Static and Dynamic State Estimation Applications in Power Systems Protection and Control Engineering." I have examined the final electronic copy of this dissertation for form and content and recommend that it be accepted in partial fulfillment of the requirements for the degree of Doctor of Philosophy, with a major in Electrical Engineering.

Kevin L. Tomsovic, Major Professor

We have read this dissertation and recommend its acceptance:

Seddik M. Djouadi, Dan Wilson, Olufemi A. Omitaomu

Accepted for the Council:

Dixie L. Thompson

Vice Provost and Dean of the Graduate School

(Original signatures are on file with official student records.)

. . .

To the Graduate Council:

I am submitting herewith a dissertation written by Ibukunoluwa O. Korede entitled "Static and Dynamic State Estimation Applications in Power Systems Protection and Control Engineering." I have examined the final paper copy of this dissertation for form and content and recommend that it be accepted in partial fulfillment of the requirements for the degree of Doctor of Philosophy, with a major in Electrical Engineering.

Kevin Tomsovic, Major Professor

We have read this dissertation
and recommend its acceptance:

Kevin L. Tomsovic

Seddik M. Djouadi

Dan Wilson

Olufemi A. Omitaomu

Accepted for the Council:

Dixie L. Thompson

Vice Provost and Dean of the Graduate School

To the Graduate Council:
I am submitting herewith a dissertation written by Ibukunoluwa O. Korede entitled "Static and Dynamic State Estimation Applications in Power Systems Protection and Control Engineering." I have examined the final electronic copy of this dissertation for form and content and recommend that it be accepted in partial fulfillment of the requirements for the degree of Doctor of Philosophy, with a major in Electrical Engineering.

Kevin Tomsovic, Major Professor

We have read this dissertation
and recommend its acceptance:

Kevin L. Tomsovic

Seddik M. Djouadi

Dan Wilson

Olufemi A. Omitaomu

Accepted for the Council:

Dixie L. Thompson

Vice Provost and Dean of the Graduate School

(Original signatures are on file with official student records.)

Static and Dynamic State Estimation Applications in Power Systems Protection and Control Engineering

A Dissertation Presented for the

Doctor of Philosophy

Degree

The University of Tennessee, Knoxville

Ibukunoluwa O. Korede

December 2023

To my late parents, Elder Emmanuel Korede and Mrs. Temilade Korede

Continue to rest in the bosom of the Lord

Acknowledgements

I would to express my deep gratitude and appreciation to my advisor, Dr. Kevin Tomsovic, for his unwavering support and guidance throughout my Ph.D. program. I also want to thank him for his support during my military career, never complaining when I was on military assignments or missions. I am extremely grateful for your invaluable contributions to my dissertation. It has been an honor to work with a distinguished professor of your caliber.

I would also like to extend my sincerest appreciation to Dr. Seddik Djouadi, Dr. Dan Wilson, and Dr. Olufemi Omitaomu for their unwavering support and patience throughout my academic journey. Your presence on the committee has been truly invaluable, and I am deeply grateful for all the comments, feedback, and responses you provided in relation to my dissertation and requests.

I would like to extend my appreciation to my esteemed colleagues and friends at Dominion Energy Electric Transmission for their support and constant motivation. Their professionalism and expertise have been a source of inspiration, and I am honored to have had the privilege of working alongside such talented individuals.

I wish to express my gratitude to my family, especially my wife and daughter, for their constant love, support, and encouragement throughout my doctoral program. Their constant presence and encouragement have been invaluable in helping me stay focused and motivated. Their unwavering support has been a source of inspiration, and I am forever indebted to them for their unwavering commitment to my success.

This research received support from the U.S. National Science Foundation (NSF) and the Department of Energy (DOE) through the Center for Ultra-Wide Area Resilient Electric Energy Transmission Networks (CURENT) Engineering Research Center (ERC).

Strive to be a dream chaser, not just a dreamer.

Abstract

The developed methodologies are proposed to serve as support for control centers and fault analysis engineers. These approaches provide a dependable and effective means of pinpointing and resolving faults, which ultimately enhances power grid reliability. The algorithm uses the Least Absolute Value (LAV) method to estimate the augmented states of the PCB, enabling supervisory monitoring of the system. In addition, the application of statistical analysis based on projection statistics of the system Jacobian as a virtual sensor to detect faults on transmission lines. This approach is particularly valuable for detecting anomalies in transmission line data, such as bad data or other outliers, and leverage points. Through the integration of remote PCB status with virtual sensors, it becomes possible to accurately detect faulted transmission lines within the system. This, in turn, saves valuable troubleshooting time for line engineers, resulting in improved overall efficiency and potentially significant cost savings for the company.

When there is a temporary or permanent fault, the generator dynamics will be affected by the transmission line reclosing, which could impact the system's stability and reliability. To address this issue, an unscented Kalman filter (UKF) and optimal performance iterated unscented Kalman filter (IUKF) dynamic state estimation techniques are proposed. These techniques provide an estimate of the dynamic states of synchronous generators, which is crucial for monitoring generator states during transmission lines reclosing for temporary and permanent fault conditions. Several test systems were employed to evaluate reclosing following

faults on transmission lines, including the IEEE 14-bus system, Kundur's two-area model, and the reduced Western Electricity Coordinating Council (WECC) model of UTK electrical engineering hardware test bed (HTB). The developed methods offer a comprehensive solution to address the challenges posed by unbalanced faults on transmission lines, such as line-to-line, line-to-line-ground, and line-to-ground faults. Utilities must consider these faults when developing protective settings. The effectiveness of the solution is confirmed by monitoring the reaction of dynamic state variables following transmission lines reclosing after temporary faults and transmission line lockout from permanent faults.

Table of Contents

List of Tables

List of Figures

Nomenclature

δ	Rotor angle
ω	Rotor speed
D	Damping coefficient
E_{dp}	d-axis transient voltage
E_{dq}	q-axis transient voltage
E_{fd}	Field voltage
H	Inertia constant
P_e	Active power
P_M	Mechanical power
Q_e	Reactive power
T'_{do}	d-axis transient time constant
T'_{qo}	q-axis transient time constant
X_d	d-axis synchronous reactance
X'_d	d-axis transient reactance
X_q	q-axis synchronous reactance
X'_q	q-axis transient reactance

Chapter 1

Introduction

State estimation is a very important topic in power systems, especially for control center engineers who utilize the state estimator tool for supervisory control and monitoring due to the increased complexities of the systems and increased load and generation. Power systems state estimation is needed due to the increase in the system generation and load, which makes power flow patterns more difficult to predict or estimate. The necessity for real-time state estimation becomes imperative for proper system monitoring and control with the aid of an Energy Management System (EMS). At control centers, the Energy Management Systems (EMS) team depends on the state estimator tool to estimate the real-time state variables from available Supervisory Control and Data Acquisition (SCADA) device measurements to predict the current or future states [2, 3]. The state estimate can enhance operation with assessment for transient stability and voltage stability. Other supported advanced applications include power flow sensitivities [4, 5], load forecasting, real-time nodal prices in electricity markets, automatic gain control (AGC), security analysis, contingency analysis, and generally ensuring that the system is operated in normal secure states [6, 7].

1.1 State Estimation Background

An example of power system state estimation importance could be seen from the July 13th, 1977, blackout in New York which caused damage of about $130 million according to the report of New York Times in 1978. The blackout was mainly due to a lack of accurate data about the system network status, which could have been prevented by proper application of state estimation in the EMS [6]. Long before the implementation of power system state estimation, monitoring of the power system network was carried out using only the (SCADA) device used in the EMS, which was prone to errors[8, 9]. State estimation was mathematically formulated in the 1970s which was implemented in the 1980s and then extended more in the 1990s. It now is now the backbone of EMS monitoring and control [6].

The state estimation principle was pioneered by Fred Schweppe who introduced the concepts to power systems for estimating the state of the system network [10, 11, 12]. This formulation was used to estimate the state of the system by taking real-time snapshots of the measurements (power flows, power injections, voltages) from SCADA. The state vector was estimated for a specific duration. This field of research in the power systems industry has then been a growing topic of interest for researchers as the modern grid had to accommodate increasing levels of renewables and new complicated market structures [13].

1.2 Problem Description and Previous Works

A static state means a state of no interest, a state that is not changing or prone to any kind of movement or motion according to the Oxford Learned Dictionary. In Physics, according to Newton's 2nd law of static equilibrium, the sum of forces on an object is zero [14]. The power system can also be viewed as a quasi-static system; a system that evolves slowly to establish the stability of the system during changes in loads, generation, line flows, or bus complex phasor voltages [13, 15].

A quasi-static state of the system can also be represented mathematically to show the current state or operating condition of a real-time power system of different areas connected together at a specific time interval from the measurements obtained [4, 5, 16]. Static state estimation is the computation of the power system state vector from measurements obtained remotely from the interconnected system network. The static state estimator procedure can be summarized using the flow chart in Figure 1.1 below. The measurement data are post-processed using an algorithm to obtain the estimated operating state or static state vector of the network buses. The estimated state of the system is the vector of the complex phasor voltage [17, 18, 19]. The static state estimator also accounts for any uncertainties in the data collected, data errors, and detection and identification of any bad data in the system.

Network observability is a crucial aspect of power system analysis that enables the estimation of the state of a power system network. This estimation is based on the available measurements, which include real power injection, reactive power injection, transmission line power flows, voltage, current, and angle measurements. Before carrying out state estimation, the system undergoes observability analysis to ensure that it forms a complete spanning tree using the available measurements without any unobservable islands.

Observability testing is a critical step in the process, as it confirms that the network is observable and free of any unobservable islands. This testing can be conducted either offline or online, depending on the system's requirements. The goal of observability testing is to ensure that the network is forming a complete spanning tree using the measurements without any unobservable island.

By ensuring that the network is observable, network observability plays a crucial role in maintaining the stability and reliability of the power system. It enables power system operators to detect and correct any issues that may arise, ensuring that the system operates efficiently and effectively.

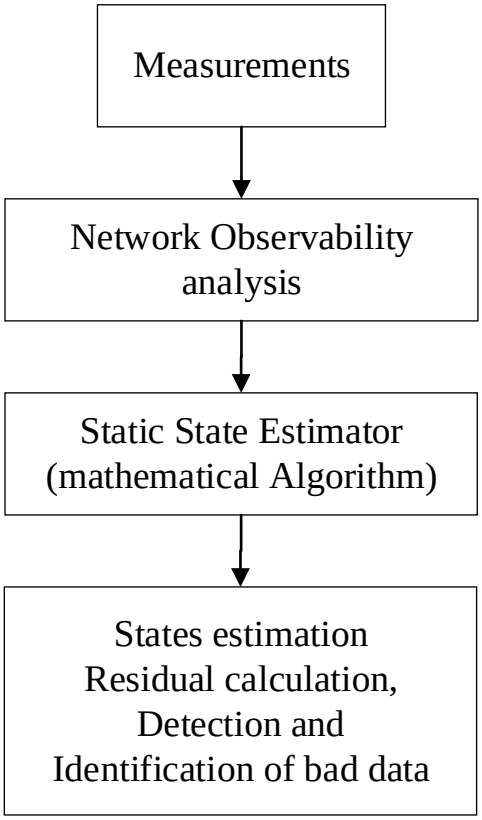

Figure 1.1: Static State Estimator Representation.

If unobservable islands occur in the system, which may be due to topology changes, communication errors, and so on, then a unique estimated state of the systems cannot be determined. Observability testing could be carried out using either a topology approach or numerical approach using the available measurements [20, 21, 22]. The topological method is carried out using the network topology, connectivity, location, and type of measurements. Formation of a full-spanning tree using the measurements helps in the computation of the phase angles that make the system observable. This approach method does not involve any calculation as compared to the numerical method. The numerical approach involves the calculation of unobservable states and the bus incidence matrix, whose multiplication gives the flow in the network branches. Using the D.C. decoupled measurement approach to compute the Jacobian with the following assumptions: all the lines have a reactance of one per unit, the voltage magnitudes have one per unit, and the phase angles have zero values. If the system is observable then there will be zero flow in the branches, if unobservable then there exist unobservable branches in the system with non-zero flow [6, 22].

After the observability testing, state estimation can now be computed using a mathematical model, load flow, probability, and statistics. With the help of statistical estimation procedures such as likelihood function, maximum likelihood estimation, maximum posterior probability, and weighted least square estimate. One can estimate future occurrence based on priori probability, and data, or use measurement samples to estimate the state of the system. Static state estimator employ either the maximum likelihood estimation method or the weighted least square method with the objective of maximizing the likelihood function of a measurement set or minimizing the sum of weighted squares of deviation of the measured value from the true value [23]. The state estimator is trying to compute the likely state using the data measured from the system. The measurements taken from the system are assumed to have errors with the probability distribution function (PDF) which is Gaussian with parameters that are known (mean and variance). The likelihood function is then maximized using the parameters stated above to give maximum likelihood estimates (MLE) of

the parameters. In this case, the log-likelihood function is considered because it is monotonically increasing [23, 24].

The need for the detection of bad measurements and identification of bad measurements or data in the system is also carried out to detect modeling errors in the network. State estimator can be used to detect errors in measurements, and identify and remove the errors. Errors could be due to telecommunication failure, wrong connections, meter issues, faults in transmission lines, generator or load pattern changes, and so on. Bad data may be single or multiple (non-interacting, non-conforming, conforming and interacting) depending on the number of error measurements, location, and type [6, 17, 18]. Some of the methods used for detection and identification using the WLS approach or algorithm are: the largest normalized residual, the chi-square distribution test, and hypothesis testing [25, 26, 27, 28, 29, 30, 31].

The operation of static state estimation is performed at a short interval, but with increased loads (complex loads and technological demands like the internet of things and electric vehicles) and generation, like the integration of distributed energy resources (DERs), it becomes computationally complicated and expensive to carry out due to the dynamics of the system. Hence, the need to consider the time-varying nature of the system model is necessary with the help of a dynamic state estimator to help with the dynamic of the system properties.

The dynamic state estimator is able to estimate or compute the system state vector at time t+1, which provides more accuracy and computes the next time ahead as compared to the static estimator at time t only [4, 32, 33]. This approach provides accuracy and better analysis of the system dynamics at the next sampling time for real-time control and monitoring of power systems. The integration of Phasor Measurement Units (PMUs) into the power system helps to achieve real-time monitoring and control using the Global Positioning System (GPS) providing synchronized time sampled measurements [34, 35, 36].

Dynamic state estimation has been proposed using the Extended Kalman filter (EKF) or the unscented Kalman filter (UKF) to compute the present and future state of the system at t+1 for stability and security analysis [33, 37]. The observability of the system is based on using the observability matrix in control systems with full rank H matrix or by using the Lie derivative approach with rank n [38, 39]. The implementation of composite load model (static load model and induction motor in parallel) to represent the load dynamics using the generalized maximum likelihood iterative extended Kalman filter (GM-IEKF) to account for dominant parameters of the model, measurements and noise [40]. The implementation of EKF and UKF in DSE may lack robustness in handling observation (loss of PMU communication channel, cyber-attacks loss of synchronization) and innovative (impulsive noise in the dynamic state model) outliers. These outliers undermined the performance of EKF and UKF. The implementation of generalized maximum likelihood also known as GM-IEKF was used to overcome these outliers due to its robustness to compute power system states when it experiences large disturbance [41] or any of the outliers.

Application of least absolute value (LAV) based estimator (also known as linear phasor estimator) and UKF by Ali Abur [42] was used as fast and robust DSE in the absence of local generator PMU raw measurements, which is robust with respect to bad data.

For the interconnected power system, the approach uses the various measurements from each area or zone (containing a number of buses) as inputs into the LAV-based estimator operated in each zone, the output of the linear phasor estimator is then used as measurements and estimated inputs into the UKF to estimate the state of the system. This approach can be carried out online and does not consume large memory. However, it experiences delay in receiving the estimated measurements, which can be corrected by a short-term predictor that enhances the performance of the DSE. It however does not account for any innovation or observation outliers. The correlation between calculated P-Q pairs and voltage phasors can be modeled using the nonlinear unscented transformation method [33]. This helps to calculate the error covariance

measurement matrix estimate using the current as inputs, voltage, and P-Q as the transformed outputs.

The UKF also overcomes the limitations of EKF of low accuracy because of the linearization output and Jacobian matrix calculation, which is not applicable to UKF [43]. The unscented transformation utilizes the sigma point approach to approximate a Gaussian distribution for better accuracy, efficiency, and consistency [44, 45]. The sigma point approach utilizes the so-called weighted statistical linear regression to linearize nonlinear random variables through linear regression between selected r points obtained from the random variable prior distribution and the nonlinear function true evaluation.

The ability of DSE to predict the system state at time t+1 makes it useful for forecasting-aided state estimation (FASE) when monitoring changes in the system operation and predicting future states that could be used to replace missing measurements to ensure the security and reliability of the system. However, FASE does have some limitations associated with it. The use of EKF with known linearization error limitation and inadequate complete analysis of the system[46].

1.3 Motivation and Contribution

Detection of temporary or permanent faults in the power system protection and control world is a very interesting topic in power grid operations. The ability to detect and identify faults help to ensure system reliability, security, and uninterrupted power supply to the customers. Substation equipment measurements and phasor measurements can be used to identify and detect temporary or permanent faults from the transmission control center.

Control centers can backup a substation solution using a topology-less substation, node-breaker model to include power circuit breaker (PCB), zero-impedance branches, and phasor measurements to detect the status of a PCB and detection of faults on transmission lines using virtual sensors.

The proposed solution is state estimation based and can be used to detect fault location using breaker status and virtual sensors to identify fault on a transmission line. This work uses the least absolute value (LAV) robust state estimation method to estimate the augmented states including the flows on the PCBs for supervisory monitoring of the topology and measurement error-free system. Further statistical analyses are executed as virtual sensors to detect or sense bad data, outliers, and leverage points using formulations in the form of virtual sensors that can be clipped on the transmission line to help detect faults. The virtual sensor simulation result is expected to conform with the PCB status to detect the state of the system for various bus configurations and the associated PCB status associated with the faulty line. This will also help to detect lines affected by open breaker status for proper fault isolation, hence increasing fault detection and identification accuracy. This approach can save troubleshooting time for line engineers and save the company a lot of money.

Fault conditions in a generator can be in the form of single-phase or unbalanced current, over-speed, overload, out-of-step, or faults in the winding. These abnormal conditions could result in damage to the generators and interrupted power supply to the customers. Hence, the need for fault detection and isolation to prevent unwanted damages and injuries. The proposed dynamic state estimation could help to determine the synchronous generators' state variables used to monitor and supervise fault detection and isolation. This dissertation proposes a state estimation-based protection for synchronous generators from unbalanced faults like line-to-ground (LG), line-to-line-to-ground (LLG), or line-to-line (LL) to help monitor the state variables associated with the generators. The approach monitors dynamic state variables for transmission line reclosing, both for unbalanced and balanced temporary and permanent faults. This can assist protection engineers in developing generator protection and aid fault analysis engineers in troubleshooting transmission line faults.

1.4 Dissertation Outline

The objective of this dissertation is to show how protection and control engineers could help to protect generators from balanced and unbalanced faults that could affect the normal secure operation of the synchronous generator using the estimated or predicted states of the synchronous generators.

Chapter 2 will focus on the modeling of various state estimators that are considered in this dissertation. The static state estimator under various algorithms, the breaker-node modeling, least absolute variable model with optimization application and the dynamic state estimation using the UKF to model the two-axis synchronous generator.

Chapter 3 presents SSE and its application on the UTK HTB WECC model.

Chapter 4 focuses on the detection of transmission line fault location using the node-breaker model to accurately detect breaker status and using the virtual sensor to detect the faulty line from the remote end open breaker.

In Chapter 5, the dynamic state estimator will be used to show how the generators react to balanced faults using the IEEE 14-bus system, Kundur's two-area system, and the UTK HTB model to simulate balanced faults.

Finally, In Chapter 6, the dynamic state estimator is extended to how generators respond to unbalanced faults using Kundur's two-area system and the UTK HTB and PSCAD WECC models to simulate such faults.

The conclusion of the dissertation and future work will be covered in chapter 7.

Chapter 2

State Estimation Protection and Control Power System Modeling

2.1 The Swing Equation

The transient stability study and analysis of the power system during planning and simulation is critical to ensure that the system can withstand events or disturbances, such as faults, line outages, large load application or removal, and so on. This study helps protection engineers develop accurate settings that could be used to mitigate or isolate the faulty portion of the system. The synchronous generator mechanics is governed by Newton's second law of motion [14]. The swing equation shows the rotor mechanics motion as it accelerates or decelerates with respect to the rotating field. Transient stability or the new operating power angle of the rotor depends on how the rotor changes state between the initial state or another state when there is a change in power due to transient events, generations, or loads [47].

The swing equation of a synchronous generator is formulated using the driving mechanical torque $T_m(N.m)$, the developing electromagnetic torque $T_e(N.m)$.

With losses like friction and windage ignored and running at a steady state.

$$T_m = T_e \tag{2.1}$$

The equation of motion for unbalanced conditions generates a net torque $T_a(N.m)$ (accelerating or decelerating) [48, 49]

$$T_a = T_m - T_e \tag{2.2}$$

$$T_a = \frac{d\omega_m}{dt} = J\frac{d^2\theta_m}{dt^2} = T_m - T_e \tag{2.3}$$

J is the turbine and generator's combined moment of inertia.

ω_m is the angular velocity of the rotor measured in rad/s .

θ_m measured in rad is the angular motion of the rotor with respect to the stator's stationary axis.

$$\theta_m = \omega_{synm}t - \delta_m \tag{2.4}$$

θ_m is the synchronous angular velocity of the rotor measured in rad/s.

δ_m is the initial rotor position at $t = 0$ measured in rad.

The rotor angular angular velocity ω_m and angular acceleration are derived from the derivatives of (2.4)

$$\omega_m = \frac{d\theta_m}{dt} = \omega_{synm} + \frac{d\delta_m}{dt} \tag{2.5}$$

$$\frac{d^2\theta_m}{dt^2} = \frac{d^2\delta_m}{dt^2} \tag{2.6}$$

Equation 2.6 is substituted into equation 2.3 to give

$$J\frac{d^2\delta_m}{dt^2} = T_m - T_e \tag{2.7}$$

Both sides of (2.7) are multiplied by ω_m, the angular velocity to give

$$J\omega_m\frac{d^2\delta_m}{dt^2} = T_m\omega_m - T_e\omega_m \tag{2.8}$$

In terms of power, equation 2.8 is presented as

$$J\omega_m\frac{d^2\delta_m}{dt^2} = P_m - P_e \tag{2.9}$$

Where:

P_m is the input mechanical power measured in W.

P_e is the output electrical power measured in W.

$J\omega_m$ is denoted by M, the inertia constant measured joules-second per mechanical radian [47, 3].

Equation 2.9 is simplified as

$$M\frac{d^2\delta_m}{dt^2} = P_m - P_e \tag{2.10}$$

In terms of kinetic energy W_k, 2.10 is denoted as [47]

$$W_k = \frac{1}{2}M\omega_m \tag{2.11}$$

$$M = \frac{2W_k}{\omega_m} \tag{2.12}$$

The per unit or normalized inertia constant H is given as [47]

$$H = \frac{kinetic\ energy\ in\ MJ\ at\ rated\ speed}{machine\ rating\ in\ MVA} = \frac{W_k}{S_B} \tag{2.13}$$

$$M = \frac{2H}{\omega_{synm}} S_B \tag{2.14}$$

Substitute (2.8) into (2.10) to give

$$\frac{2H}{\omega_{synm}} \frac{d^2\delta_m}{dt^2} = \frac{P_m - P_e}{S_B} = P_{m(pu)} - P_{e(pu)} \tag{2.15}$$

The simplified per-unit representation of equation 2.15 is given as [3, 47, 48, 49]

$$\frac{2H}{\omega_{synm}} \frac{d^2\delta_m}{dt^2} = P_m - P_e \tag{2.16}$$

Equation 2.16 could also be written in terms of frequency f_0, which is also per unitized with the damping power P_D added to the equation

$$\frac{H}{\pi f_0} \frac{d^2\delta_m}{dt^2} = P_m - P_e - P_D \tag{2.17}$$

2.2 The Two-Axis Synchronous Generator Model

Consider the dynamic equation associated with a synchronous generator. The nonlinear dynamics of the generator is given as

$$\dot{x} = f(x, u, w) \tag{2.18}$$

where:

x is the state vector with the dynamic state variables.

u denotes the input vector and w denotes the modeling errors.

The dynamics corresponding to the two-axis model of a synchronous generator are given as [50, 51]

$$\dot{\delta} = \omega - \omega_0 \tag{2.19}$$

$$\frac{H}{\pi f_0}\frac{d^2\delta_m}{dt^2} = P_m - P_e - D\frac{\omega - \omega_0}{\omega_0} \tag{2.20}$$

$$T_{do}^{'}\dot{E}_q^{'} = -E_q^{'} - (X_d - X_d^{'})I_d - E_{fd} \tag{2.21}$$

$$T_{do}^{'}\dot{E}_q^{'} = -E_q^{'} - (X_d - X_d^{'})I_d - E_{fd} \tag{2.22}$$

$$T_{qo}^{'}\dot{E}_d^{'} = -E_d^{'} - (X_q - X_q^{'})I_q - E_{fd} \tag{2.23}$$

$$\begin{bmatrix} V_d \\ V_q \end{bmatrix} = \begin{bmatrix} sin(\delta) & -cos(\delta) \\ cos(\delta) & sin(\delta) \end{bmatrix} \begin{bmatrix} Vcos(\theta) \\ Vsin(\theta) \end{bmatrix} \tag{2.24}$$

$$I_d = \frac{E_q^{'} - V_d}{X_q^{'}} \tag{2.25}$$

$$I_q = \frac{E_d^{'} - V_d}{X_q^{'}} \tag{2.26}$$

$$P_e = V_d I_d + V_q I_q \tag{2.27}$$

$$Q_e = -V_d I_q + V_q I_d \tag{2.28}$$

where the definition of the elements in the above equations are:

δ	is the rotor angle,
ω	is the rotor speed,
P_m	is the input mechanical power,
$E_d^{'}$ and $E_q^{'}$	are the q-axis and d-axis transient voltages,
H	is the inertia constant in *sec*,

D	is the damping coefficient in pu,
$T_{qo}^{'}$ and $T_{do}^{'}$	are the q-axis and d-axis transient time constants,
X_q and X_d	are the q-axis and d-axis synchronous reactances in pu,
$X_q^{'}$ and $X_d^{'}$	are the q-axis and d-axis transient reactances in pu,

2.3 Balanced Three-Phase Fault

Protection engineers in the power industry develop and continuously review relay settings to ensure coordination and isolation of faulted parts of the system whenever a fault occurs in the system due to known or unknown factors. The balanced three-phase fault is an uncommon fault, the simulated fault in software like ASPEN or CAPE is used to set a relay that can send a trip signal to the associated circuit breaker. The current transformer (CT) is used to sense the secondary current that is used by the relay to make the decision when the received current goes beyond a set threshold.

The exposure of a generator to an extended balanced fault could result in unwanted damage to the generator. Hence, the generator needs to be protected from a balanced three-phase fault with the help of the CT and relay. The type or magnitude of short circuit current depends on the synchronous generator's internal impedance and that of the system attached to it [47, 52]. As the name implies, the balanced three-phase fault occurs along all the phases or all three phases shorted to ground. The duration of the fault could be for a few cycles (subtransient period), last longer than a few cycles (transient period), or last longer for some cycles until a trip is issued by the relay to change the state of the affected equipment or transmission lines. The reactances, synchronous reactance (X_d), transient reactance ($X_d^{'}$), and the subtransient reactance ($X_d^{''}$), are used to solve or analyze the network using Thevenin's approach [47, 48]. The bus impedance matrix formulation will be discussed later in the dissertation.

2.4 Unbalanced Faults

Contrary to the balanced three-phase fault above, unbalanced faults occur much more frequently in power systems. Unbalanced faults in power systems are single line-to-ground faults (LG), line-to-line (LL) faults, and double-line (LLG) faults [47]. Unbalanced faults could result in a high short circuit current magnitude that is capable of heating the machines more severely than the balance three-phase fault. For example, the motor rotates twice the rated speed due to the induced negative sequence current. If the fault is not isolated within a few cycles, it could lead to rotor structure damage [52].

Unbalanced fault currents in generators could also be due to an open bus or conductor leading to single phasing, slow reclosing during intentional single phasing trip test, relaying failure, unbalanced fault conditions, or unbalanced generator step-up transformer (GSU) [53]. Thus, the need for a detailed analysis of the generator protection, to ensure that generators or the network are protected from temporary or permanent faults. The control center receives an alarm whenever a fault is detected in the system. A permanent fault requires the operator to isolate the generator from the rest of the system for troubleshooting before bringing the generator back online.

In a generator, unbalanced faults, such as, LG, LL, or LLG are not easy to analyze because of the $d-q-0$ model of the synchronous generator. This also makes the numerical solution complicated. The following sub-section will discuss more on the various unbalanced faults.

2.4.1 Line-to-Ground Fault

The majority of faults in power systems are LG faults. LG faults could be due to bad weather like snow or rain storms, wind, vegetation, animals, or other human errors like poor protection settings leading to misoperation, or deliberate attacks on a substation or transmission tower. The Figure 2.1 below illustrates a single LG fault. I_a, I_b, and I_c are the currents for phases a,b, and c respectively.

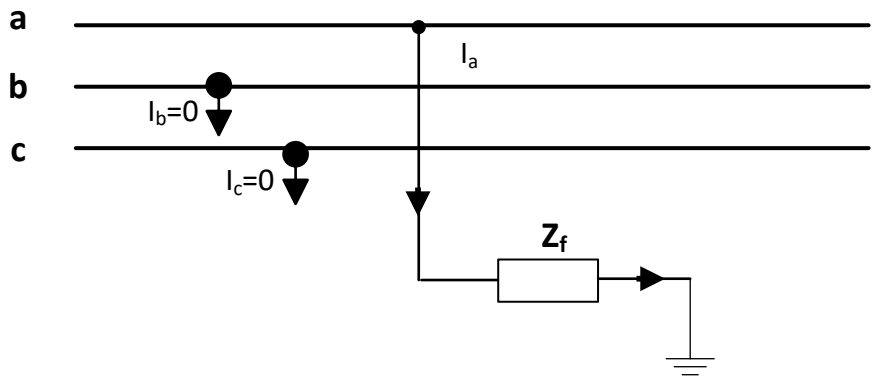

Figure 2.1: Single Line-to-Ground Fault.

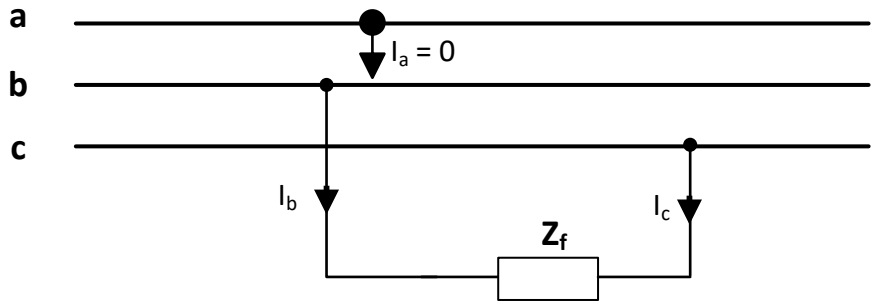

Figure 2.2: Line-to-Line Fault.

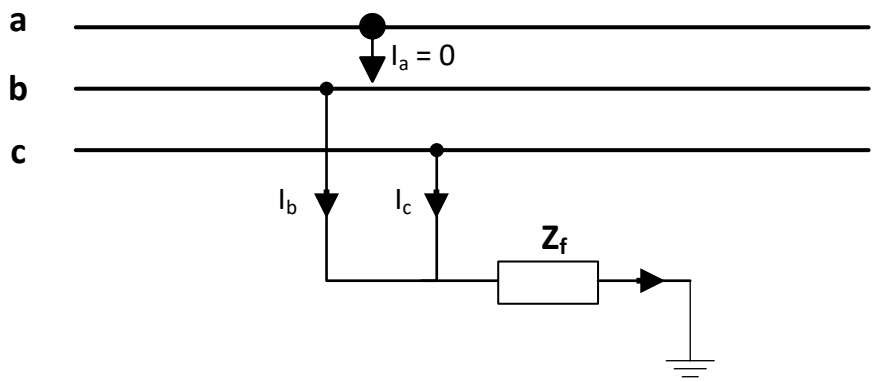

Figure 2.3: Double Line-to-Ground Fault.

The fault current I_a goes through the fault impedance Z_f.Phases a and b currents $I_b = 0$, and $I_c = 0$ [52, 54].

2.4.2 Line-to-Line Fault

LL fault is a type of unbalanced fault that occurs across two phases. Transmission lines faults constitute just a few percent of LL faults. LL faults could also be caused by factors listed above in LG faults. Transmission lines may close back during temporary faults or trips when the line locks out due to persistent faults on the line. Whenever there is a line lockout, the line crew needs to patrol the line using a company truck, drone, or helicopter, depending on the right of way and geographical area of the fault location. This leads to a lot of man hours and money wasted. Later in the dissertation, a virtual sensor solution is proposed for the accurate detection of a remote line attached to a network breaker.

The Figure 2.2 below shows a simple explanation of of LL fault. I_a, I_b, and I_c are the currents for phases a,b, and c respectively. The fault current I_b, and I_c goes through the fault impedance Z_f, and phase a current $I_a = 0$ [52, 54].

2.4.3 Double Line-to-Ground Fault

LLG fault occurs across two phases to ground. LLG faults occur in our system due to various reasons similar to the ones listed for LG faults. The Figure 5.4 below shows a simple explanation of the LL fault. I_a, I_b, and I_c are the currents for phases a,b, and c respectively. The fault current I_b, and I_c goes through the fault impedance Z_f to ground, and phase a current $I_a = 0$ [52, 54].

2.5 The Symmetrical Components

The solution of the unbalanced network described above can be found by using symmetrical components to represent them in three balanced circuits. This enables

the elements of unbalanced voltages and currents to be represented with balanced symmetrical components [47, 48].

Symmetrical components are a powerful technique that enables protection engineers to design and implement effective relay settings for a wide range of equipment, including generators, breakers, and transmission lines. By using symmetrical components, engineers can simulate and study faults on a three-phase network, which helps them to develop the best possible relay settings. This is particularly useful when using power system software like ASPEN or CAPE, which can provide detailed fault simulation data that can be used to optimize relay settings based on symmetrical components. Overall, symmetrical components resolution is an essential tool for any protection engineer looking to ensure the safe and reliable operation of complex electrical systems.

The visualized time current curves (TCC) from ASPEN or CAPE also help system protection engineers develop the proper settings using symmetrical components. Protection or relay engineers can develop phase settings for phase relays using three-phase fault simulation, and ground settings using single phase-to-ground simulation results [52].

The three symmetrical components, the positive, negative, and zero sequence, will be briefly discussed in this section. The Figures 2.4 to 2.6 below represent the symmetrical components for positive sequence, negative sequence, and zero sequence respectively. The elements of the positive sequence consist of balanced, three balanced phasors of equal magnitude.

The phase sequence is 120^0 out of phase with rotation counterclockwise. The positive phasors are in order of abc, the negative sequence phasors are in order of acb, and the zero sequence phasors are all in phase with one another. Details of symmetrical components formulation are contained in the appendix [47, 48, 52, 53].

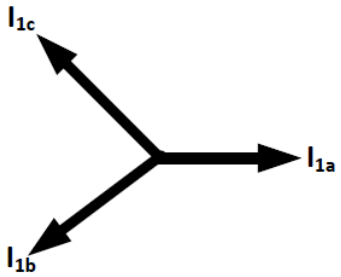

Figure 2.4: Positive Sequence

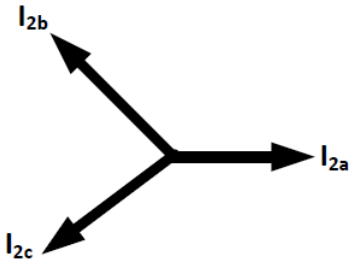

Figure 2.5: Negative Sequence.

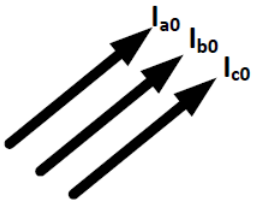

Figure 2.6: Zero Sequence.

2.6 Static State Estimation

Static state estimation for balanced steady-state power systems is used to estimate bus phasors (magnitude and angle). Static state estimation is accomplished using available measurements, including bus injections (real and reactive power), line flows, voltage magnitude, current magnitude, transformer taps, breaker status, reactors, shunt capacitors. The following steps are involved in static state estimation: data processing, topological processing, observability analysis, state estimation, and bad data processing. The next subsection discusses some of the solutions used for static state estimation for this dissertation, in more detail [20, 55, 56, 57].

2.6.1 Weighted Least Square

Consider a set of measurement sets, with the likelihood function given as

$$f_n(z) = \prod_{k=1}^{n} f(z_k) \tag{2.29}$$

where $k = 1, 2, 3, \cdots, n$, and z_k is the kth measurement. And

$$f(z_k) = \frac{1}{\sqrt{2\Pi}\sigma_k} exp - \frac{1}{2}(\frac{z_k - \mu_k}{\sigma_k})^2 \tag{2.30}$$

The objective function is

$$\text{Maximize} \qquad \log f_n(z) \tag{2.31}$$

OR

$$\text{Minimize} \qquad \sum_{k=1}^{n}(\frac{z_k - \mu_k}{\sigma_k})^2 \tag{2.32}$$

- Weights $W_{kk} = \sigma_k^{-2}$
- Measurements expectation $E(z_k) = h_k(x)$, where x is the state vector and h_k is a nonlinear function of the kth measurement.
- Residual, $r_k = z_k - E(z_k)$

The objective is to minimize the above function or optimize the above function subject to constraint. The optimization could be

$$\begin{aligned} &\text{Minimize} && \sum_{k=1}^{n} W_{kk} r_k^2 \\ &\text{Subject to} && z_k = h_k(x) + r_k \end{aligned} \tag{2.33}$$

The above optimization solution is known as the Weighted Least Square (WLS) estimation for the state vector x. The measurement model for a given set of measurements is given as

$$z = h(x) + e \tag{2.34}$$

$$\begin{bmatrix} z_1 \\ z_2 \\ \vdots \\ z_n \end{bmatrix} = \begin{bmatrix} h_1(x_1, x_2, ..., x_m) \\ h_2(x_1, x_2, ..., x_m) \\ \vdots \\ h_n(x_1, x_2, ..., x_m) \end{bmatrix} \tag{2.35}$$

where e is the measurement error vector, x is the state vector of the system, h_k is a nonlinear function that expresses the relationship between the kth measurement and the state vector x. The following assumptions are made

- The expected value of error of each measurement is zero i.e. $E(e_k) = 0, k = 1, 2, 3, \cdots, n$
- The measurements errors are statistically independent i.e. $E[e_i e_j] = 0$

so

$$R = Covariance(e) = E[ee^T]$$

$$\begin{bmatrix} \sigma_1^2 & 0 & 0 & 0 \\ 0 & \sigma_1^2 & 0 & 0 \\ \vdots & \vdots & \ddots & \vdots \\ 0 & 0 & \cdots & \sigma_n^2 \end{bmatrix} \tag{2.36}$$

The WLS estimator then performs the function of minimizing the objective function:

$$\begin{aligned} J(x) &= \sum_{k=1}^{n} \frac{(z_k - h_k(x))^2}{R_{kk}} \\ \text{with} \quad R_{kk} &= \frac{1}{W_{kk}} \end{aligned} \tag{2.37}$$

WLS Algorithm

The WLS state estimator is executed using the following iterative algorithm. The first step in the WLS algorithm is to find the linear approximation of the non-linear measurements using first-order Taylor's expansion approximation for measurement.

$$z = h(x) + e \tag{2.38}$$

Taylor expansion gives

$$\begin{aligned} z &= h(x_0) + H(x_0)\Delta x + e + H.O.T. \\ z - h(x_0) &= H(x_0)\Delta x + e \\ \Delta z = z - h(x_0) &= H(x_0)\Delta x + e \end{aligned} \tag{2.39}$$

The linearized measurement could be considered as

$$\begin{aligned} &\Delta z = H\Delta x + e \\ &\text{with} \\ &\Delta x = x^{k+1} - x^k \\ &H = \frac{\partial h(x^k)}{\partial x} \end{aligned} \tag{2.40}$$

The gain matrix is calculated using the objective function from (9), by finding the minimum of the optimality condition

$$\begin{aligned} \frac{\partial J(x)}{\partial x} &= -H^T(x)R_{-1}[z - h(x)] = 0 \\ g(x_k) &= -H^T(x)R_{-1}[z - h(x)] \end{aligned} \tag{2.41}$$

Applying Newton's method to (13) gives the following

$$\begin{aligned} \Delta x^{k+1} &= \frac{g(x^k)}{G(x^k)} \\ G(x^k) &= \frac{\partial g(x^k)}{\partial x} = H^T(x^k)R^{-1}H(x^k) \end{aligned} \tag{2.42}$$

In order to achieve stability and convergence during the iteration process, it is crucial to ensure that the maximum value of Δx is less than or equal to a specified value of ε. This can be achieved by ensuring that the system is observable, which means that the gain matrix is full rank, positive definite, and symmetric.

To perform the necessary computations, Cholesky decomposition is used due to the sparsity of the matrix. This method allows for the efficient computation of the gain matrix, which is essential for ensuring the stability and convergence of the iteration process. By using Cholesky decomposition, the computation time is reduced, and the accuracy of the results is improved.

The update Δx is calculated from

$$\Delta \widehat{x} = G^{-1}H^T R^{-1}\Delta z \tag{2.43}$$

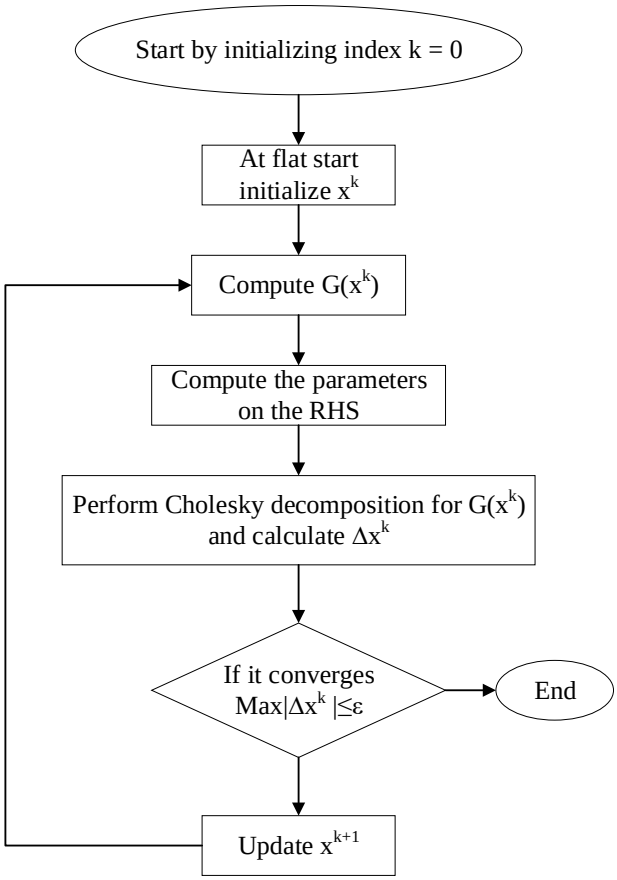

Figure 2.7: WLS Algorithm.

2.6.2 Least Absolute Value

Different researchers have proposed in the past the use of LAV with the notion that it is robust in handling bad data efficiently, saves computation time, has better storage, and improves accuracy [58] relative to the WLS method. The LAV approach presented in this review [46] considers systems with PMU measurements enough to make the system observable. However, LAV could be vulnerable to parameter errors caused by variations in operating conditions, data entry errors, unreported device upgrades, or status of device changes. This could lead to the rejection of good data over bad data [59]. As an alternative to WLS estimation and bad data rejection; LAV estimation is implemented by minimizing the absolute value of the measurement residuals or L1 norm of the measurement residual vector [60] with the aim of estimating results that are robust against bad data. LAV is based on the following equations:

$$\sum_{i=1}^{2m} |r_i| = c^T |r| \tag{2.44}$$

$$\begin{aligned} c^T &= [1, 1, ..., 1] \\ r_i^r &= [r_1^r, r_2^r, ..., r_m^r, r_1^i, r_1^i, ..., r_m^i] \\ r_i^r &= z_i^{m,r} - \widehat{z}_i^r \\ r_i^i &= z_i^{m,i} - \widehat{z}_i^i \end{aligned} \tag{2.45}$$

c^T is a vector consisting of ones and dimension (1 x 2m)

. r_i^r and r_i^i are real and imaginary part of the ith measurement residual.

. $z_i^{m,r}$ and $z_i^{m,i}$ are real and imaginary part of the ith measurement.

. $\widehat{z}_i^r$ and $\widehat{z}_i^i$ are real and imaginary ith estimated measurements.

.

$$\overline{z} = H\overline{x} + \overline{r} \tag{2.46}$$

LAV estimation can be solved as a linear programming problem by

$$\begin{aligned} & min\ c^T|\overline{r}| \\ & st \quad \overline{z} - H\overline{x} = \overline{r} \end{aligned} \tag{2.47}$$

The above equations are rearranged with some new non-negative variables defined

$$\begin{aligned} & min\ c^T|\overline{r}| \\ & st \quad My = b \\ & y \geq 0 \end{aligned} \tag{2.48}$$

where

$$\begin{aligned} c^T &= \begin{bmatrix} Z_n & O_m \end{bmatrix} \\ y &= \begin{bmatrix} X_a & X_b & U & V \end{bmatrix}^T \\ M &= \begin{bmatrix} H & -H & I & -I \end{bmatrix} \\ b &= \overline{z} \end{aligned} \tag{2.49}$$

Z_n and O_m are (1 x 2n) vector of zeros and ones respectively. U and V are 1 x n vector, X_a and X_b are also 1 x n vector. The estimated states and residual are computed as

$$\begin{aligned} \overline{x} &= X_a^T - X_b^T \\ \overline{r} &= U^T - V^T \end{aligned} \tag{2.50}$$

2.6.3 Static State Estimation Using Quadratic Programming

Aside from the linear programming applied earlier in the LAV approach for SSE, quadratic programming could also be used for a modified quadratic function of the original objective function subject to linear constraints. This approach will be used to estimate the state of the IEEE 14-bus system as compared to the results obtained by the previous approaches of WLS and LAV. Moreover, this approach is used to optimize the quadratic objective function subject to the given constraints. For this case, a linear approach was considered, and linear constraints of the power flow

model to better estimate the state of the system. A standard quadratic programming mathematical expression is expressed below.

$$\begin{aligned} \min_{x} \quad & \frac{1}{2}x^T Hx + c^T x \\ such \quad that & \\ & A.x \leq b \\ & Aeq.x = beq \\ & lb \leq x \leq ub \end{aligned} \tag{2.51}$$

where H, A, and A_{eq} are matrices and f, b, beq, lb, ub, and x are vectors.

$$\begin{aligned} \min_{x} \quad & f(x) \\ such \quad that & \\ & c(x) \leq 0 \\ & ceq(x) = 0 \\ & Ax \leq b \\ & Aeqx = beq \\ & lb \leq x \leq ub \end{aligned} \tag{2.52}$$

where

A and Aeq are matrices

b, and beq are vectors.

$c(x)$ and $ceq(x)$ are the inequality and equality nonlinear constraints and

$f(x)$ is the objective function of the problem.

2.6.4 Breaker-Node Model

As previously mentioned, the substation node-breaker model consists of branches with zero impedance or admittance, which represent the status of equipment such as PCBs, disconnect switches, or capacitor banks. Therefore, the topology processor

is not required for this model. To depict the relationship between flow state and measurements, a PCB incidence matrix (M) is utilized. The incidence matrix M includes entries of the PCB measurements. The k^{th} PCB flow measurement in the i^{th} column and j^{th} row of M can be expressed as:

$$M_{i,j} = \begin{cases} 1 & \text{if } j = k, \text{ and flow is measured at the from bus of PCB j} \\ -1 & \text{if } j = k, \text{ and flow is measured at the to bus of PCB j} \\ 0 & \text{otherwise} \end{cases}$$

$$z = [H\ M][\beta] + e \tag{2.53}$$

where β is the augmented state of the system and the flow through the PCB. The augmented state is expressed as

$$\beta = [x^T f^T] \tag{2.54}$$

H and M can be used to form a new matrix D. The measurement equation (8) could be expressed in a more compact form as

$$z = D\beta + e \tag{2.55}$$

where H is the jacobian of non-PCB measurements, M is the PCB incidence matrix, x is the state vector with size $(2n \times 1)$, t is the PCB flow vector with size $(2l \times 1)$, e is the measurement error vector, z is the measurement vector with size $(2m \times 1)$, n, l, and m are the number of voltage phasor, PCBs, and measurements respectively.

2.7 Node-Breaker LAV Problem Formulation

Different papers in the past emphasized the use of LAV-based estimation because of the robust handling of bad data, saving computation time, better storage, and improving accuracy [58] against the WLS method discussed earlier in this review. The LAV approach presented in this dissertation assumes the system contains PMU

measurements sufficient to make the system observable. Still, LAV may be vulnerable to parameter errors caused by variations in operating conditions, data entry errors, unreported device upgrades, or the status of the device changed. This could lead to the rejection of good data over bad data [59]. As an alternative to WLS estimation and bad data rejection, LAV estimation is implemented by minimizing the absolute value of the measurement residuals or L1 norm of the measurement residual vector [60] with the aim of results that are robust against bad data. LAV is based on the following equations

$$\begin{aligned} &min \sum_{i=1}^{2m} \omega_i |z_i - D_i \beta| = min \sum_{i=1}^{2m} \omega_i |r_i| \\ &s.t.\, r = z - D\beta \end{aligned} \tag{2.56}$$

$$\begin{aligned} r &= r_a - r_b, \quad r_a, r_b \geq 0 \\ \beta &= \beta_a - \beta_b, \quad \beta_a, \beta_b \geq 0 \end{aligned} \tag{2.57}$$

The expressed (2.56) above is a weighted LAV objective function where the weights and residual are represented by ω_i and r_i respectively. The above equations are rearranged with new non-negative variables to convert the linear program into a standard form as

$$\begin{aligned} min \quad & C^T \beta \\ s.t. \quad & M\beta = z \end{aligned} \tag{2.58}$$

where

$$\begin{aligned} C^T &= \begin{bmatrix} Z_{n+l} & Z_{n+l} & \Omega_m & \Omega_m \end{bmatrix} \\ y &= \begin{bmatrix} \beta_a & \beta_b & r_a & r_b \end{bmatrix}^T \\ M &= \begin{bmatrix} D & -D & I_m & -I_m \end{bmatrix} \end{aligned} \tag{2.59}$$

$$min \quad \begin{bmatrix} Z_{n+l} & Z_{n+l} & \Omega_m & \Omega_m \end{bmatrix} \begin{bmatrix} \beta_a \\ \beta_b \\ r_a \\ r_b \end{bmatrix} \tag{2.60}$$

$$s.t. \begin{bmatrix} D & -D & I_m & -I_m \end{bmatrix} \begin{bmatrix} \beta_a \\ \beta_b \\ r_a \\ r_b \end{bmatrix} = z \tag{2.61}$$

$$\begin{bmatrix} z_e \\ z_r \end{bmatrix} = \begin{bmatrix} D_e \\ D_r \end{bmatrix} .\hat{\beta} + \begin{bmatrix} 0 \\ r_r \end{bmatrix} \tag{2.62}$$

$$\begin{aligned} z_e &= D_e.\hat{\beta} \\ \hat{\beta} &= D_e^{-1}.z_e \end{aligned} \tag{2.63}$$

$$Covariance(\hat{\beta}) = \Psi_\beta = D_e^{-1} Cov(z_e) D_e^{-T} \tag{2.64}$$

$$\Psi_\beta = \begin{bmatrix} \Psi_x & \Psi_{xf} \\ \Psi_{fx} & \Psi_f \end{bmatrix} \tag{2.65}$$

$$f_{norm}^i = \frac{|\hat{f}|_i}{\sqrt{\Psi_{f(i,i)}}} \tag{2.66}$$

z_{n+l} and Ω_m are (1 x 2n) vectors of zeros and weights, respectively. I is the identity matrix, u and v are 1 x n vector, X_a and X_b are also 1 x n vector. The estimated augmented states and residuals are computed as

$$\begin{aligned} \overline{x} &= X_a^T - X_b^T \\ \overline{r} &= U^T - V^T \end{aligned} \tag{2.67}$$

$$
\begin{aligned}
c^T &= [1, 1, ..., 1] \\
r_i^r &= [r_1^r, r_2^r, ..., r_m^r, r_1^i, r_1^i, ..., r_m^i] \\
r_i^r &= z_i^{m,r} - \widehat{z}_i^r \\
r_i^i &= z_i^{m,i} - \widehat{z}_i^i
\end{aligned}
\tag{2.68}
$$

c^T is a vector consisting of ones and dimension $(1x2m)$. r_i^r and r_i^i are real and imaginary part of the i^{th} measurement residual. $z_i^{m,r}$ and $z_i^{m,i}$ are real and imaginary part of the i^{th} measurement. $\widehat{z}_i^r$ and $\widehat{z}_i^i$ are real and imaginary i^{th} estimated measurements.

2.8 Dynamic State estimator

2.8.1 Extended Kalman Filter

In estimating the dynamic state of the system, the correct mathematical model [4] is vital to achieving a desired result. The dynamic state estimation typically utilizes the Extended Kalman filter (EKF) to determine the dynamic state of the system. The mathematical model [61] includes the modeling of the components of the power system and the system's nonlinearity to achieve the best estimate. The EKF algorithm [37] will be discussed here, which depends on the prediction and filtering algorithms. Consider the model below for EKF

$$
\begin{aligned}
\dot{x} &= f(x, u, w) \\
z &= h(x, u, v)
\end{aligned}
\tag{2.69}
$$

From (2.69) above, $f(\cdot)$ is a non-linear function that represents the system dynamics in time, and $h(\cdot)$ is the non-linear measurement function. The process and measurement noise are w and v respectively with zero mean and covariance of Q and R. The set of discrete time equations for the EKF algorithm is expressed below

$$\begin{aligned} x_k &= x_{k-1} + f(x_{k-1}, u_{k-1}, w_{k-1})\Delta t \\ z_k &= h(x_k, v_k) \end{aligned} \tag{2.70}$$

Here, the $k-1$ in the $f(\cdot)$ function represents the present time index, while k is the next or future time index and Δt is the time step. The non-linear function $h(\cdot)$ represents the measurement at time instant k, the state variables and measurement noise are x and v respectively. The process and measurement covariance are Q_k and R_k respectively.

$$\begin{aligned} w_k &\sim (0, Q_k) \\ v_k &\sim (0, R_k) \end{aligned} \tag{2.71}$$

The filter is initialized using the expression

$$\begin{aligned} \widehat{x}_0^+ &= E(x_0) \\ P_0^+ &= E[(x - \widehat{x}_0^+)(x - \widehat{x}_0^+)^T] \end{aligned} \tag{2.72}$$

$\widehat{x}_0^+$ is the initial state, while P_0^+ is the initial state of the covariance matrix. Prediction is computed from the partial derivative matrices at $\widehat{x}_{k-1}^+$, which is the current state.

$$\begin{aligned} F_{k-1} &= \frac{\partial f_{k-1}}{\partial x}|_{\widehat{x}_{k-1}^+} \\ L_{k-1} &= \frac{\partial f_{k-1}}{\partial w}|_{\widehat{x}_{k-1}^+} \end{aligned} \tag{2.73}$$

where F_{k-1} is the partial derivative of the function f with respect to x, which is the Jacobian matrix at x_{k-1}^+. L_{k-1} is the partial derivative of the function f with respect to w, which is the Jacobian matrix at x_{k-1}^+. The next step is the time update of the state estimate and the error covariance matrix.

$$\begin{aligned} P_k^- &= F_{k-1} P_{k-1}^+ F_{k-1}^T + L_{k-1} Q_{k-1}^+ L_{k-1}^T \\ \widehat{x}_k^- &= f(x_{k-1}^+, u_{k-1}, 0) \end{aligned} \tag{2.74}$$

The – sign indicates a prior estimate and + a posterior estimate. Compute the partial derivative of h with respect to x and v to derive the Jacobian matrices needed for measurement update.

$$\begin{aligned} H_k &= \frac{\partial h_k}{\partial x}|_{\widehat{x}_k^-} \\ M_k &= \frac{\partial f_k}{\partial v}|_{\widehat{x}_k^-} \end{aligned} \tag{2.75}$$

where H_k is the partial derivative of the measurement h with respect to x, which is the Jacobian matrix at $\widehat{x}_k^-$. M_k is the partial derivative of the measurement h with respect to v, which is the Jacobian matrix at $\widehat{x}_k^-$. Measurement update calculation is done by computing the update of the state and the covariance.

$$\begin{aligned} K_k &= P_k^- H_k^T (H_k P_k^- H_k^T + M_k R_k M_k^T)^{-1} \\ x_k^+ &= x_k^- + K_k(y_k - h_k(x_k^-, 0)) \\ P_k^+ &= (I - K_k H_k) P_k^- \end{aligned} \tag{2.76}$$

where:

I: Identity matrix

x_k^+: Updated state estimate

P_k^+: Is the updated state error covariance

K_k: Is the Kalman gain

DSE uses an extended Kalman filter (EKF) to compute the state of the system and also forecast the state at time t+1. This is achieved by incorporating new measurements and the predicted state (using prior state estimates) into the DSE model known as a two-stage DSE [22]. Difficulties that could arise using this approach are the complexity of modeling the system dynamics and computational time. The process thus goes through a prediction (using the predicted states from the predicted measurement) and filtering/correction (to obtain high-quality estimates at time t+1) stages to estimate the state vector [37] computed at a sufficiently small time step

for stability and consistency [43]. EKF linearization can be a problem if higher-order terms are significant. This may introduce errors in the mean and covariance of Gaussian random variables, affecting the filter's performance. The EKF algorithm above could be used to estimate the dynamic variables of a generator or a multi-machine system with the consideration of both small and large disturbances.

2.8.2 Unscented Kalman Filter

The correlation between calculated P-Q pairs and voltage phasors can be modeled using the nonlinear unscented transformation method [33]. This helps to compute the error covariance measurement matrix estimate using the current as inputs, with voltage and P-Q as the transformed outputs. The UKF also overcomes the limitations with EKF of low accuracy due to the linearization and Jacobian matrix calculation, which is not applicable to UKF [43].

The unscented transformation utilizes the sigma point approach to approximate a Gaussian distribution for better accuracy, efficiency, and consistency [44, 45]. The sigma point approach leverages the so-called weighted statistical linear regression to linearize nonlinear random variables through regression between selected r points obtained from the random variable prior distribution and the nonlinear function true evaluation. The sigma point [45] is selected to account for important statistical properties of the previous random variables x with mean $\overline{x}$ and covariance P_{xx}. The proposed number of sigma points required is $r = 2L + 1$, where L represents the dimension of x. Let us begin by considering a nonlinear function

$$y = f(x) \tag{2.77}$$

which is evaluated at r points (χ_i, γ_i) The term χ_i is the set of sigma points. The sigma points and weights used by UKF for unscented transformation are

$$\begin{aligned} \chi_0 &= \overline{x} \\ \chi_i &= \overline{x} + (\sqrt{(L+\lambda)P_{xx}})_i \\ i &= 1, ..., L \end{aligned} \tag{2.78}$$

$$\begin{aligned} \chi_{i+n} &= \overline{x} - (\sqrt{(L+\lambda)P_{xx}})_i \\ i &= L+1, ..., 2L \end{aligned} \tag{2.79}$$

$$\begin{aligned} w_0^m &= \frac{\lambda}{L+\lambda} \\ w_0^c &= \frac{\lambda}{L+\lambda} + (1-\alpha^2+\beta) \\ w_i^m &= w_i^c = \frac{\lambda}{2(L+\lambda)} \end{aligned} \tag{2.80}$$

where $\lambda = \alpha^2(L+\kappa) - L$ is the proposed scaling factor and α is usually set to a very small value suggested to be around $10^{-4} \leq \alpha \leq 1$ and κ is the proposed secondary scaling parameter with values $\kappa = 0$ or $\kappa = 3 - L$. The $\omega(s)$ are the weights and β is a scalar parameter with an extra degree of freedom to provide any prior knowledge of the random variable x distribution, which is usually set to two for the best result [45]. The quantity $(\sqrt{(n+\lambda)P_{xx}})_i$ is termed as the i^{th} row or column of the matrix square root of P_{xx} usually computed numerically using Cholesky factorization. The sigma points are propagated via a nonlinear function

$$\begin{aligned} \gamma_i &= f(\chi_i) \\ i &= 0, 1, ..., 2n \end{aligned} \tag{2.81}$$

The resulting mean and covariance of the propagated points are

$$\begin{aligned} \overline{y} &= \sum_{i=0}^{2n} w_i^m \gamma_i \\ P_{yy} &= \sum_{i=0}^{2n} w_i^c (\gamma_i - \overline{y})(\gamma_i - \overline{y})^T \end{aligned} \tag{2.82}$$

The UKF algorithm based on unscented transformation can be used to solve the nonlinear problem of

$$\begin{aligned} x_{k+1} &= f(x_k) + q_k \\ y_{k+1} &= h(x_{k+1}) + r_{k+1} \end{aligned} \tag{2.83}$$

where, x and y are the discrete-time state vector and measurement respectively, q is Gaussian noise and r is the measurement of Gaussian noise, both having a mean of zero and covariance matrices of Q and R, respectively. The calculation of sigma points assumes initial state vector and covariance as x_0 and P_0, Q as process noise covariance, and R as measurement noise covariance based on prior information of the system. The computation of $2L + 1$ sigma points is implemented using the below expression based on the prior state

$$\begin{aligned} X_{k-1} &= [x_{k-1} \cdots x_{k-1}] ... \\ &+ \sqrt{(L+\lambda)} \begin{bmatrix} 0 & \sqrt{P_{k-1}} & \sqrt{P_{k-1}} \end{bmatrix} \end{aligned} \tag{2.84}$$

In the state prediction stage, the sigma points are propagated through the function

$$\chi^*_{k|k-1} = f(\chi_{k-1}) \tag{2.85}$$

The predicted state mean and predicted covariance matrix are computed using

$$\begin{aligned} \overline{x}_{k|k-1} &= \sum_{i=0}^{2L} w_i^m \chi^*_{i,k|k-1} \\ \overline{P}_{k|k-1} &= \sum_{i=0}^{2L} w_i^c [(\chi^*_{i,k|k-1} - \overline{x}_{k|k-1})(\chi^*_{i,k|k-1} - \overline{x}_{k|k-1})^T] + Q \end{aligned} \tag{2.86}$$

The sigma points associated with the predicted parameters above are computed using

$$\chi_{k|k-1} = [\overline{x}_{k|k-1}, \overline{x}_{k|k-1} \pm \sqrt{(L+\lambda)P_{k|k-1}}] \tag{2.87}$$

These estimated sigma points are now propagated through the updated measurement function as

$$\gamma_{k|k-1} = h(\chi_{k-1}) \tag{2.88}$$

The propagated points are computed using

$$\overline{y}_{k|k-1} = \sum_{i=0}^{2L} w_i^m \gamma_{k|k-1} \tag{2.89}$$

The measurement covariance and cross-covariance are computed from

$$\begin{aligned} P_{yy} &= \sum_{i=0}^{2L} w_i^c [(\gamma_{i,k|k-1} - \overline{y}_{k|k-1})(\gamma_{i,k|k-1} - \overline{y}_{k|k-1})^T] + R \\ P_{xy} &= \sum_{i=0}^{2L} w_i^c [(\chi_{i,k|k-1} - \overline{x}_{k|k-1})(\gamma_{i,k|k-1} - \overline{y}_{k|k-1})^T] \end{aligned} \tag{2.90}$$

The updated measurement of the state estimate is estimated using

$$\begin{aligned} K_k &= P_{xy} P_{yy}^{-1} \\ \overline{x}_k &= \overline{x}_{k|k-1} + K_k(y_k - \overline{y}_{k|k-1}) \\ P_k &= P_{k|k-1} - K_k P_{yy} K_k^T \end{aligned} \tag{2.91}$$

Chapter 3

Static State Estimation (SSE) Simulation and Results

The presented algorithms in chapter 2 are used to estimate or compute the static state of the reduced UTK HTB WECC model. This model is depicted or illustrated in Figure 3.1, and the algorithms implemented in this chapter play an essential role in predicting its static behavior. The use of this analog 3-phase system allows higher fidelity testing. The chapter compares and discusses results from various SSE estimators modeled using PSSE and PSAT simulation software.

3.1 PSSE and PSAT Results

The UTK WECC model was simulated using PSSE software. The power flow function was used to estimate the voltage phasor at the buses. These voltage phasors represent the static states of the system, which are essential for monitoring the system's health. Table 3.1 is the power flow result of the WECC PSSE model. The voltage phasor result of the system represents the static state of the WECC system.

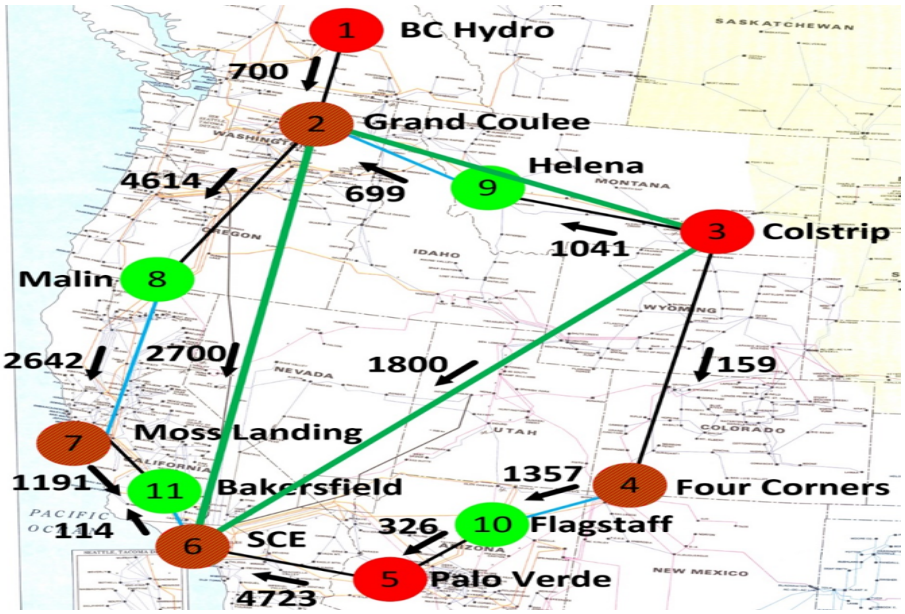

Figure 3.1: UTK HTB WECC Summer Model

Table 3.1: PSSE Model Result

Bus No	Voltage (pu)	Angle (Degree)
1	1.05	0.000
2	1.05	-0.884
3	1.05	11.225
4	1.05	1.591
5	1.05	-8.938
6	1.05	-44.881
7	1.05	-36.098
8	0.993	-24.033
9	1.023	0.511
10	1.025	-9.471
11	1.023	-43.279

The PSSE power flow is used as the base case to validate the SE approaches considered in this chapter. To verify the accuracy of the results obtained from PSSE, the WECC model was also simulated using PSAT. The Table 3.2 below displays the simulation results. It is clearly apparent that the results obtained from the PSAT are in line with those from the PSSE. Thus, the UTK WECC model's system phasor has been successfully estimated using PSSE and PSAT.

3.2 Weighted Least Square (WLS) Results

In chapter 2 of the dissertation, the WLS method was explained as one of the SSE methods used for static state estimation. Figure 3.2 shows the result of the voltage magnitude of the estimated state and Figure 3.3 shows the angle of the estimated state using the WLS approach for the UTK HTB WECC model.

The phasor result for the reduced WECC system is shown in Table 3.3 below. Normally distributed random number using 10% of the standard deviation was used as added noise into the system. The mean squared error (MSE) of the estimated states and true states was calculated using (3.1) below. The voltage magnitude MSE is $1.16e^{-}6$ and the voltage angle MSE is 0.0799. The relative error plot of the estimated and true state is shown in Figures 3.4, and 3.5.

$$MSE = \sqrt{\frac{1}{N}\sum_{j=1}^{N}(x_j^i - \hat{x}_j^i)^2} \tag{3.1}$$

Where

x_j^i is the true state of the ith element contained in the associated state vector

$\hat{x}_j^i$ is the estimated state of the ith element of the associated state vector

N is the aggregate number of simulation steps.

Table 3.2: PSAT Model Result

Bus No	Voltage (pu)	Angle (Degree)
1	1.05	0.000
2	1.05	-0.884
3	1.05	11.225
4	1.05	1.591
5	1.05	-8.938
6	1.05	-44.881
7	1.05	-36.098
8	0.993	-24.033
9	1.023	0.511
10	1.025	-9.471
11	1.023	-43.279

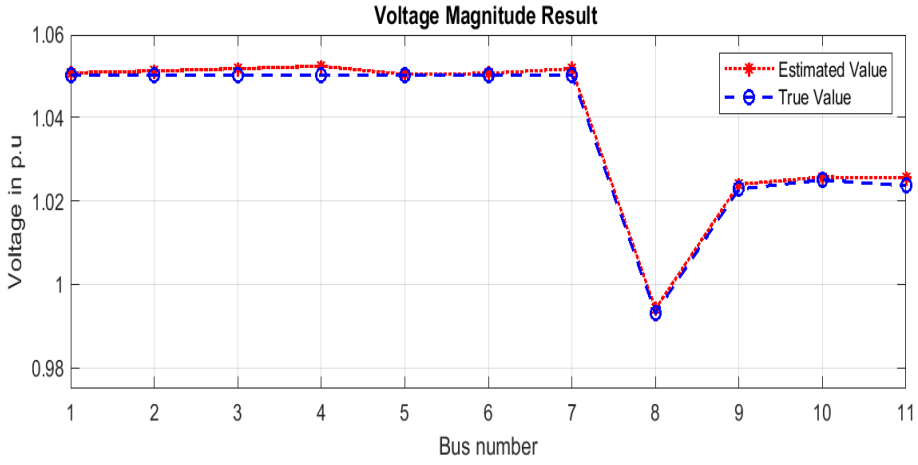

Figure 3.2: WLS Voltage Magnitude

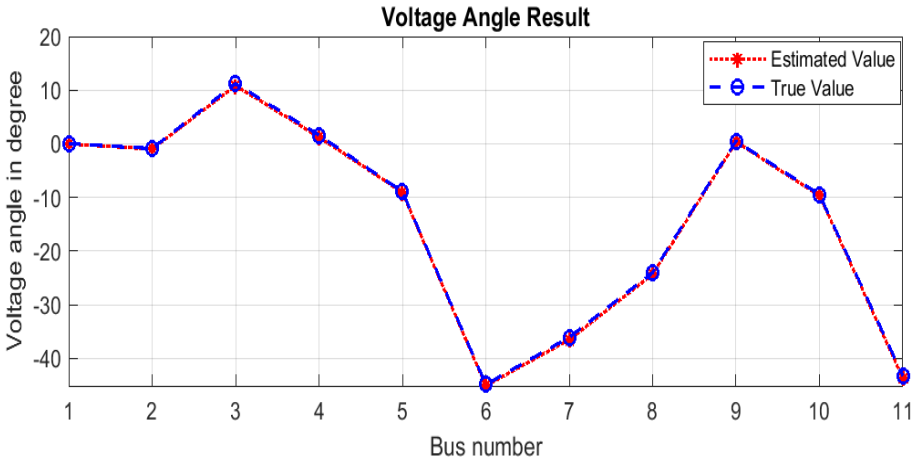

Figure 3.3: WLS Angle

Table 3.3: SSE: WLS

Bus No	Voltage (pu)	Angle (Degrees)
1	1.0507	0.000
2	1.0511	-0.9677
3	1.0517	10.8488
4	1.0523	1.2494
5	1.0503	-9.0612
6	1.0505	-45.1406
7	1.0517	-36.5303
8	0.9941	-24.3481
9	1.0240	0.3181
10	1.0257	-9.6223
11	1.0256	-43.7087

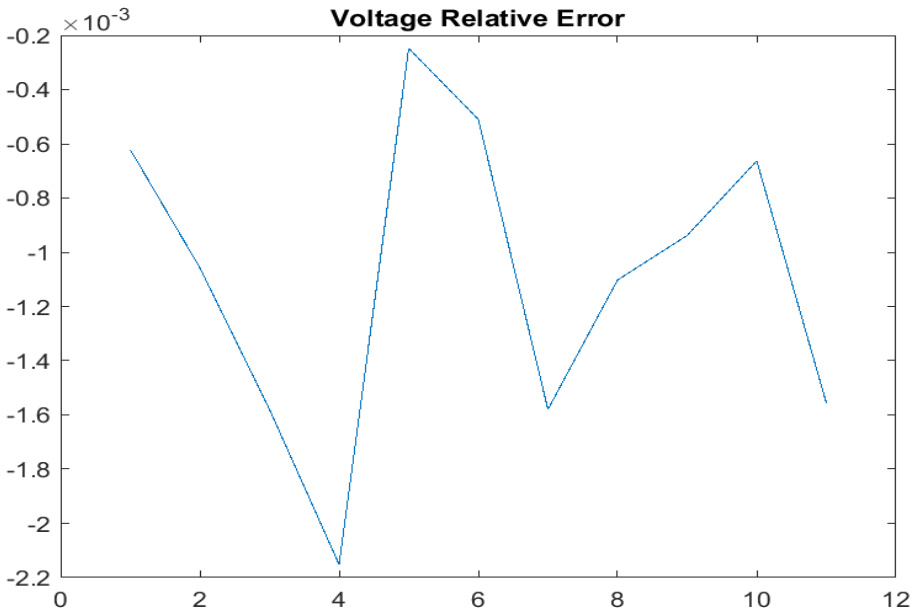

Figure 3.4: WLS Voltage Relative Error

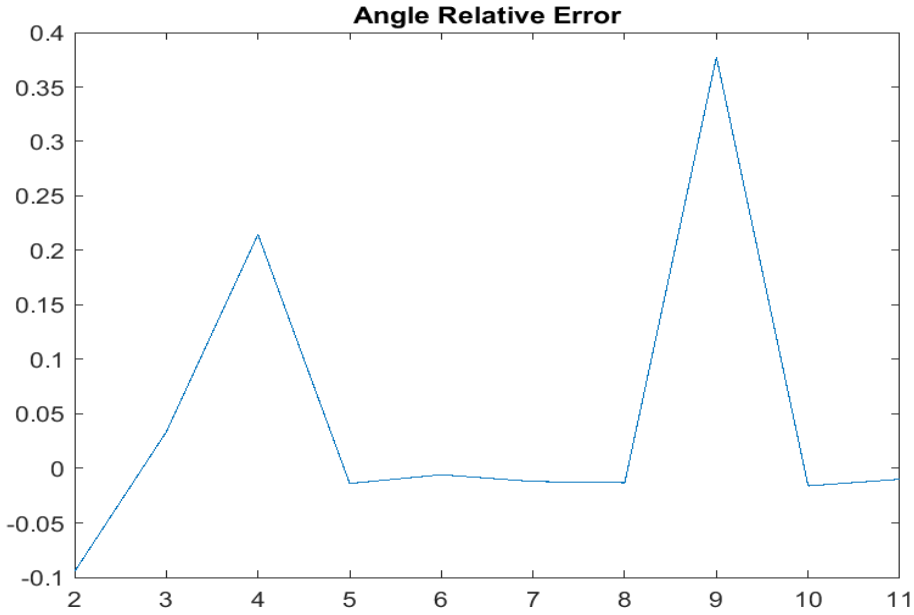

Figure 3.5: WLS Angle Relative Error

3.3 Least Absolute Value Results

The LAV method is used to estimate the states of the WECC system. Compared to the WLS method, LAV is a more reliable state estimator that performs better in the presence of bad data. You can find the details of the formulation in chapter 2 of this dissertation. To estimate the state of the WECC system, we use linear programming with the objective of minimizing the $L1$ norm or absolute value of the residuals. The computed states of the WECC system are presented in Figures 3.6 and 3.7.

Additionally, Table 3.4 provides the tabulated results from the LAV robust state estimator, which were found to be consistent with the results obtained from PSSE and PSAT. No bad data was detected or identified using the chi-square test and normalized residual method. Similarly with the WLS approach, normally distributed random numbers using 10% of the standard deviation were used as added noise into the system. The mean squared error (MSE) of the estimated states and true states was calculated using (3.1). The voltage magnitude MSE is $3.75e^{-}7$ and the voltage angle MSE is 0.0177. The MSE of the LAV method is lower than that of the WLS approach to show LAV as a robust estimator in the presence of bad data. The relative error plot of the estimated and true state is shown in Figures 3.8 and 3.9.

3.4 Quadratic Programming Results

The quadratic programming method was also utilized to compute the static state variables of the WECC model. The algorithm was discussed in chapter 2. The state estimates for the WECC system were estimated using the Matlab quadratic programming (quadprog) routine. The computed states of the voltage phasors are shown in Figures 3.10 and 3.11 below.

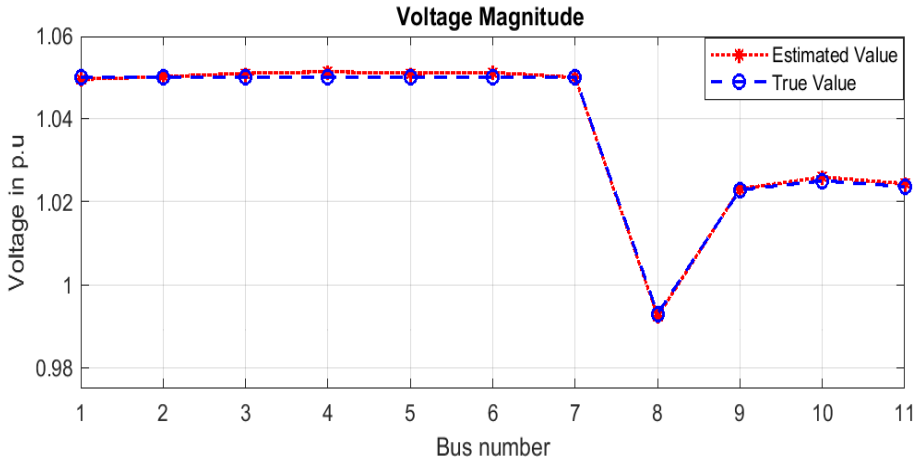

Figure 3.6: LAV Voltage Magnitude

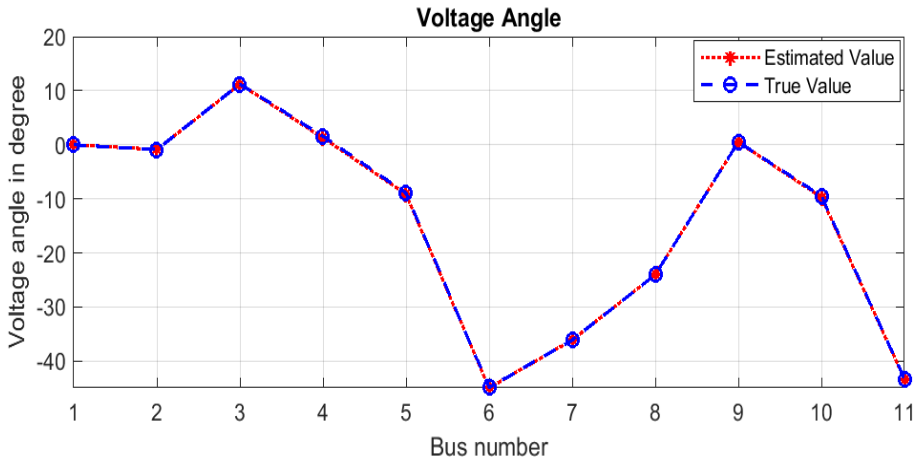

Figure 3.7: LAV Angle in Degrees

Table 3.4: SSE: Least Absolute Value

Bus No	Voltage (pu)	Angle (Degree)
1	1.0494	0.000
2	1.0496	-0.8606
3	1.0505	11.1946
4	1.0511	1.3285
5	1.0505	-9.1839
6	1.0506	-44.9253
7	1.0497	-36.1118
8	0.9923	-23.9949
9	1.0225	0.5321
10	1.0256	-9.7154
11	1.0234	-43.2918

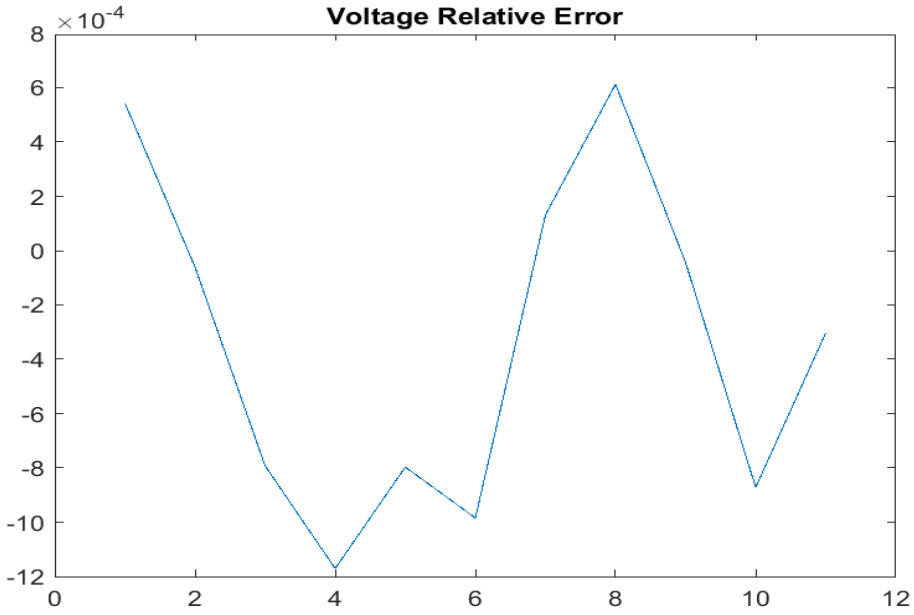

Figure 3.8: LAV Voltage Relative Error

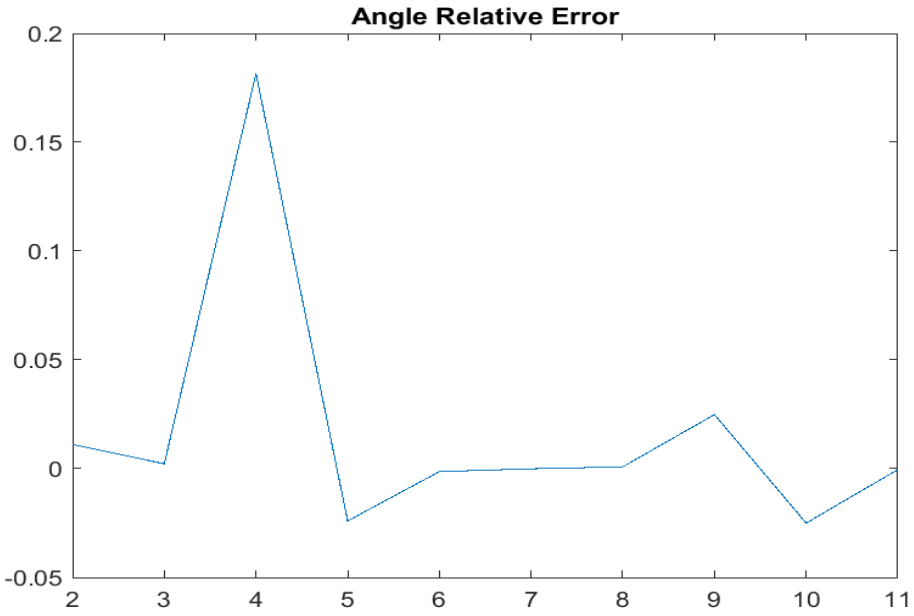

Figure 3.9: LAV Angle Relative Error

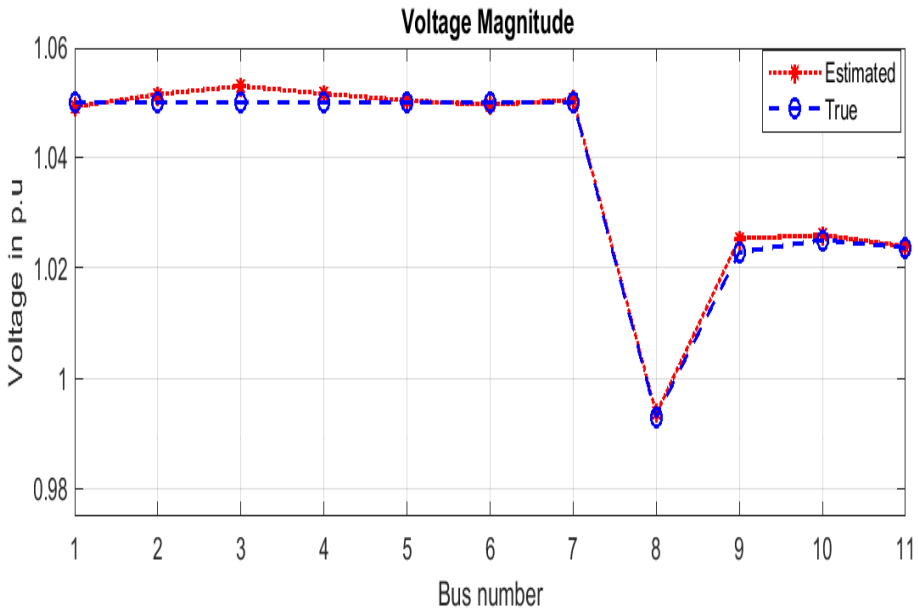

Figure 3.10: Quadratic Programming Voltage Magnitude Estimate

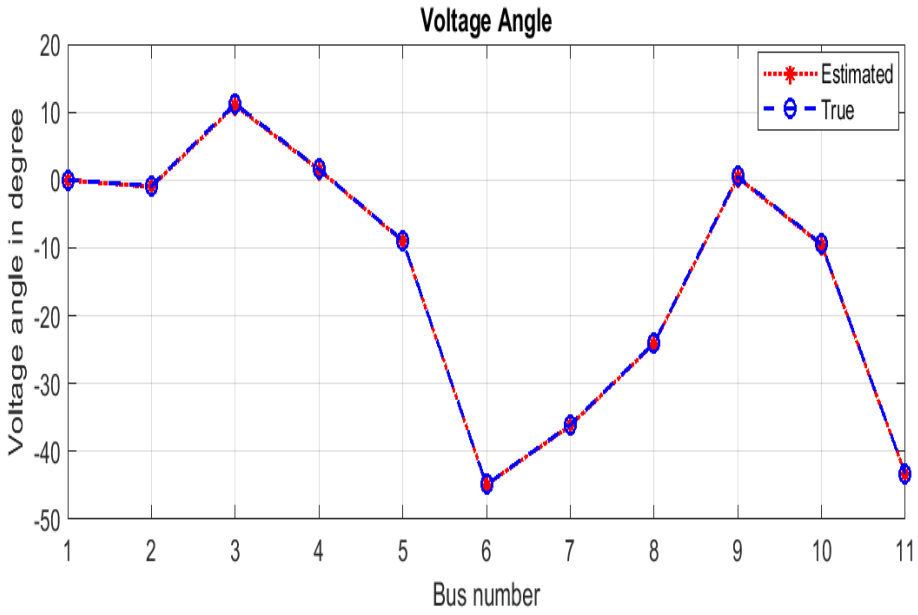

Figure 3.11: Quadratic Programming Angle Estimate in Degrees

Table 3.5: SSE: Quadratic Programming

	Voltage (pu)	Angle (Degrees)
1	1.0490	0.000
2	1.0507	-0.9920
3	1.0528	10.9473
4	1.0505	1.3819
5	1.0503	-9.1208
6	1.0492	-45.0135
7	1.0500	-36.2179
8	0.9935	-24.1245
9	1.0243	0.3285
10	1.0251	-9.6910
11	1.0235	-43.3737

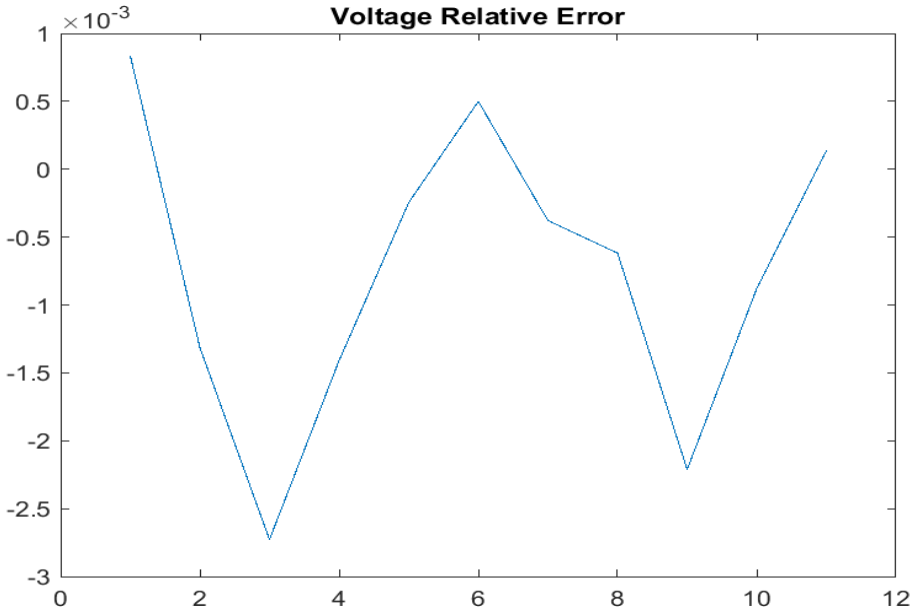

Figure 3.12: Quadratic Programming Voltage Estimate Relative Error

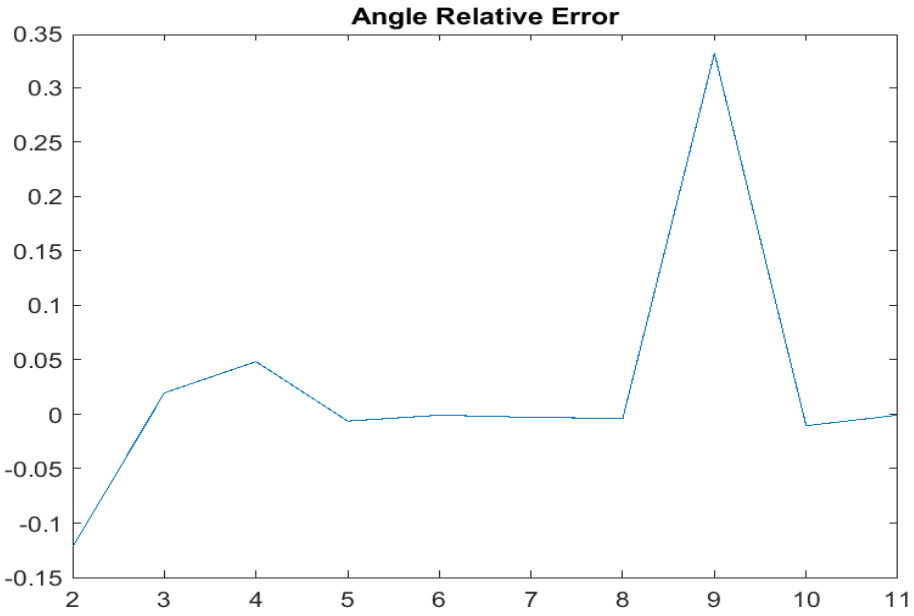

Figure 3.13: Quadratic Programming Angle Estimate Relative Error

Table 3.6: Mean Squared Error

State Estimator	Voltage	Angle
WLS	$1.6e^{-6}$	0.0799
LAV	$3.75e^{-7}$	0.0177
QUAD	$1.13e^{-6}$	0.0270

The Table 3.5 also shows the tabulated results using the quadratic state estimation approach. The results were consistent with the results from PSSE and PSAT. No bad data was suspected or detected using the chi-square test and normalized residual method. Similarly with the LAV approach, normally distributed random numbers using 10% of the standard deviation were used as added noise into the system.

The calculated mean squared error (MSE) between the estimated states and the true states was determined using the equation in reference 3.1. The voltage magnitude MSE is 1.13×10^{-6}, while the voltage angle MSE is 0.0270. The MSE obtained for the Quadratic Programming method was lower than that of the WLS approach. This indicates that this approach may be a better state estimator, especially as a robust estimator in the presence of bad data, similar to the LAV state estimator. For a visual representation, you can refer to the relative error plots of the estimated and true state in Figures 3.12 and 3.13.

As shown in Table 3.6, the accuracy of the static state estimators used by power utility companies to estimate their system's static states is confirmed. Among these estimators, LAV and Quadratic Programming are more reliable than the WLS estimator for estimating over erroneous data. Additionally, LAV and Quad have significantly faster computational speeds compared to the typical computational speed of the WLS estimator.

Chapter 4

Transmission Line Trip Detection and Identification Using Node-Breaker Approach

Power utility companies rely on the efficient functioning of their electrical transmission infrastructure for uninterrupted power supply to customers. The status of breakers and timely fault detection in transmission lines are critical for ensuring seamless power delivery. However, despite efforts to control and monitor breaker status, it is not uncommon for operators to have erroneous status of breakers at the control center.

Field experience reveals that communication failure and other factors can impede the operators from accurately verifying the breaker status at the substation. Moreover, in some instances, operators may observe current flow across the breaker, but the status indicates that it is open rather than closed. These scenarios suggest alternative or backup solutions to correctly identify and validate the breaker status, even in the event of communication failure.

In this chapter, we will explore three distinct scenarios, each utilizing different bus configurations to accurately simulate specific events that occur at the substation.

In each of these scenarios, a fault is simulated on the transmission line between the nodes. The relay is responsible for monitoring the line's health and is expected to trip the breaker during the fault, while other breakers will remain closed unless there is a breaker failure or differential event.

By collecting measurements from these events, we will be able to estimate the states and flows across the breakers at the substation, which facilitates the identification of the associated transmission line. This analysis will provide a more detailed understanding of the behavior of the transmission lines under different conditions and will help in designing more efficient and reliable power systems.

The early detection and location of faults in transmission lines is critical to ensure the smooth functioning of the power grid. One innovative solution to achieve this is by using a virtual sensor. This sensor is designed to analyze the topology and measurements of the system to identify any potential leverage points or outliers that could indicate a fault in the transmission line. By leveraging this technology, power grid operators can quickly and accurately identify and locate faults, allowing them to take prompt action to restore power and prevent further damage.

To identify these leverage points, the projection statistics algorithm is used. This algorithm uses the Jacobian matrix of the system to identify leverage data points from the rest of the measurement data. After calculating the projection statistics, they are compared with the cutoff values used to identify the leverage points associated with the measurement data.

If the calculated projection statistics are greater than the cutoff value, then a leverage measurement is identified. This identified measurement corresponds to the faulty transmission line, which might have momentarily tripped or reclosed. By using this method, the transmission control center can quickly identify the fault location, making it easier and faster to take corrective actions and avoid potential power outages.

4.1 Simulation and Results

This study provides a comprehensive analysis of the various bus configurations that are commonly employed in power systems. Specifically, we will be examining the main-transfer, breaker, and half bus configuration, and the double breaker-double bus configuration. To accurately model these configurations, we will be utilizing the PSSE power system simulation tool. This tool allows us to create a node-breaker model for a substation with zero-impedance branches, which will enable us to obtain precise and reliable results.

The different bus configurations are the main-transfer bus, breaker and half, and double breaker, double bus configurations. These configurations are illustrated in Figures 4.1 - 4.3. We use various trip scenarios to simulate events at the substations and transmission lines, which help us model the system bus configuration. To identify faulty lines, we utilize robust state estimation, virtual sensors, and node-breaker models. We also take into account the associated breaker status, which helps us make accurate predictions and recommendations.

4.1.1 Case I: Main Bus Transfer Bus

In this scenario, a fault is introduced on the transmission line connecting node 2 and node 3 using the main and transfer buses. During the fault event, the local or remote line breaker is expected to open for fault isolation. In the event of a permanent fault, which is a type of electrical fault that persists even after the fault has been removed, it is expected that both breakers will trip. This is a safety measure that helps to prevent further damage to the electrical system and protect against potential hazards.

In this particular case, the breaker located between nodes 2 and 3 should trip when a fault occurs on the transmission line. This breaker is designed to detect and respond to faults by opening the circuit and interrupting the flow of electricity. Figure 4.4, which provides a visual representation of the expected behavior of the breakers during a fault event.

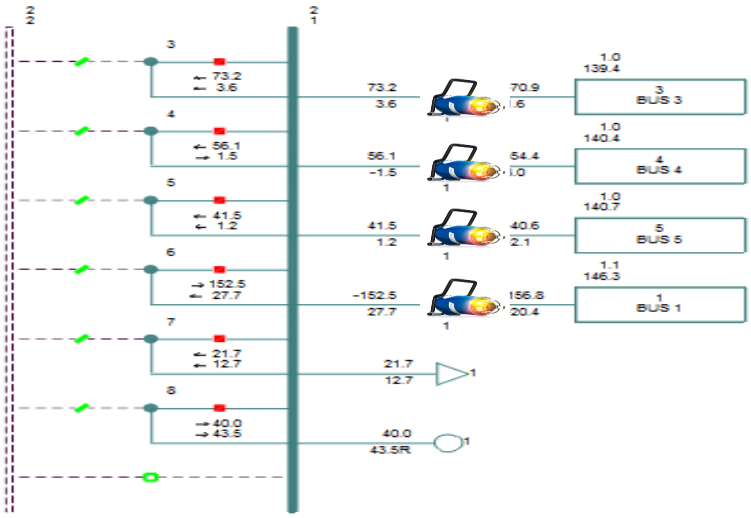

Figure 4.1: Main and Transfer Bus Configuration.

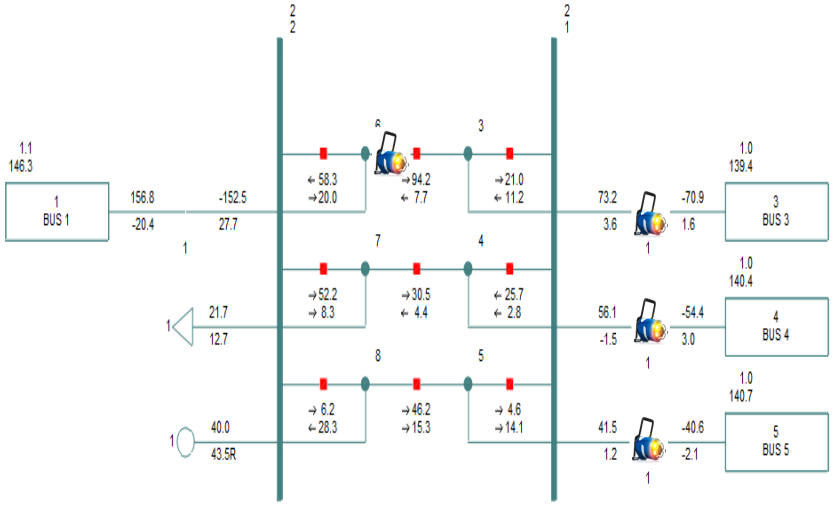

Figure 4.2: Breaker-and-a-Half Bus Configuration.

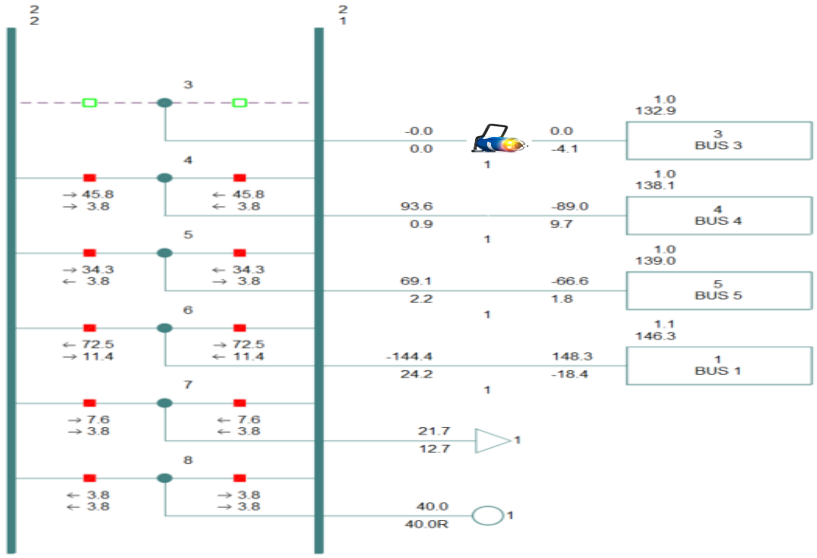

Figure 4.3: Double Breaker - Double Bus Configuration.

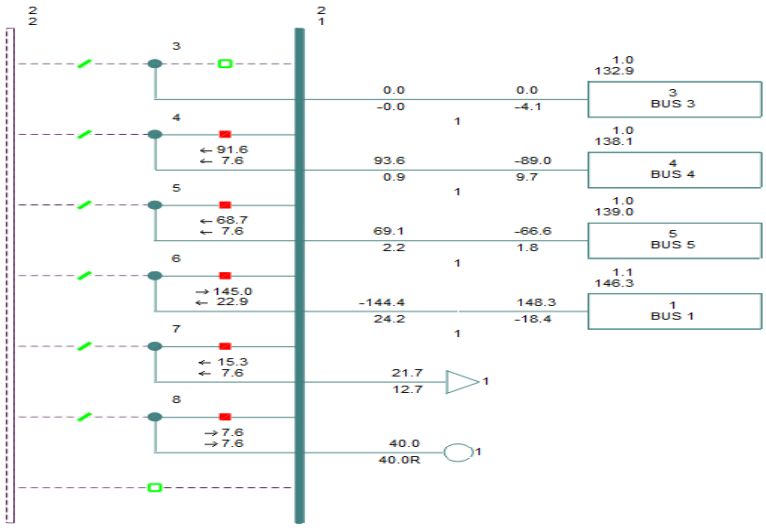

Figure 4.4: Case I: Open breaker between node 2 - 3.

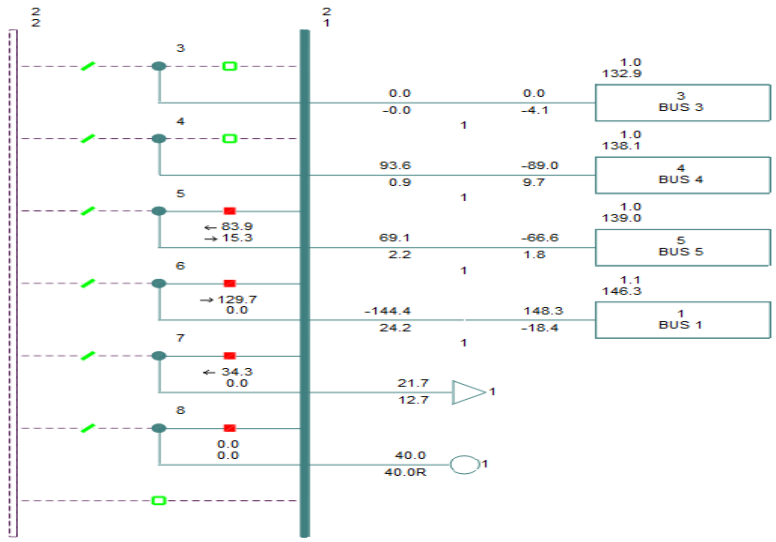

Figure 4.5: Case II: Open breaker between node 2-3, and 2-4.

During the NB simulation, the breaker located between nodes 2 and 3 tripped when a fault occurred on the transmission line between these nodes. Although control center operators can observe analog measurements of the flow across the breaker, they are unable to confirm the open or closed status of the transmission line. This may be due to issues with telemetry or communication, as mentioned earlier in this chapter. When the breaker $2-3$ trips, it disconnects the transmission line from the rest of the system. Table 4.1 displays the estimated flow across the breaker, with the status of the breaker indicated as 1 or 0 to represent closed or open breakers respectively. A threshold value of 3 was made, which approximates to be equivalent to a 1% probability of false alarm. When the flow is below the set threshold, the breaker associated with the transmission line is assumed to be open. On the other hand, when the flow exceeds the threshold of 3, the breaker is assumed to be closed. Random Gaussian measurement error was used as input measurement noise to estimate the flow across the circuit breakers.

4.1.2 Case II: Main Bus Transfer Bus

Here, the breakers associated with two (2) transmission lines are simulated to be open when a fault is introduced into the system that causes the breakers to trip. In this scenario, two breakers are open between nodes 2 and 3 and buses 2 and 4 to simulate a fault event on the transmission lines by tripping the breaker associated with both nodes as shown below. The breakers are assumed to have tripped instantaneously to isolate the faulty line from the rest of the system. The scenario is represented with the Figure 4.5. As shown in Table 4.2, When the flow is below the set threshold, the breaker associated with the transmission line is assumed to be open. Random Gaussian measurement error was used as input measurement noise to estimate the flow across the circuit breakers.

Table 4.1: Case I PCB Status

From Bus	To Bus	Flow	Status
2	1	6.8169	1
2	3	0.1102	0
2	4	5.1269	1
2	5	5.3126	1
6	5	10.6229	1
6	11	9.3398	1
6	12	6.7960	1
6	13	6.5317	1
7	4	5.1274	1
7	8	8.8459	1
7	9	9.3046	1
9	4	7.8016	1
9	7	6.1989	1

Table 4.2: Case II PCB Status

From Bus	To Bus	Flow	Status
2	1	5.1695	1
2	3	0.4596	0
2	4	2.5271	0
2	5	3.0164	1
6	5	5.9626	1
6	11	3.2610	1
6	12	3.1594	1
6	13	3.4248	1
7	4	3.9507	1
7	8	5.7600	1
7	9	6.2244	1
9	4	5.1955	1
9	7	3.0168	1

4.1.3 Case III: Breaker and Half Bus with Open Breakers

In this scenario, the breaker-and-a-half is made up of two normally energized buses with three breakers connected between the buses. A bus fault is simulated on one of the buses to open the breakers associated with the bus. An additional breaker is open to isolate the line between buses 2 and 3 as shown below. The breakers are assumed to have tripped on a permanent fault to isolate the fault from the system. The scenario is represented with Figure 4.6 to show the simulated bus fault. The result of the node-breaker estimated flow across the breaker is shown in Table 4.3, the breaker status is shown as either closed (1) or opened (0).

4.1.4 Case IV: Double Breaker-Double Bus

The final scenario considered in this chapter is the double breaker-double breaker bus configuration. This bus configuration takes advantage of the two normally energized buses and two connected circuit breakers for the circuits. Hence, any of the PCBs can be removed for maintenance or replacement without interrupting the circuit. This means that a fault on any of the breakers does not affect the other circuit. However, for this study, the two breakers on both circuits are assumed to be open due to a fault that instantaneously tripped both breakers to isolate the transmission line between buses 2 and 3. The breakers are assumed to have tripped on a permanent fault to isolate the fault from the system. The scenario is represented in Figure 4.7 to show the simulated bus fault. The result of the node-breaker estimated flow across the breaker is shown in Table 4.4, the breaker status is shown as either closed (1) or opened (0).

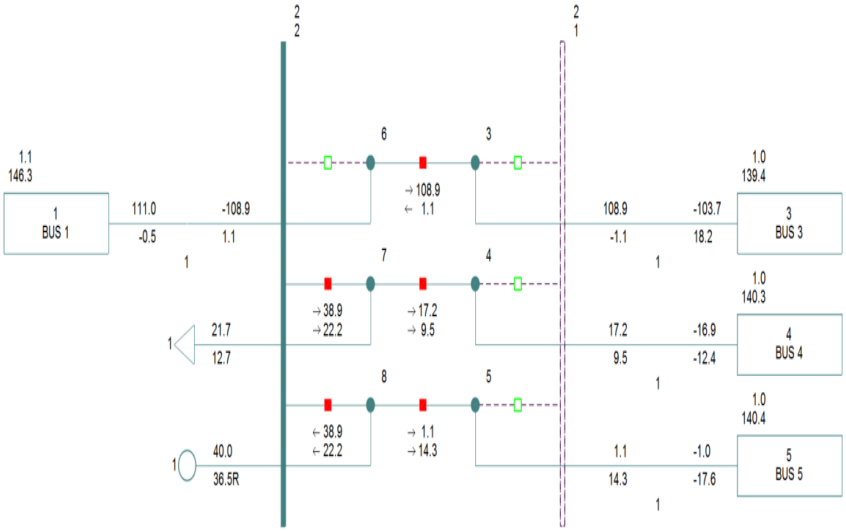

Figure 4.6: Case III: bus fault with open breakers

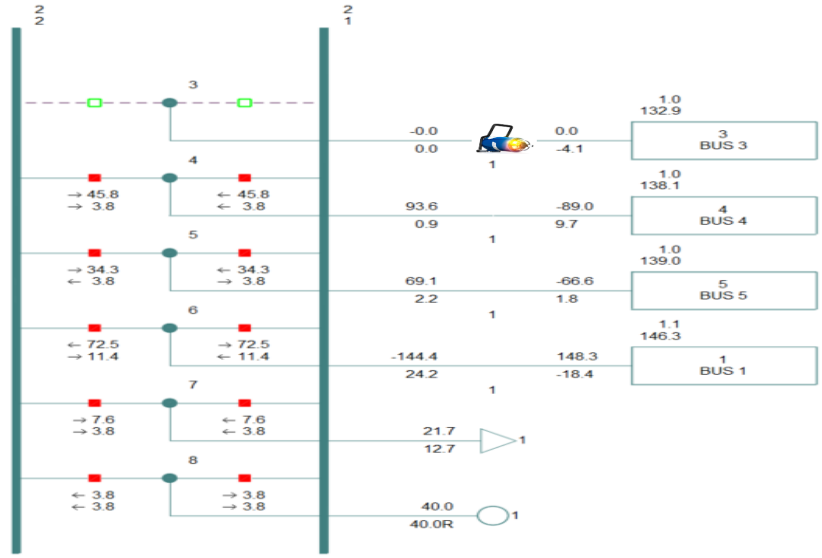

Figure 4.7: Case IV: Open breaker between node 2 - 3.

Table 4.3: Case III PCB Status

From Bus	To Bus	Flow	Status
2	3	2.4336	0
2	4	2.0553	0
2	5	2.7312	0
2	1	2.2038	0
6	5	11.8817	1
6	11	4.4365	1
6	12	12.2170	1
6	13	6.4052	1
7	4	4.5774	1
7	8	5.4610	1
7	9	5.2564	1
9	4	3.1897	1
9	7	6.8994	1

Table 4.4: Case IV PCB Status

From Bus	To Bus	Flow	Status
2	1	4.1329	1
2	3	2.8018	0
2	4	3.6643	1
2	5	3.6766	1
6	5	4.9801	1
6	11	4.1921	1
6	12	4.1307	1
6	13	4.1224	1
7	4	3.3969	1
7	8	4.6964	1
7	9	4.8154	1
9	4	4.4203	1
9	7	3.9231	1

4.2 Virtual Sensor

As systems become increasingly complex and automated, it is essential that they are able to perform at a high level and provide excellent quality of service. These growing complexities come with new challenges, including the need for innovative ideas, controllers, designs, and sensors to ensure system reliability and efficiency [62]. This is particularly true for fault detection and identification on transmission lines, where the proposed node-breaker model can be used to model a transmission or distribution substation. To achieve this, the proposed virtual sensor will use real-time measurement sensors to detect faults and trigger a trip. This can be done by either rolling the lockout relay or sending a trip command to the PCBs associated with the transmission line. The main goal is to ensure that the system is capable of detecting and responding to true faults while avoiding false alarms.

The proposed virtual sensor is a technology that functions similarly to the SEL fault indicator, which is a device that is attached to transmission lines to identify and locate faults. The virtual sensor (VS), also known as a soft sensor, is an inferential statistical model that utilizes the transmission line sensor to predict and recommend actions [63]. The VS model relies on the supervisory control and data acquisition (SCADA) system's measurements to analyze and make conclusions through the local remote terminal unit (RTU) at the substation. This type of transmission line virtual sensor is data-driven, which means it's designed for monitoring and protection [64, 65].

Statistical inferential analysis will be utilized to draw conclusions and predictions about the transmission line or the system's condition. The analysis will incorporate different models to provide a comprehensive understanding of the system. Projection statistics, chi-square, normalized residual, and auto-regression analysis are among the models that will be examined. These models will help to analyze data sets, identify patterns and trends, and provide useful insights to improve the system's performance. By utilizing these models, we can develop a better understanding of

the system and its potential issues, allowing for more effective decision-making and proactive maintenance.

4.2.1 Projection Statistics Algorithm

Projection statistics is a robust method of identifying leverage measurement [66, 67, 41]. The projection statistics algorithm is given as

$$PS_i = \max_{H_k} \frac{|H_i^T * H_k|}{S_m} \qquad for \quad k = 1, 2, 3, ..., m \tag{4.1}$$

$$Sm = \gamma . lomed_i lomed_{j \neq 1} |H_i^T . H_k + H_j^T . H_k| \quad 1 \leq i, j, k \leq m \tag{4.2}$$

where γ= 1.1926 and $lomed_i\{x\}$ is low median expressed as $\left[\frac{(m+1)}{2}\right]$ - th order of the m numbers in x [67], where $x = x_1, x_2, ..., x_m$ and $[x]$ represents the integer of x . For instance, if m =8, then the low median will be 4.

The denominator S_m in (4.2) represents the dispersion of the numerator about the origin in (4.1). The projection statistics algorithm is expected to follow the chi-square distribution. The degree of sparsity in the Jacobian matrix H_i corresponds to the degree of freedom (DOF) of the chi-square distribution for the measurement i.A leverage point can be identified when the value of PS_i, which is the leverage measurement, exceeds a certain cutoff threshold. This threshold serves as a point of reference to distinguish normal data points from those that exhibit a higher degree of leverage.

$$\begin{aligned} PS_i &> \eta \\ \eta &= \chi^2_{k,0.975} \end{aligned} \tag{4.3}$$

Table 4.5: Projection Statistics: Case I

Meas.	PS_i	ω_i
I_{2-1}(real)	8.7968	11.1433
I_{2-1}(imag)	8.5292	11.1433
I_{2-3}(real)	18.5748	11.1433
I_{2-3}(imag)	16.4445	11.1433
I_{2-4}(real)	9.0203	11.1433
I_{2-5}(imag)	9.1595	11.1433
I_{2-4}(imag)	7.0943	11.1433

Table 4.6: Projection Statistics: Case II

Meas.	PS_i	ω_i
V_3(real)	702.9838	7.3778
V_2(real)	702.9838	7.3778
V_3(imag)	9.4179	5.0239
V_2(imag)	1.6674	5.0239
I_{2-3}(real)	1405.9704	11.1433
I_{2-3}(imag)	1677.0116	11.1433
I_{2-4}(real)	702.9859	14.4494
I_{2-4}(imag)	1118.0077	11.1433

Table 4.7: Projection Statistics: Case III

Meas.	PS_i	ω_i
V_3(real)	41.2385	7.3778
V_2(real)	61.8352	7.3778
V_3(imag)	7.5757	5.0239
V_2(imag)	1.3344	5.0239
I_{2-3}(real)	61.3204	11.1433
I_{2-3}(imag)	976.0201	11.1433
I_{2-4}(real)	702.9859	14.4494
I_{2-4}(imag)	1118.0077	11.1433

As mentioned earlier, leverage measurement i can be identified as a leverage point if the associated PS_i is greater than the cutoff ω_i. The PS virtual sensor information is given in Table 4.5 for case I where the line between nodes 2 and 3 tripped due to fault. As shown in the Table 4.5, the tripped line measurements (real and imaginary) are expected to show up as leverage measurements with the value s of PS_i greater than the cutoff ω_i. Measurements, I_{2-3} (real) and I_{2-3} (imaginary) show up as the leverage measurements to validate the measurement of the trip line as the leverage measurements sensed by the VS on the line.

More leverage measurements are expected from Case II due to more tripped transmission lines. The measurements associated with nodes 2, 3, and 4 are expected to show up as leverage measurements as shown in Table 4.6. The table shows that both the real and the imaginary measurements PS are greater than the cutoff. This table also validates the VS sensor of sensing tripped lines measurements as leverage measurements.

Case III, which is the breaker-and-a-half bus configuration, is a unique case with a bus fault simulated at the bus to trip all the breakers and transmission lines associated with the breakers. Table 4.7 shows the result of the VS projection statistics to sense leverage measurements of the tripped lines. The table 4.7 validates that the tripped lines measurements show up as leverage measurements. Real and imaginary measurements associated with buses 2,3, and 4 have PS greater than the cutoff to validate the measurements as leverage measurements.

Chapter 5

Dynamic State Estimation: Balanced Fault Simulation

Performing static state estimation at short intervals becomes computationally complicated and expensive when there are increased loads and generation due to the dynamics of the system. Therefore, it is necessary to use a dynamic state estimator that considers the time-varying nature of the system model. Dynamic state estimators can compute the system state vector at the next time step, providing greater accuracy and analysis for real-time control and monitoring of power systems. This approach is useful for estimating the next sampling time and integrating Phasor Measurement Units (PMUs) into power system operations. Using the Global Positioning System (GPS), synchronized time-sampled measurements can be used for real-time monitoring and control [4, 32, 33, 34, 35, 36].

The dynamic state estimation is carried out using Kundur's two-area model, and the reduced University of Tennessee, Knoxville (UTK) Hardware Test Bed (HTB) WECC model to simulate several fault events. Different faults were simulated on the different models to see how the dynamic states reacted to fault events. Balanced and unbalanced faults were simulated to study the effect of faults on the systems and how the dynamic states of synchronous generators react to these faults.

Similar to the UTK HTB model, the simulation can be scaled to a large-scale simulation. This chapter will focus on different case studies using the data from the system to estimate the dynamic states to comparing the true and the estimated states.

5.1 UTK HTB Reduced WECC System

The University of Tennessee WECC Hardware Test Bed model is a transmission network that approximates the true large-scale WECC model using converters that emulate generators and loads. Figure 5.1 shows the different interconnections modeled on the HTB to simulate the large-scale models with integrated real-time protection, control, and communication. Figures 5.2 and 5.3 show the power flow of the reduced HTB WECC model in MW. The summer model was selected and used for the dynamic state estimation. The data from the model was used as input measurements for the dynamic simulation. Different cases were used to test the HTB model from using the HTB measurements to estimate the dynamic states to comparing the states of the HTB with the dynamic state estimator using the robust unscented Kalman filter (UKF).

To conduct the initial simulation using the HTB WECC model, the parameter data obtained from the HTB simulation was used. The generator's active power (P_e), reactive power (Q_e), and terminal voltage (V_T) are input measurements for the estimator. This helps in accurately estimating the dynamic states of the generator in the interconnection system. The reclosing protection system was tested on transmission lines to assess its response to fault conditions. The simulation included one-shot, two-shot, and lock-out reclosing protection events, and demonstrated the impact of transmission line faults on the dynamic states of generators. The results provide insights into how generators behave in response to transmission line faults.

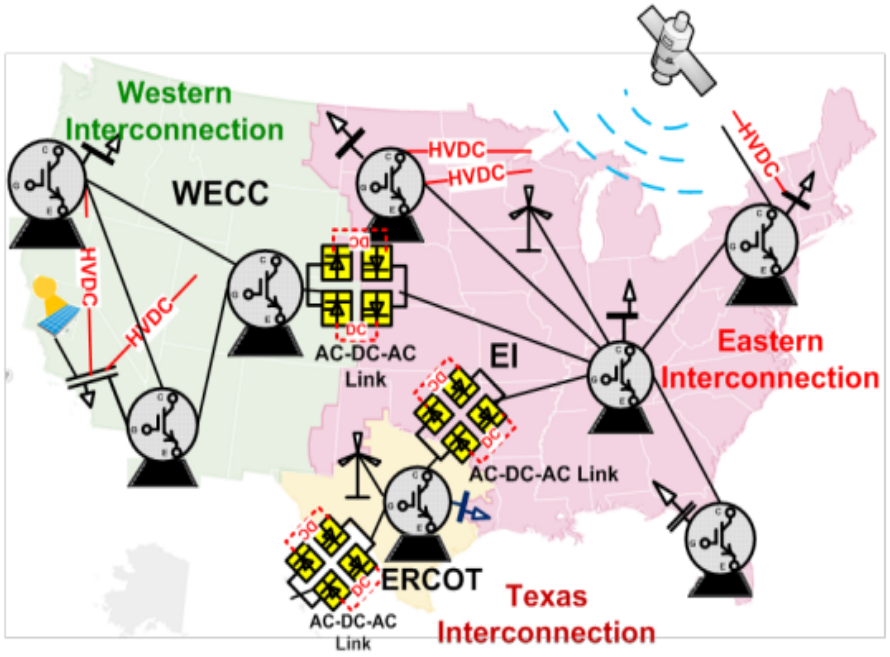

Figure 5.1: UTK HTB WECC Summer Model

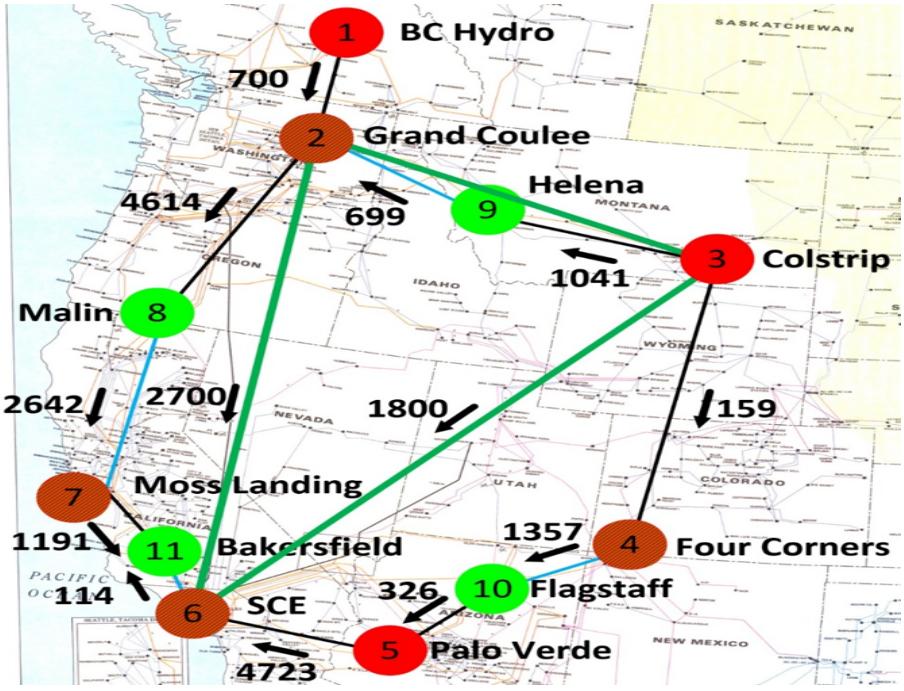

Figure 5.2: UTK HTB WECC Summer Model

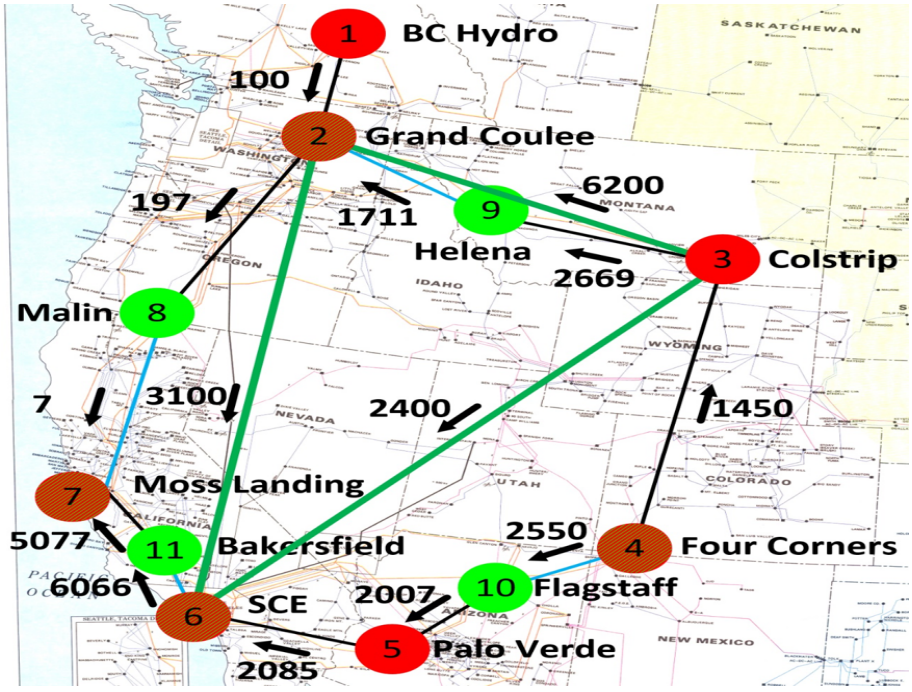

Figure 5.3: UTK HTB WECC Winter Model

5.1.1 Unscented Kalman Filter

$$\begin{aligned} x_{k+1} &= g(x_k, k) + \omega_k \\ z_k &= h(x_k, k) + \vartheta_k \end{aligned} \tag{5.1}$$

$g(x_k, k)$ is the noise-free dynamics evaluated at time k step

$h(x_k, k)$ is the noise-free measurement evaluated at time k step

$x_k \in \mathbb{R}^n$ is the discrete state vector at time step k

$z_k \in \mathbb{R}^m$ is the discrete measurement vector at time step k

$\omega_k \sim N(0, Q_k)$ is the process noise at time step k

$\vartheta_k \sim N(0, R_k)$ is the measurement noise at time step k

Q_k is the covariance matrix of ω_k

R_k is the covariance matrix of ϑ_k

The UKF is initialized as follows

$$\hat{x_0^+} = E(x_0) \tag{5.2}$$

$$P_0^+ = E[(x_0 - \hat{x_0^+})(x_0 - \hat{x_0^+})^T] \tag{5.3}$$

Time updates are used to propagate the state estimate and covariance from one measurement time to another. To propagate from time step (k-1) to k, sigma points are chosen as

$$\begin{aligned} \hat{x}_{k-1}^i &= \hat{x}_{k-1}^+ + x_*^i \quad i = 1, ..., 2L \\ x_*^i &= (\sqrt{(LP_{k-1}^+}\,)_i^T \quad i = 1, ..., L \\ x_*^{n+i} &= -(\sqrt{(LP_{k-1}^+}\,)_i^T \quad i = 1, ..., L \end{aligned} \tag{5.4}$$

where $(\sqrt{LP})_i$ is termed as the ith row of the matrix square root of $(\sqrt{LP})_i$ usually computed numerically using Cholesky factorization. The nonlinear system equation $f(\cdot)$ is used to transform the sigma points into $\hat{x}_k^i$ vectors

$$\hat{x}_k^i = g(\hat{x}_{k-1}^i, k-1) \tag{5.5}$$

Combining the $\hat{x}_k^i$ vectors to obtain the a priori state estimate at time k

$$\hat{x}_k^- = \frac{1}{2L}\sum_{i=1}^{2L}\hat{x}_k^i \tag{5.6}$$

Estimate the a priori error covariance with the measurement noise Q_{k-1} added

$$P_k^- = \frac{1}{2L}\sum_{i=1}^{2L}(\hat{x}_k^i - \hat{x}_k^-)(\hat{x}_k^i - \hat{x}_k^-)^T + Q_{k-1} \tag{5.7}$$

For optimal performance, the new sigma point is calculated as

$$\begin{aligned} \hat{x}_k^i &= \hat{x}_{k-1}^+ + x_*^i \quad i = 1, ..., 2L \\ x_*^i &= (\sqrt{(LP_k^-)})_i^T \quad i = 1, ..., L \\ x_*^{n+i} &= -(\sqrt{(LP_k^-)})_i^T \quad i = 1, ..., L \end{aligned} \tag{5.8}$$

Use the nonlinear measurement h(.) equation to transform the sigma point into $\hat{z}_k^i$ vectors

$$\hat{z}_k^i = h(\hat{x}_k^i, k) \tag{5.9}$$

Combine the $\hat{z}_k^i$ vectors to obtain the predicted measurement at time k

$$\hat{z}_k^- = \frac{1}{2L}\sum_{i=1}^{2L}\hat{z}_k^i \tag{5.10}$$

Estimate the covariance and cross-covariance

$$\begin{aligned} P_z &= \frac{1}{2L}\sum_{i=1}^{2L}(\hat{z}_k^i - \hat{z}_k)(\hat{z}_k^i - \hat{z}_k)^T + R_k \\ P_{xz} &= \frac{1}{2L}\sum_{i=1}^{2L}(\hat{x}_k^i - \hat{x}_k)(\hat{z}_k^i - \hat{z}_k)^T \end{aligned} \tag{5.11}$$

The measurement update of the state estimate is performed using

$$K_k = P_{xz} P_z^{-1} \tag{5.12}$$

$$\begin{aligned} \hat{x}_k^+ &= \hat{x}_k^- + K_k(z_k - \hat{z}_k) \\ P_k^+ &= P_k^- - K_k P_z K_k^T \end{aligned} \tag{5.13}$$

5.1.2 Case I: UTK HTB WECC System

To estimate the true dynamic states of the interconnection system, the HTB WECC model's parameters and measurements (identified as "WECC summer") were exported into the UKF dynamic state estimator. The generator active power (P_e), reactive power (Q_e), and terminal voltage (V_T) are used as measurements within the estimator. This allows for the accurate estimation of the generator's dynamic states.

A three-phase-ground fault is applied to one of the transmission lines, specifically L_{2-8} at 0.6 seconds. This type of fault causes a current to flow from each of the three phases to the ground. As a result, the line trips and remains disconnected for the remaining 1.4 seconds of the simulation. This fault is considered permanent, which means it requires a manual reset or intervention to restore the line to normal operation. Figures 5.4 to 5.8 showcase the estimated dynamic states that align with the two-axis model given in (2.2). These dynamic states are crucial to understanding the dynamic behavior of the system.

Figure 5.4 shows the rotor angles δ of the generators. The plot illustrates that the rotor angles diverge from the steady state to form islands during the fault. The graph in Figure 5.5 displays the rotor speeds (ω) of the generators. The plot clearly illustrates that when the fault occurred, the rotor speed deviated from the steady state, causing the formation of groups of generators (or 'islands') with similar rotor angles. Figure 5.6 displays the field voltage E_{fd} of the generator.

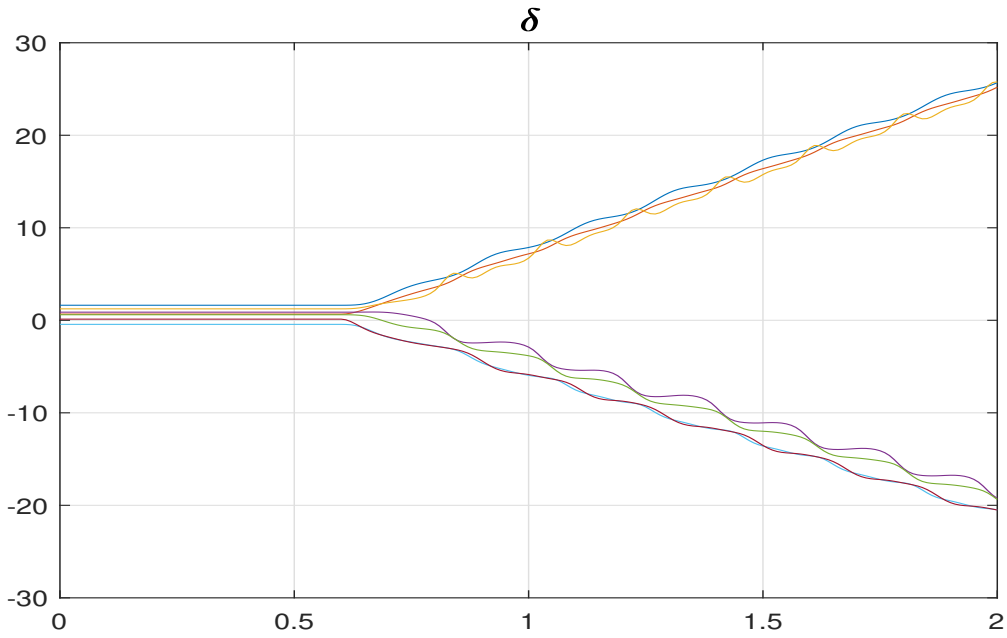

Figure 5.4: Rotor Angles

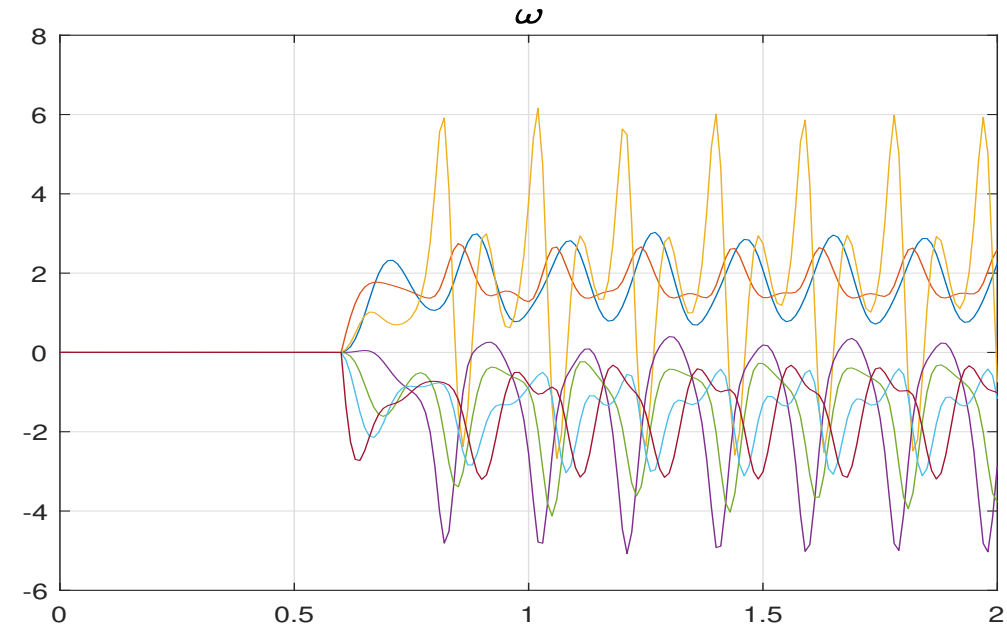

Figure 5.5: Rotor Speeds

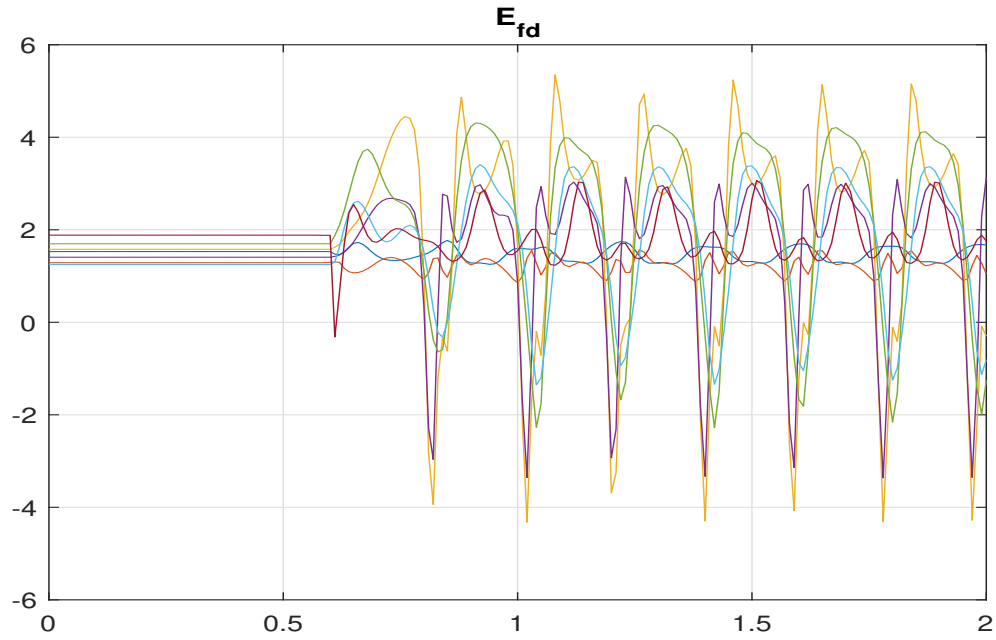

Figure 5.6: Field Voltage

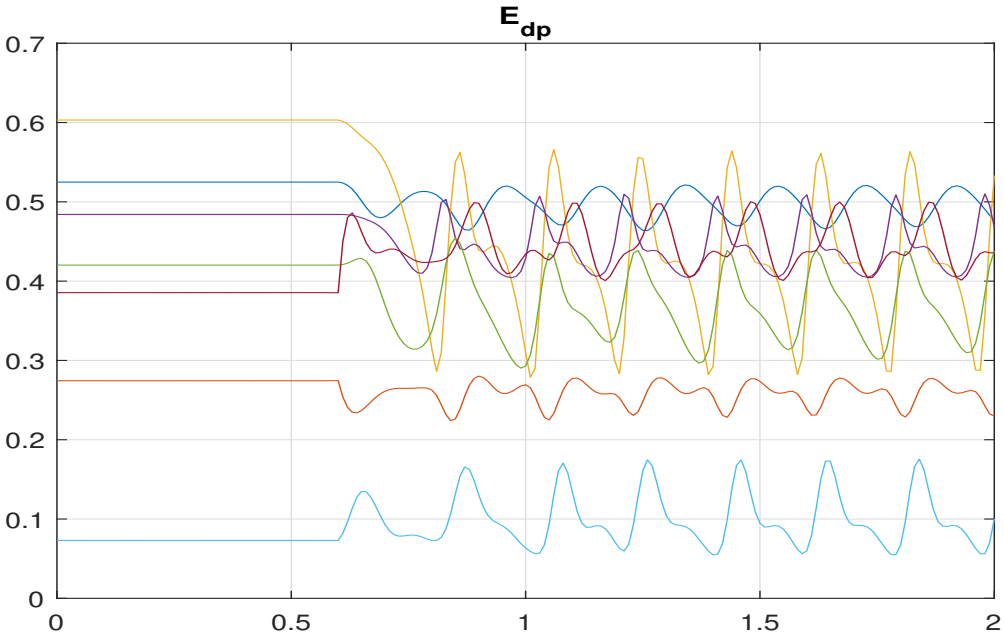

Figure 5.7: d-axis Transient Voltage

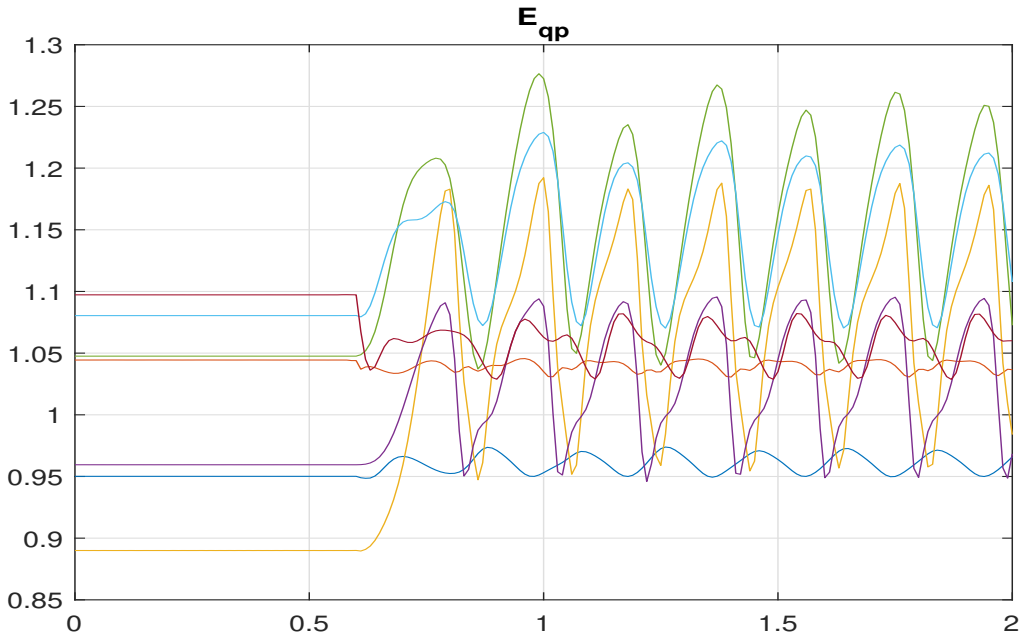

Figure 5.8: q-axis Transient Voltage

The d-axis transient voltage $E_d^{'}$ of the generator can be seen in Figure 5.7, while the q-axis transient voltage $E_q^{'}$ is illustrated in Figure 5.8.

5.1.3 Case II: WECC System without Reclosing

In this case, the true states of the generators are compared with the estimated states obtained from the dynamic estimator. The transmission line between the generators trips and there is no reclosing, which results in the system's inability to return to a steady state. Additionally, measurements from the generators were collected and processed to estimate the states of the generators. The generator's active and reactive power, denoted by P_e and Q_e, respectively, are used as measurements, as well as the generator terminal voltage V_T.

At one second of the simulation, a three-phase-ground fault is applied to the transmission line L_{2-8}. As a result, the line is tripped and remains disconnected for the remaining 4 seconds of the simulation. This fault is considered to be permanent, which means that it requires manual intervention or reset to restore the line to normal operation.

Added noise in the form of a normally distributed random number is now introduced. The accuracy of the estimated states against the true states is evaluated by calculating the Mean Squared Error (MSE) using (5.14). The MSE error of the dynamic states is summarized in Table 5.1, comparing the true and estimated values. This allowed us better to understand the differences between the estimated and true states, giving us valuable insights into the performance of our system.

The different generator states are shown in Figures 5.9 - 5.13. The red dashed line indicates the estimated dynamic states, while the blue solid line indicates the true dynamic states of the system. Figure 5.9 shows the rotor angles δ of the generators. The plot illustrates that the rotor angles diverges from the steady state to form islands of generators during the fault. The MSE for all the generators is calculated and shown in Table 5.1. To replicate real-world conditions, noise is introduced into the system

to evaluate the performance of the dynamic simulator in estimating the dynamic rotor angle. The calculated Mean Squared Error (MSE) value provides a quantitative measure of the accuracy of the simulator's performance. This assessment is crucial for ensuring the reliability and effectiveness of the estimator in practical applications.

The plot in Figure 5.10 shows the rotor speeds (ω) of the generators. The plot clearly illustrates that when the fault occurred, the rotor speed deviated from the steady state, causing the formation of groups of generators (or 'islands') with similar rotor angles, as seen in other graphs. The MSE of the rotor speeds (ω) is also calculated as shown in Table 5.1. Figure 5.11 displays the field voltage E_{fd} of the generator. The d-axis transient voltage $E_d^{'}$ of the generator can be seen in Figure 5.12, while the q-axis transient voltage $E_q^{'}$ is illustrated in Figure 5.13 as the final estimated state. The MSE for E_{fd}, $E_d^{'}$, and $E_q^{'}$ are also calculated as shown in Table 5.1.

To further analyze the behavior of synchronous generators, their relative rotor angles are simulated and plotted, with generator one used as the reference angle. The results of this simulation can be seen in Figure 5.14, which provides a visual representation of the relative angles between the generators.

$$MSE = \sqrt{\frac{1}{N}\sum_{j=1}^{N}(x_j^i - \hat{x}_j^i)^2} \tag{5.14}$$

where

x_j^i is the true state of the ith element of the associated state vector

$\hat{x}_j^i$ is the estimated state of the ith element of the associated state vector

N is the aggregate number of simulation steps.

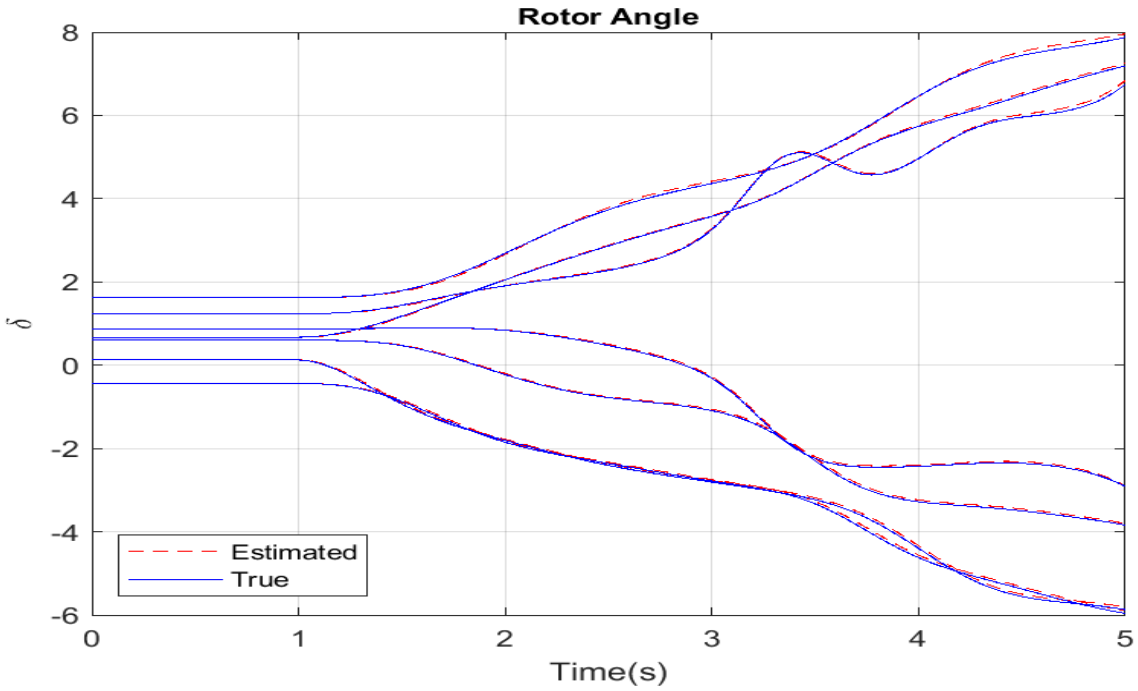

Figure 5.9: True vs. Estimated Rotor Angle

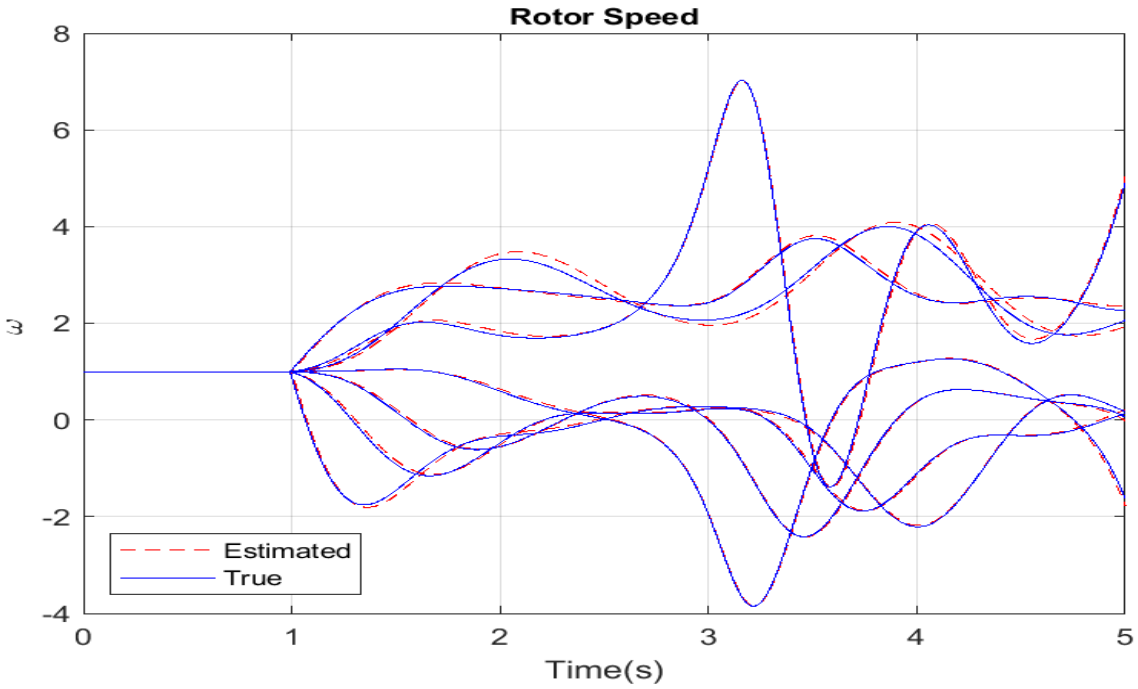

Figure 5.10: True vs. Estimated Rotor Speed

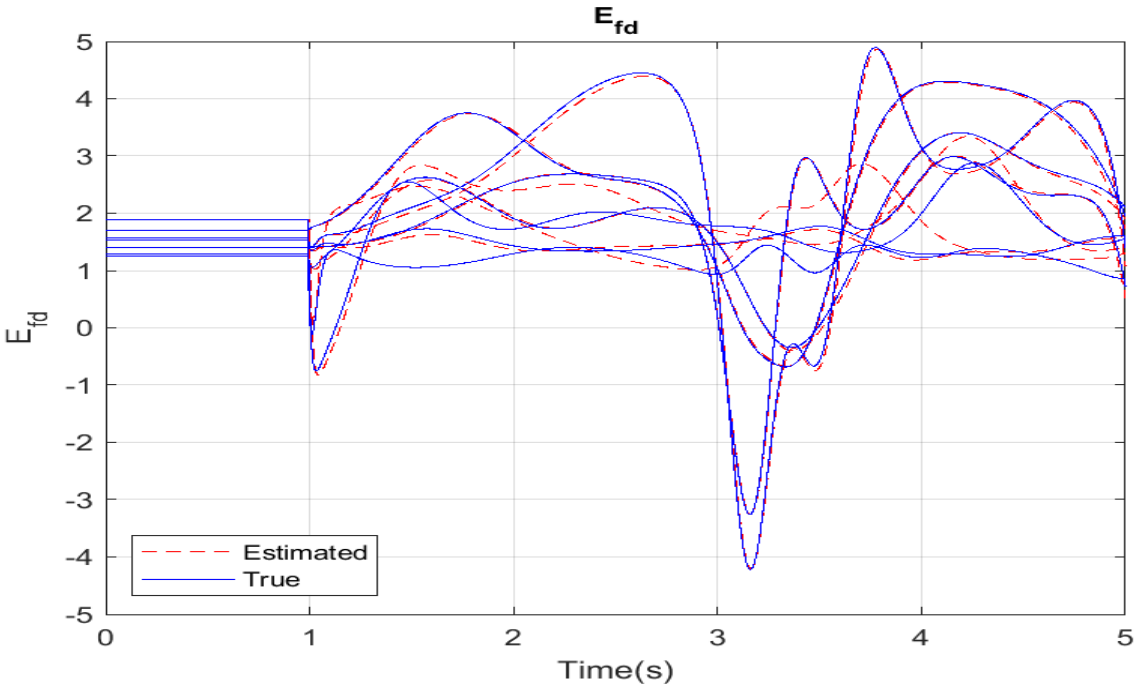

Figure 5.11: True vs. Estimated E_{fd}

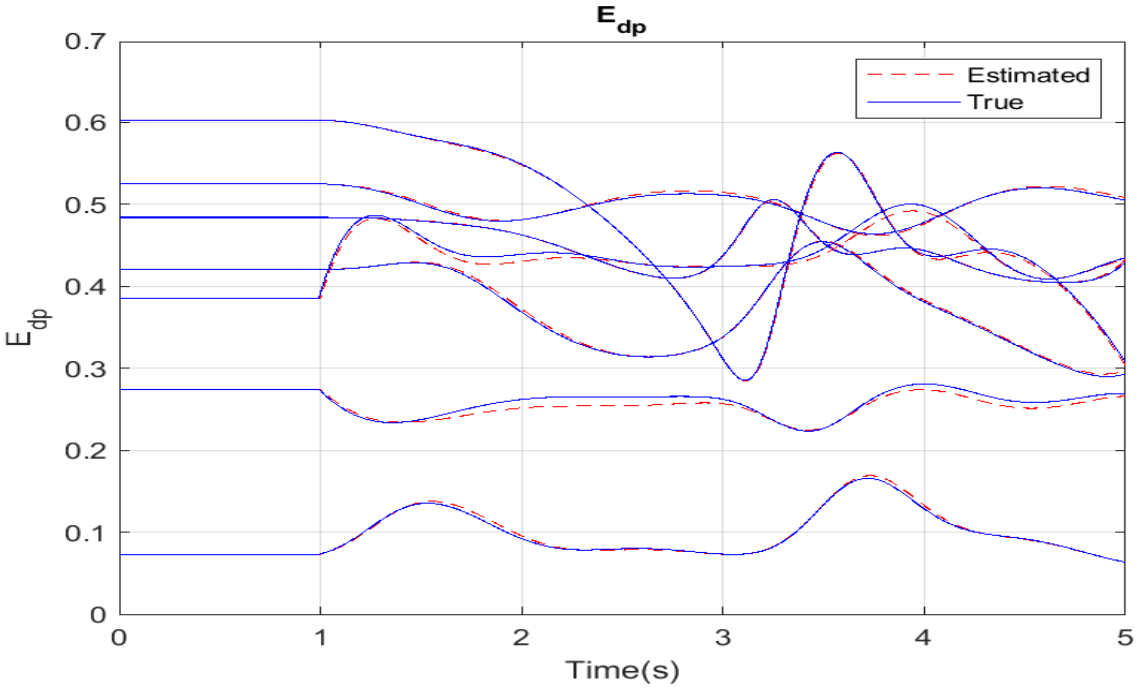

Figure 5.12: True vs. Estimated E_{dp}

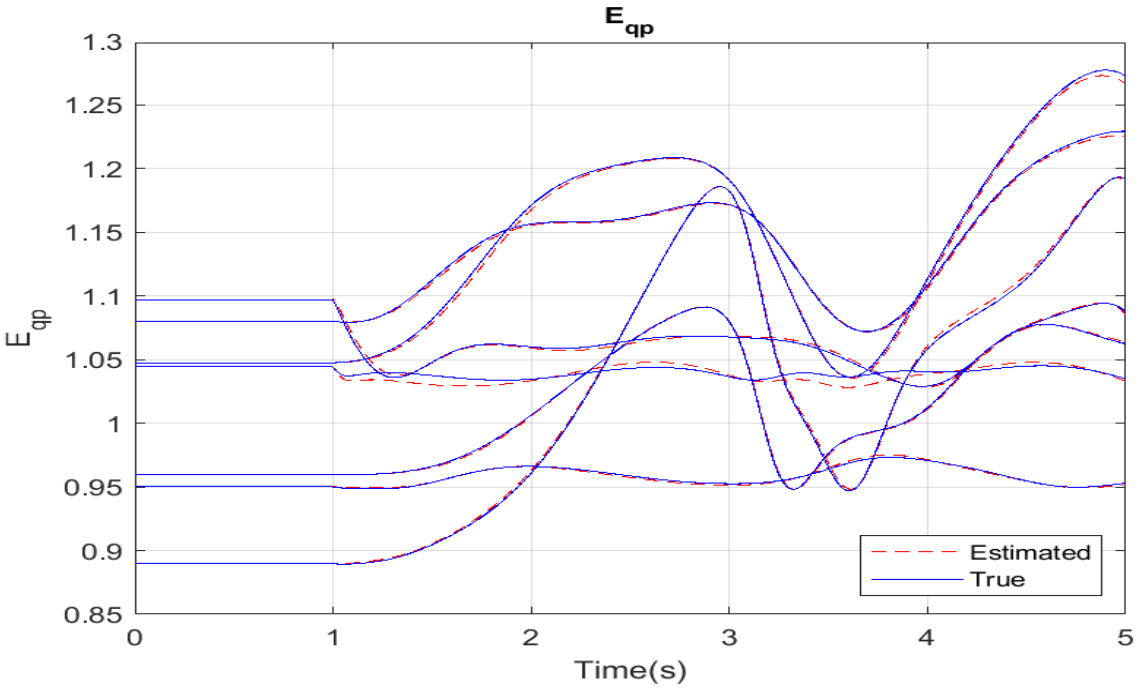

Figure 5.13: True vs. Estimated E_{qp}

Table 5.1: Mean Squared Error: WECC System without Reclosing

States	MSE
δ	0.0012
ω	0.0031
E_{fd}	0.00836
E_{dp}	$1.060e^{-5}$
E_{qp}	$3.852e^{-6}$

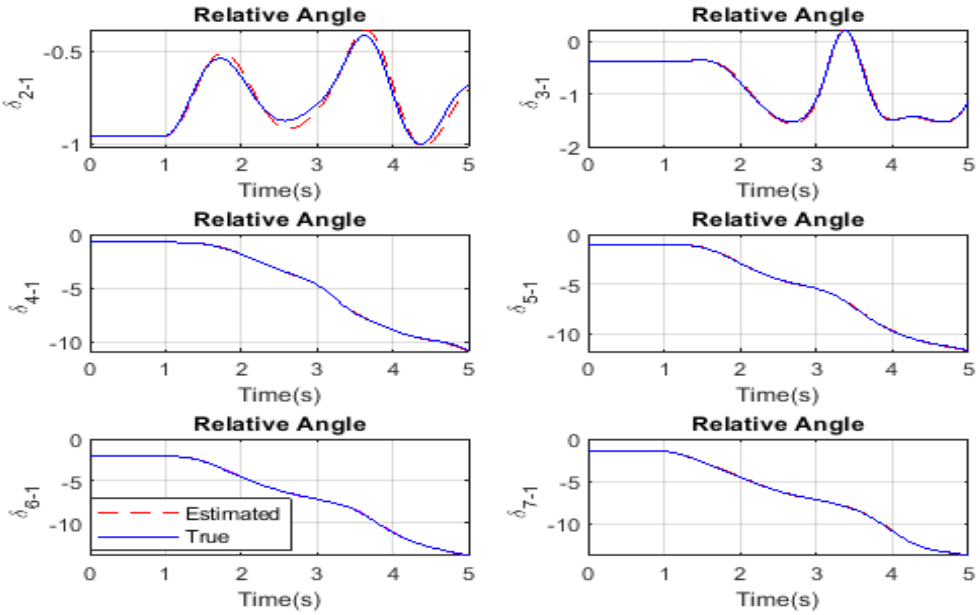

Figure 5.14: True vs. Estimated Rotor Relative Angles

5.1.4 Case III: WECC System with Reclosing

In this case, the transmission line reclosing is simulated to see how the dynamic states of the generators react to the temporary fault on a transmission line. The true states of the generators are compared with the estimated states obtained from the dynamic estimator. The transmission line between the generators trips and recloses after the fault is cleared, which allows the system to return to a steady state. Measurements from the generators are collected and processed to estimate the states of the generators. The generator's active and reactive power, denoted by P_e and Q_e respectively, are used as measurements as well as the generator terminal voltage V_T.

At two seconds of the simulation, a three-phase-ground fault is applied to the transmission line L_{2-8}. As a result, the line is tripped after a few cycles and recloses for the remaining time of the simulation. This fault is considered to be temporary, which means that it only occurs for a few cycles and does not require a manual reset to restore the line to normal operation.

This type of reclose is a single-shot reclose. When a transmission line fails to reclose after the second attempt, it may experience a two-shot reclose or lockout. This means that the reclose scheme will attempt to close the line twice before it locks out to prevent further damage or danger. In the subsequent sections of this chapter, we will delve deeper into this specific reclose scheme and its significance in maintaining a safe and reliable power transmission system.

Again to replicate real-world conditions, noise was introduced into the system to evaluate the performance of the dynamic simulator in estimating the dynamic rotor angle. The MSE provides a quantitative measure of the accuracy of the simulator's performance. This assessment is crucial for ensuring the reliability and effectiveness of the simulator in practical applications. The accuracy of the estimated states against the true states was evaluated by calculating the (5.14). Finally, the MSE error of the dynamic states is summarized in Table 5.2 comparing the true and estimated values.

This allowed us better to understand the differences between the estimated and true states, giving us valuable insights into the performance of our system.

The different generator-estimated dynamic states are shown in Figures 5.15 - 5.19. The red dashed line indicates the estimated dynamic states, while the blue solid line indicates the true dynamic states of the system. Figure 5.15 shows the rotors' relative angles δ of the generators. The rotor angle of generator one(1) is used as the reference angle. The plot illustrates a visual representation of the relative angles between the generators.

In Table 5.2, the Mean Squared Error (MSE) values are calculated for all the generators. Additionally, Figure 5.16 provides a visual representation of the rotor speeds (ω) of the generators. The plot clearly shows that when a fault occurs, the rotor speed deviation diverges from the steady state for a few cycles until the transmission line trips. Once the transmission line recloses, the rotor speed returns to its steady state. The MSE values for the rotor speeds (ω) are also calculated and presented in Table 5.2.

The Figure 5.19 shows the plot of the generator's field voltage E_{fd}. The d-axis transient voltage $E_d^{'}$ of the generator is shown in Figure 5.17, while Figure 5.18 illustrates the q-axis transient voltage $E_q^{'}$. Additionally, Table 5.1 provides the Mean Squared Error (MSE) values for E_{fd}, $E_d^{'}$, and $E_q^{'}$, which can be used to evaluate the accuracy of the dynamic state estimator.

The mean squared error (MSE) analysis of the dynamic states reveals that the Unscented Kalman Filter (UKF) is a reliable method for estimating the dynamic states of the generators in the model. The performance of the estimator is noteworthy, as it can efficiently simulate real-world scenarios even in the presence of noise. The results of the analysis demonstrate the effectiveness of the unscented Kalman filter in providing accurate and reliable estimates of the dynamic states of the generators.

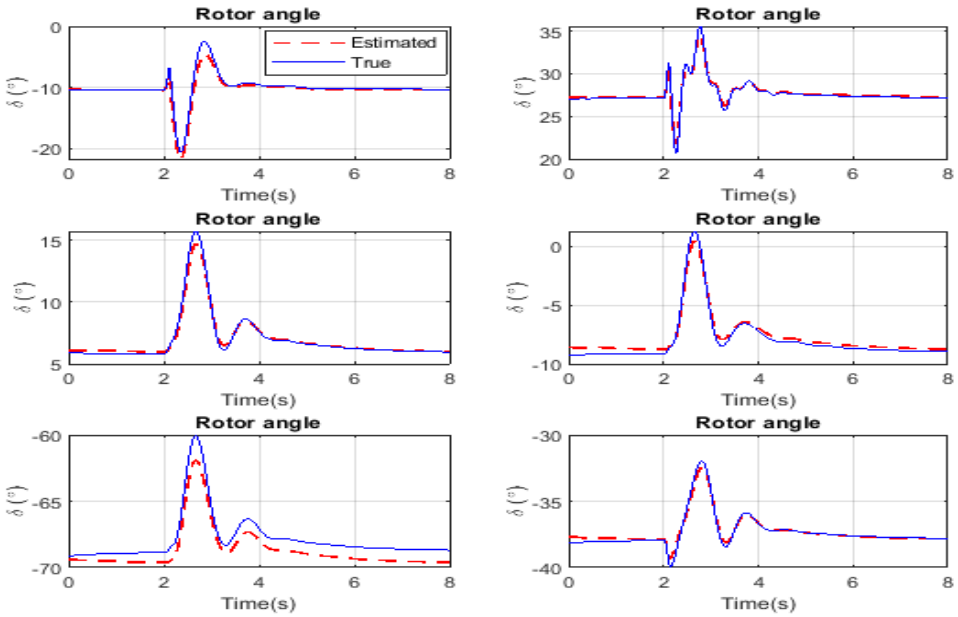

Figure 5.15: True vs. Estimated Relative Rotor Angles

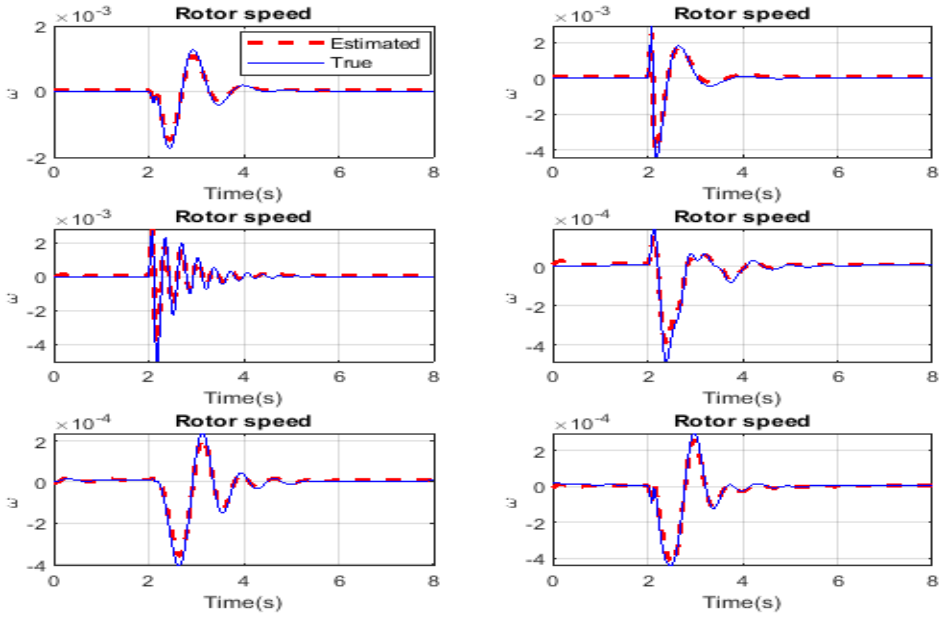

Figure 5.16: True vs. Estimated Rotor Speed

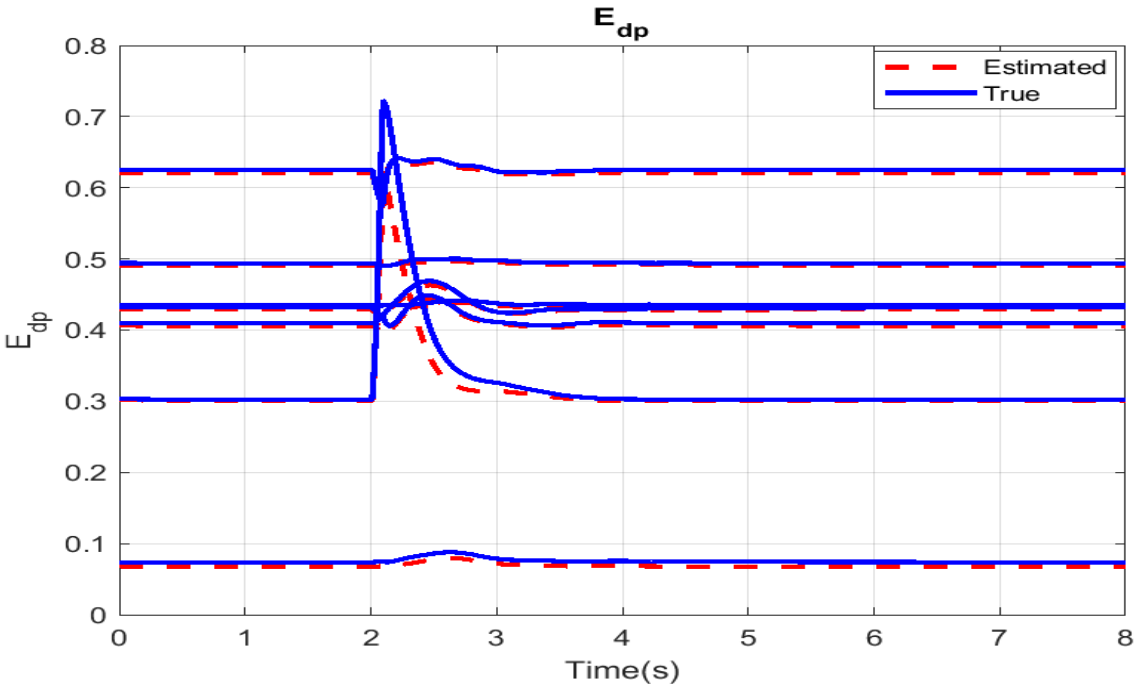

Figure 5.17: True vs. Estimated E_{dp}

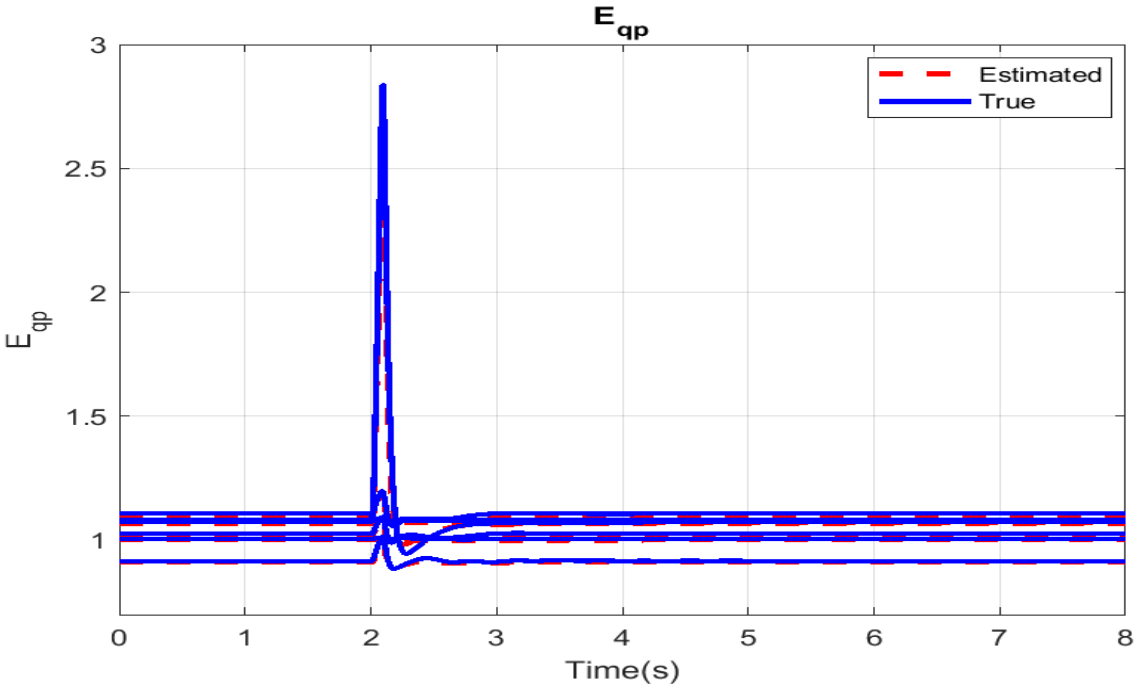

Figure 5.18: True vs. Estimated E_{qp}

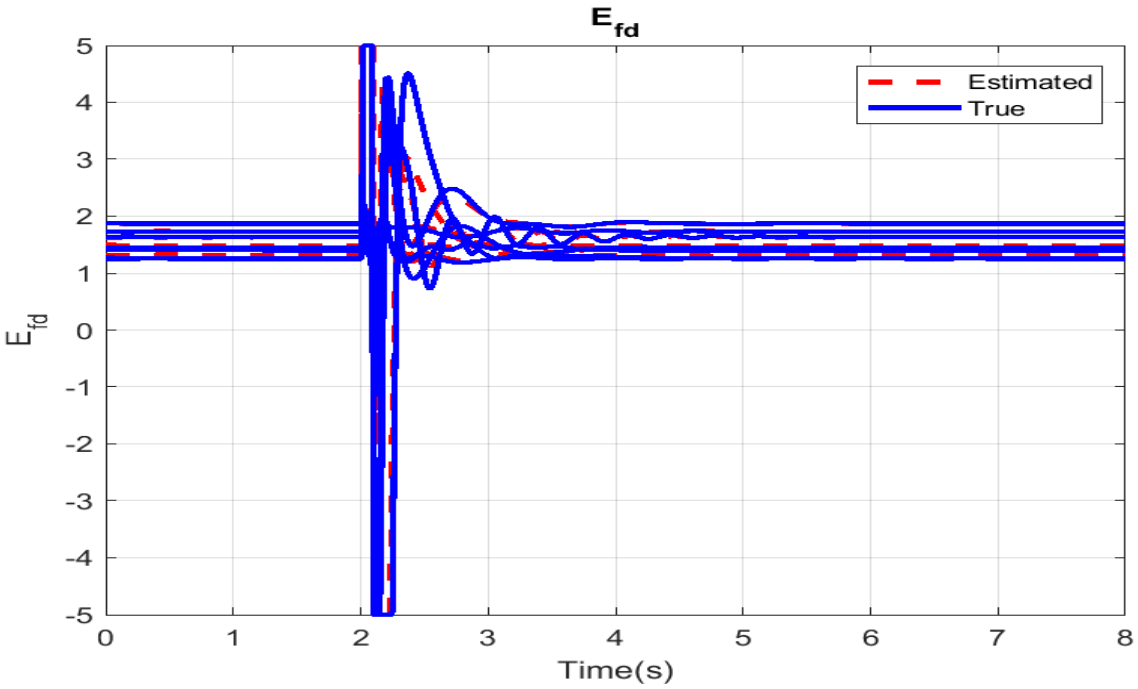

Figure 5.19: True vs. Estimated E_{fd}

Table 5.2: Mean Squared Error: WECC System with Reclosing

States	MSE
δ	0.000377
ω	$1.542e^{-06}$
E_{qp}	$6.001e^{-5}$
E_{dp}	$1.743e^{-4}$
E_{fd}	0.00672

5.2 Kundur's Two-Area System

5.2.1 Case I: Single-shot Reclosing Event

Kundur's two-area oneline parameters and measurements are used to test the UKF dynamic state estimator, as shown in Figure 5.20. The generator's active power (P_e), reactive power (Q_e), and terminal voltage (V_T) are utilized as measurements and input measurements respectively within the estimator. During the simulation of a temporary fault on a transmission line, the reclosing of the transmission line is tested. The aim is to observe how the dynamic states of the generators react to the fault. The estimated states obtained from the dynamic estimator are compared with the true states of the generators. After the fault is cleared, the transmission line between the generators trips and then recloses, which allows the system to return to a steady state. To estimate the states of the generators, measurements from the generators are collected and processed. The generator's active and reactive power, denoted by P_e and Q_e respectively, are used as measurements. Additionally, the generator terminal voltage V_T is used.

At 1 second of the simulation, a three-phase-ground fault is applied to the transmission line L_{8-9}. This fault causes a current to flow from each phase to the ground. As a result, the line is tripped for a few cycles and reclosed to go back to a steady state for the remaining time of the simulation. This fault is considered to be temporary, which means that it only occurred for a few cycles and does not require a manual reset to restore the line to normal operation. This type of reclose is a single-shot reclose. When a transmission line fails to reclose after the second attempt, it may experience a two-shot reclose or lockout. This means that the reclose scheme will attempt to reclose the line twice before it locks out to prevent further damage or danger.

Again to replicate real-world conditions, noise is introduced into the system to evaluate the performance of the dynamic simulator in estimating the dynamic rotor

angle. The MSE provides a quantitative measure of the accuracy of the estimator's performance (see 5.14). This assessment is crucial for ensuring the reliability and effectiveness of the simulator in practical applications. The MSE error of the dynamic states is summarized in Table 5.3, comparing the true and estimated values. The different generator-estimated dynamic states are shown in Figures 5.21 - 5.28. The red dashed line indicates the estimated dynamic states, while the blue solid line indicates the true dynamic states of the system. Figures 5.22 - 5.24 show the rotors' relative angles δ. The rotor angle of generator one is used as the reference angle. The plot illustrates a visual representation of the relative angles between the generators. The MSE for all the generators' rotor angles is calculated and shown in Table 5.3.

The graph in Figure 5.25 displays the rotor speeds (ω) of the generators. The plot clearly illustrates that when the fault occurred, the rotor speed deviation diverged from the steady state for a few cycles when the transmission line tripped. The rotor speed returned to steady after the transmission line reclosed. The MSE of the rotor speeds (ω) was also calculated as shown in the Table 5.3. Figure 5.28 displays the field voltage E_{fd}. The d-axis transient voltage $E_d^{'}$ of the generator can be seen in Figure 5.26, while the q-axis transient voltage $E_q^{'}$ is illustrated in Figure 5.27 as the final estimated state. The MSE for E_{fd}, $E_d^{'}$, and $E_q^{'}$ were also calculated and shown in the Table 5.3.

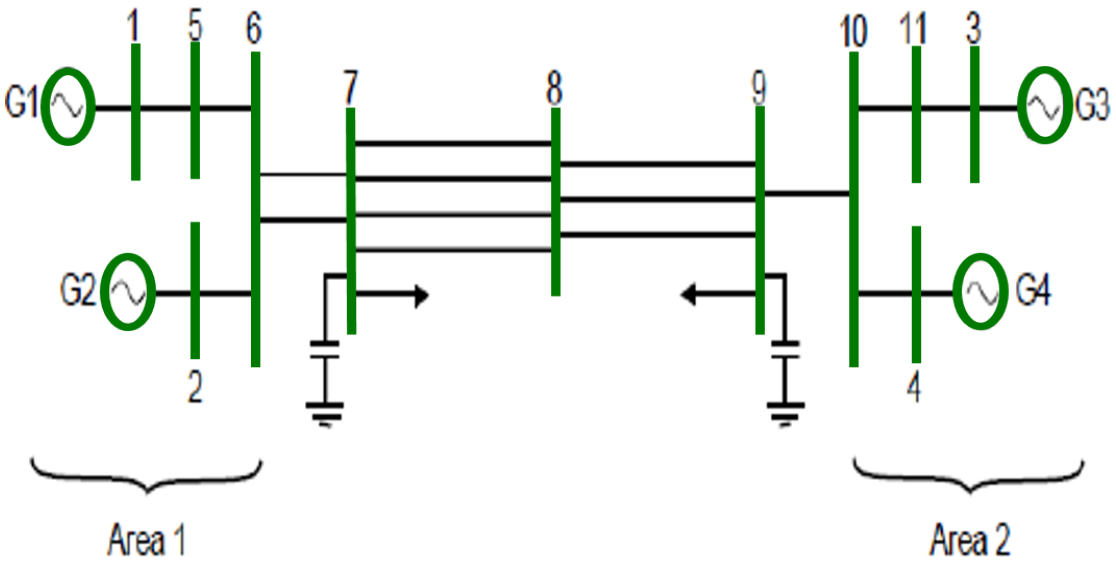

Figure 5.20: Kudur Two-Area Oneline

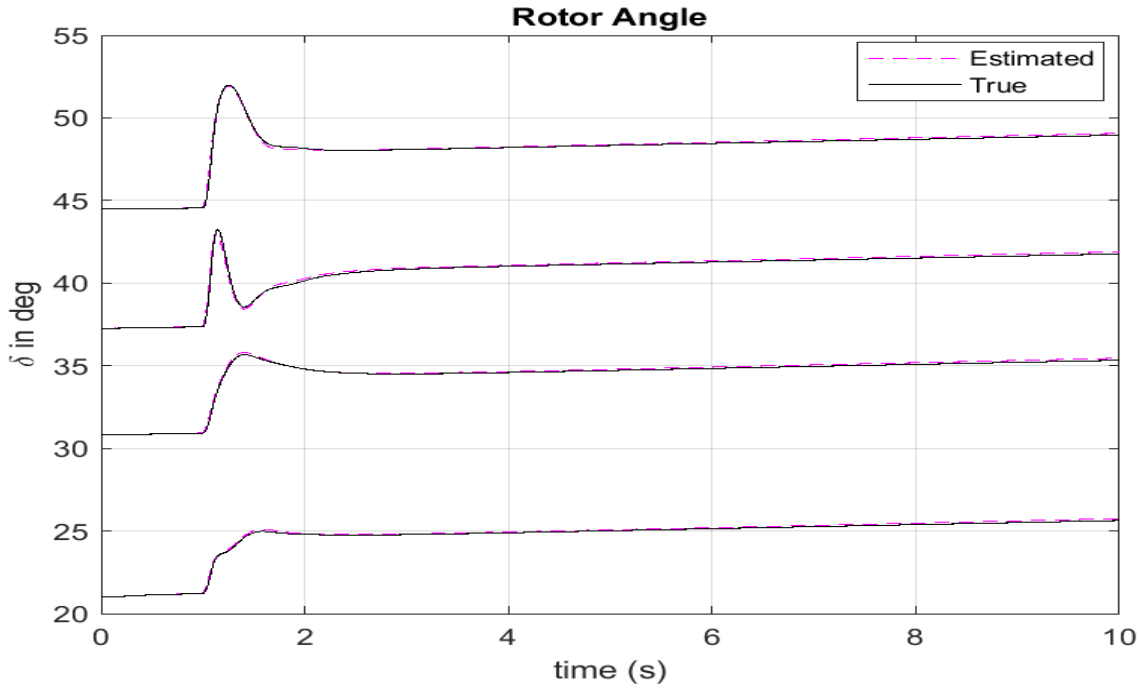

Figure 5.21: True vs. Estimated Rotor Angles

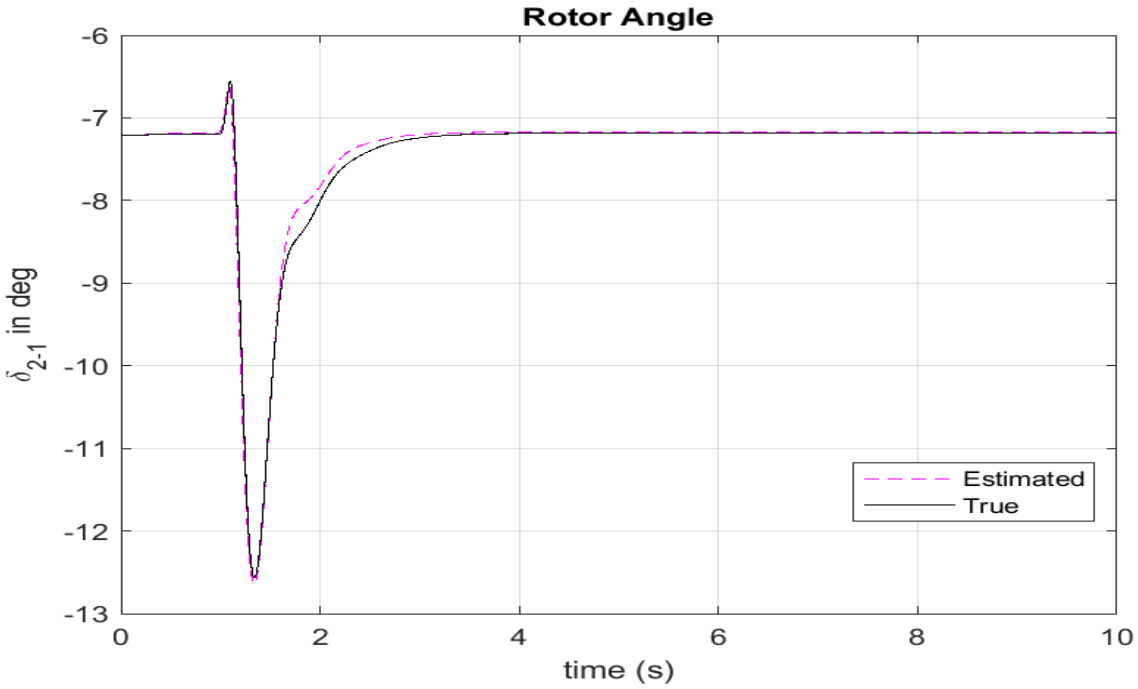

Figure 5.22: True vs. Estimated δ_{2-1}

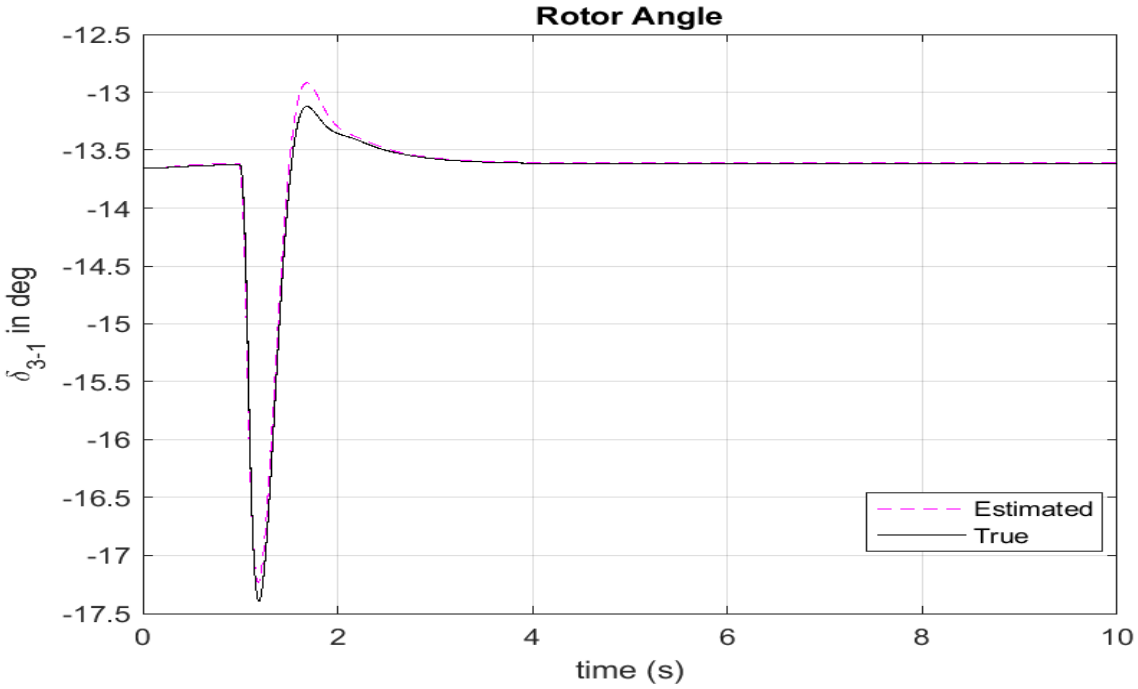

Figure 5.23: True vs. Estimated δ_{3-1}

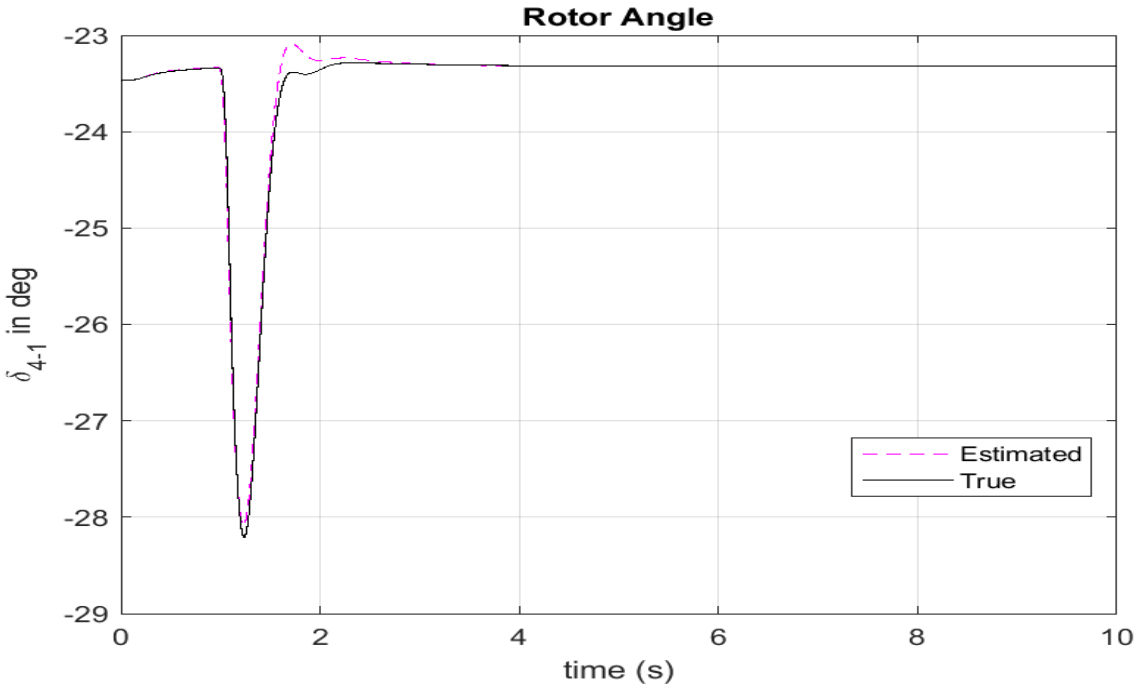

Figure 5.24: True vs. Estimated δ_{4-1}

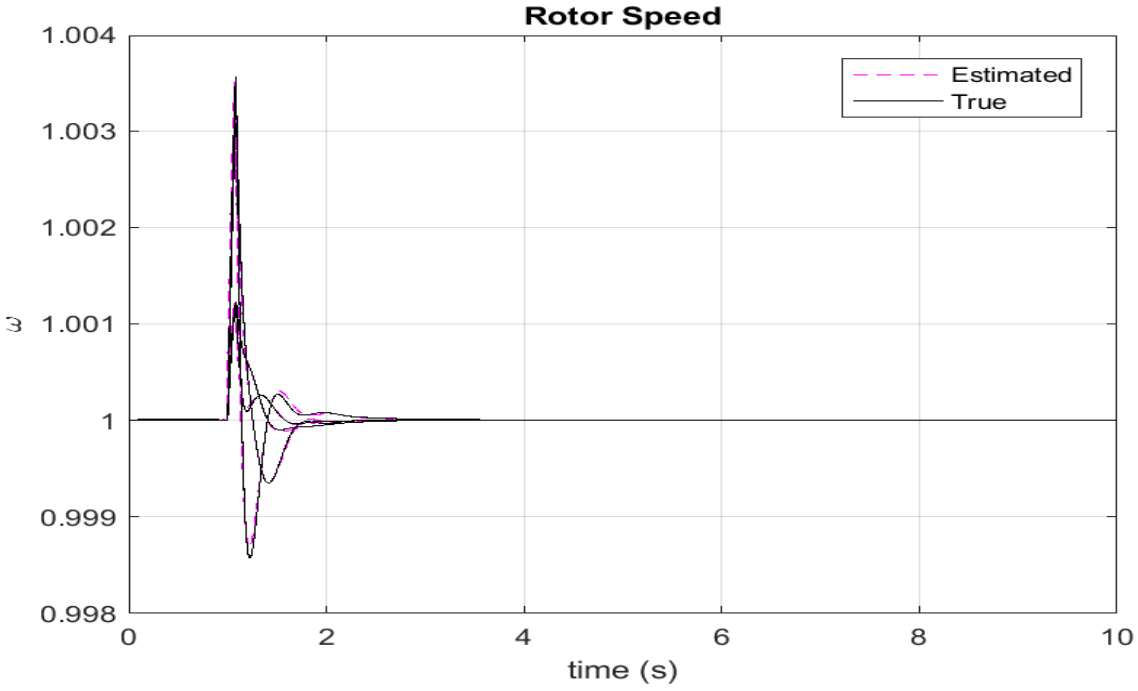

Figure 5.25: True vs. Estimated Rotor Speed

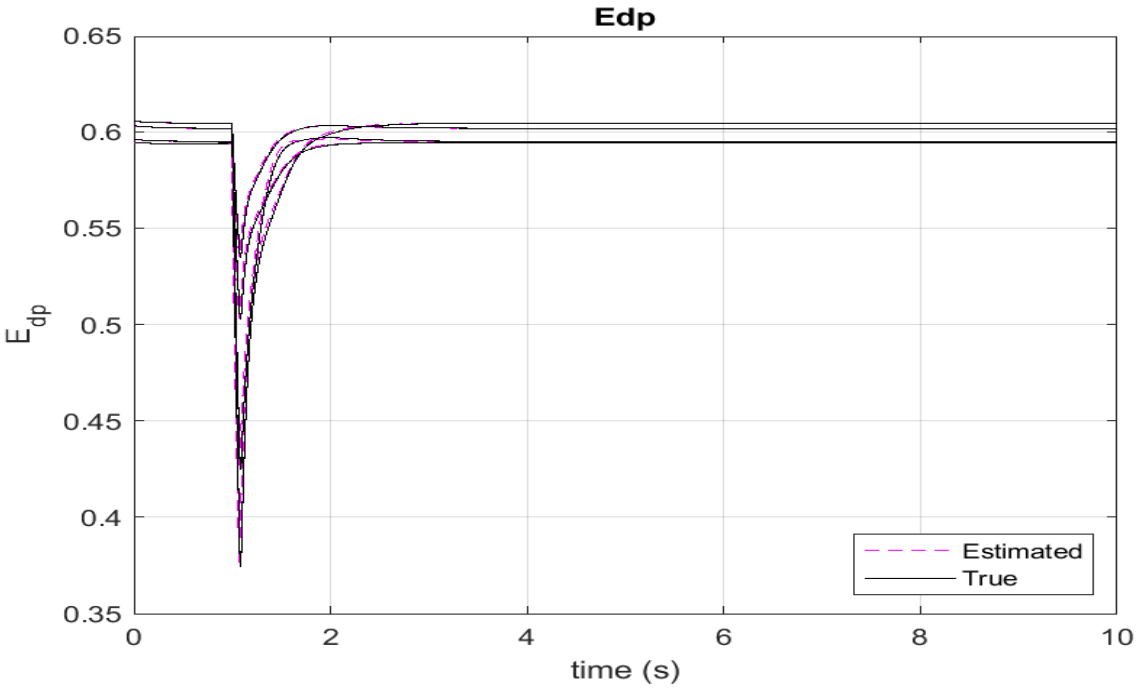

Figure 5.26: True vs. Estimated E_{dp}

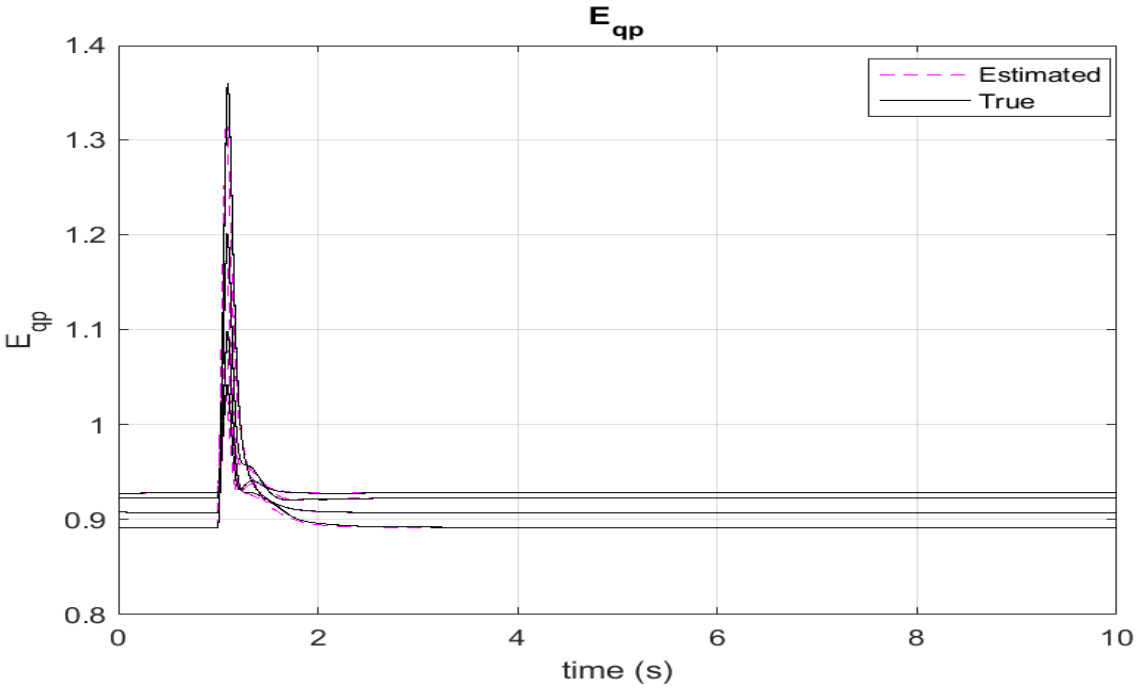

Figure 5.27: True vs. Estimated E_{qp}

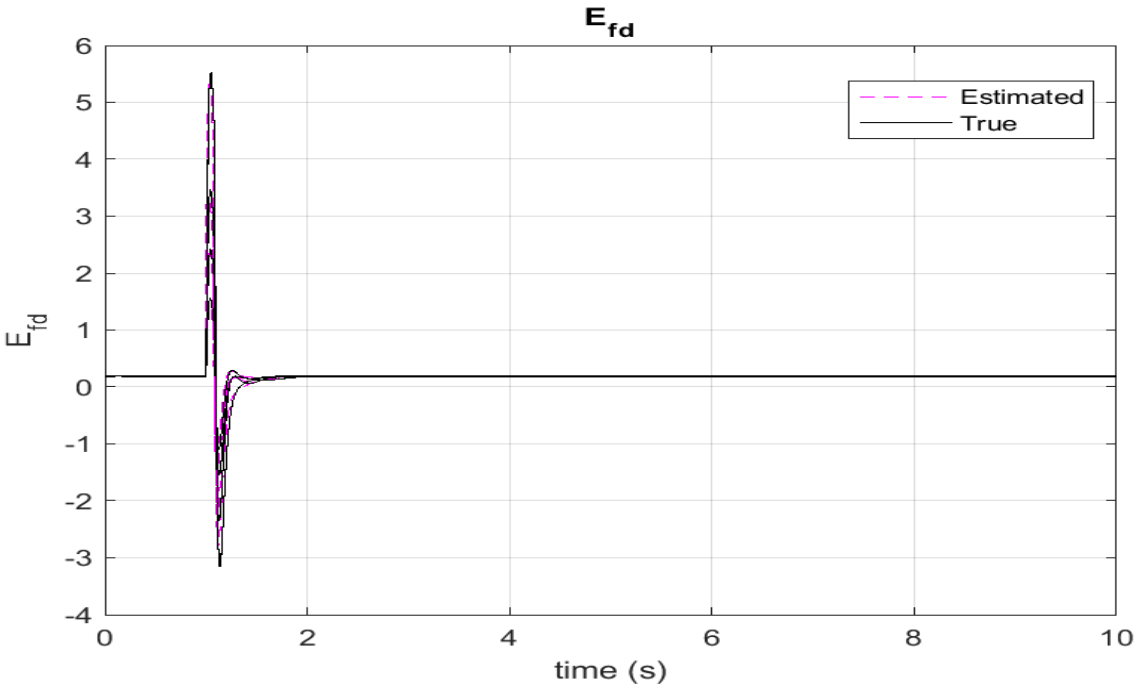

Figure 5.28: True vs. Estimated E_{fd}

Table 5.3: Case I Mean Squared Error

States	MSE
δ	$2.431e^{-06}$
ω	$1.989e^{-09}$
E_{qp}	$5.489e^{-6}$
E_{dp}	$2.732e^{-5}$
E_{fd}	0.00348

5.2.2 Case II: Two-shot Reclosing

Sometimes, a transmission line may encounter temporary faults consecutively within a few cycles. In such a case, the transmission line will initially open upon detecting a fault and then close again. However, if the fault has not cleared or another fault occurs within a short time frame, the line will open again and only close if it is a temporary fault. There will be a fault between two temporary $3-\phi-G$ connections that will last for two (2) cycles per fault before reclosing. This will happen two times and each time the fault will be cleared and the system will return to normal. As this happens, the generator dynamic states will react to the reclosing of the line and show how the machines in different areas of the interconnection are affected by the transmission line trip and reclose. The estimated states of the generators are compared with their actual states using a dynamic estimator. The details of the simulation are shown below:

At the 0.5 second of the simulation, a three-phase-ground fault is applied to the transmission lines L_{8-9}.As a result, the line is tripped for a few cycles and recloses to go back to a steady state. Another three-phase-ground fault is applied at 1.5 seconds, the transmission line L_{8-9} trips and recloses after the second fault to go back to a steady or normal state. These faults are considered to be temporary, which means that they only occur for a few cycles and do not require a manual reset to restore the line to normal operation.

Table 5.4 summarizes the MSE error of the dynamic states, comparing the estimated and true values. The different generator-estimated dynamic states are shown in Figures 5.29 - 5.33. The red dashed line indicates the estimated dynamic states, while the blue solid line indicates the true dynamic states of the system. Figure 5.29 shows the rotor angles δ of the generators. The plot illustrates that the rotor angles diverged from the steady state when the transmission line tripped and returned to the steady state when the fault cleared.

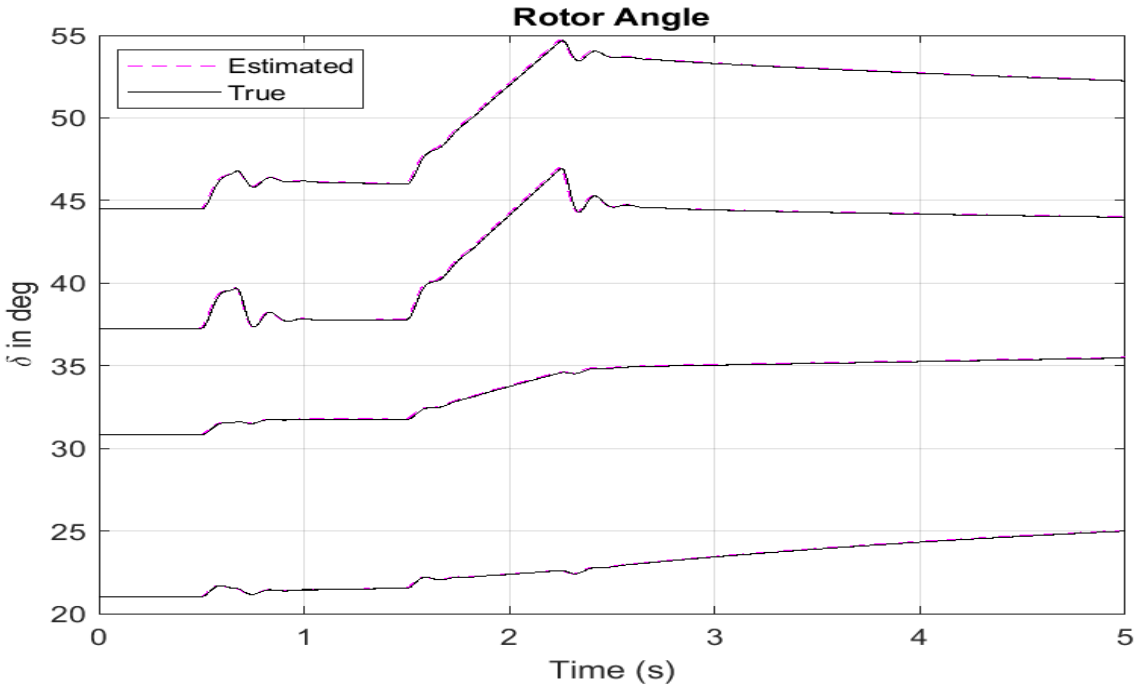

Figure 5.29: True vs. Estimated Rotor Angle

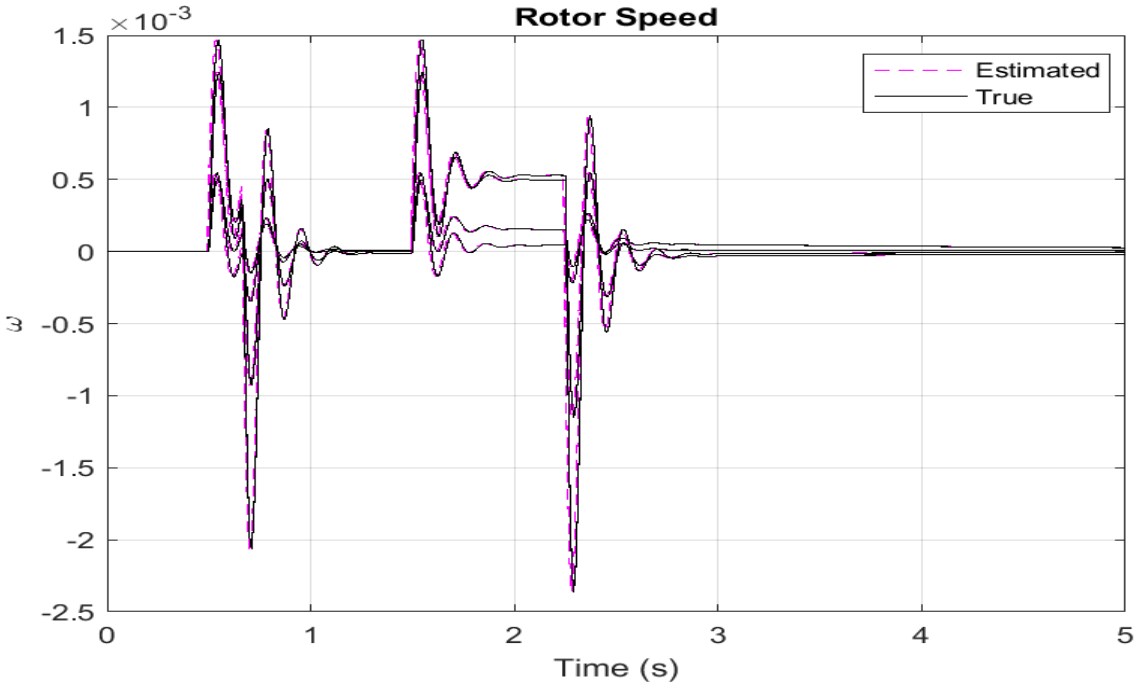

Figure 5.30: True vs. Estimated Rotor Speed

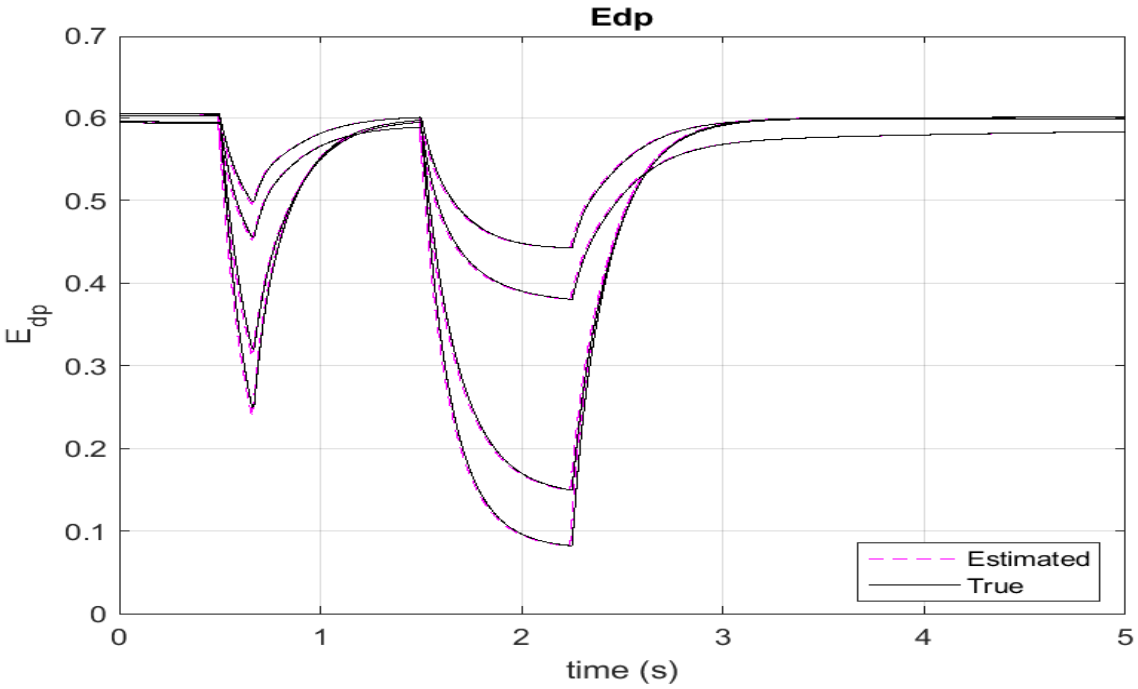

Figure 5.31: True vs. Estimated E_{dp}

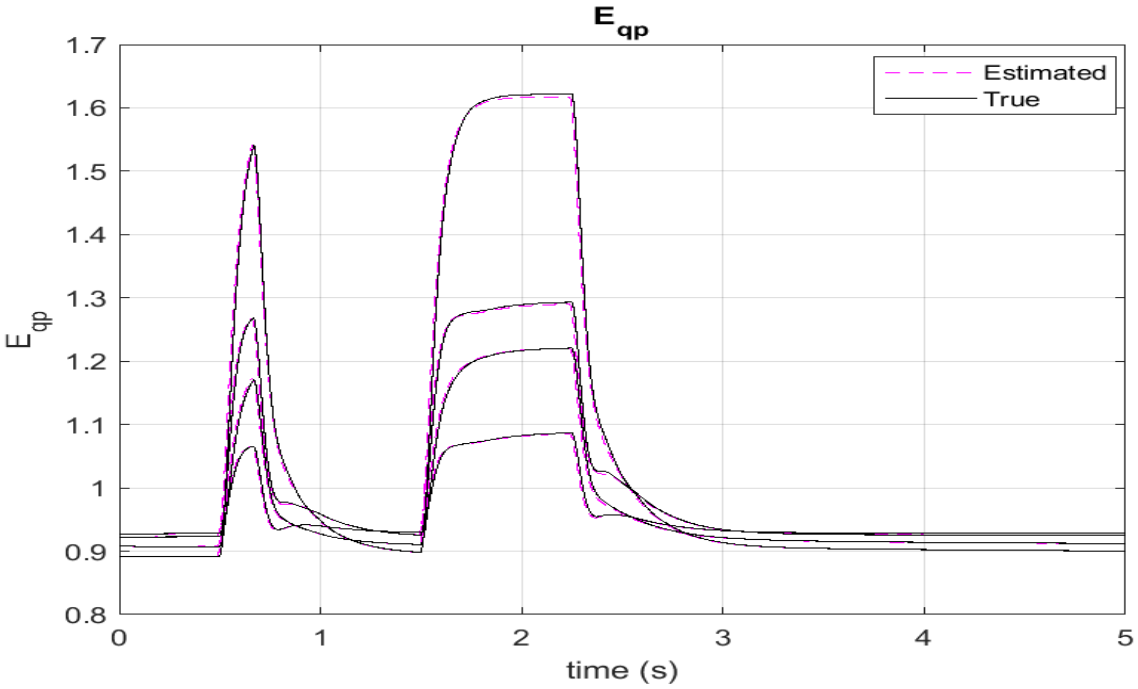

Figure 5.32: True vs. Estimated E_{qp}

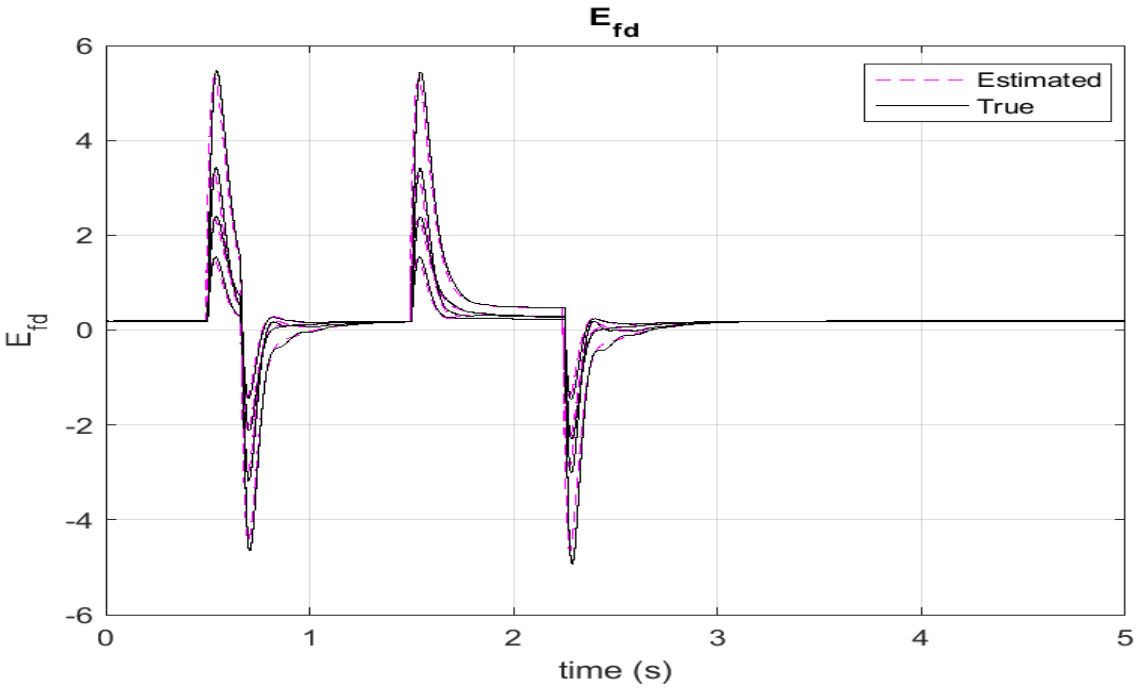

Figure 5.33: True vs. Estimated E_{fd}

Table 5.4: Case II Mean Squared Error

States	MSE
δ	$1.358e^{-06}$
ω	$5.5062e^{-09}$
E_{qp}	$2.572e^{-6}$
E_{dp}	$6.011e^{-5}$
E_{fd}	0.00739

The same process was repeated for the second fault event, the fault cleared and returned to a normal state as indicated in the plot. The MSE for all the generators' rotor angles were calculated and shown in Table 5.4.

The graph in Figure 5.30 displays the rotor speeds (ω) of the generators. The plot clearly illustrates that when the fault occurred, the rotor speed deviation diverged from the steady state for a few cycles when the transmission line trips. The rotor speed returned to steady after the transmission line recloses. The MSE of the rotor speeds (ω) was also calculated as shown in the Table 5.4. Figure 5.33 displays the field voltage E_{fd} of the generator. The d-axis transient voltage $E_d^{'}$ of the generator can be seen in Figure 5.31, while the q-axis transient voltage $E_q^{'}$ is illustrated in Figure 5.32. The MSE for E_{fd}, $E_d^{'}$, and $E_q^{'}$ are also calculated and shown in the Table 5.4.

5.2.3 Case III: Permanent Fault

Performance of the estimator for a permanent fault is studied. If the relay still detects a fault at the second attempted reclose, it will trip and lock out the line. During the simulation, a three-phase-ground fault occurs at 0.5 seconds on transmission lines L_{8-9}. As a result, the line trips for a few cycles and then recloses to return to a steady state. Another three-phase-ground fault occurs at 1.5 seconds, causing the transmission line L_{8-9} to trip and attempt to reclose after the second fault to go back to a normal state. A third fault occurs at 3.2 seconds, but the transmission line fails to reclose due to detecting a permanent fault. The system will not attempt to reclose the line for the third time. At this point, the line will trip and lock out to prevent further damage or danger to the equipment.

Table 5.5 summarizes the MSE error of the dynamic states by comparing the estimated values with the true values. The different generator-estimated dynamic states are shown in Figures 5.34 - 5.37. Figure 5.34 shows the rotor angles δ of the generators.tripped and locked out.

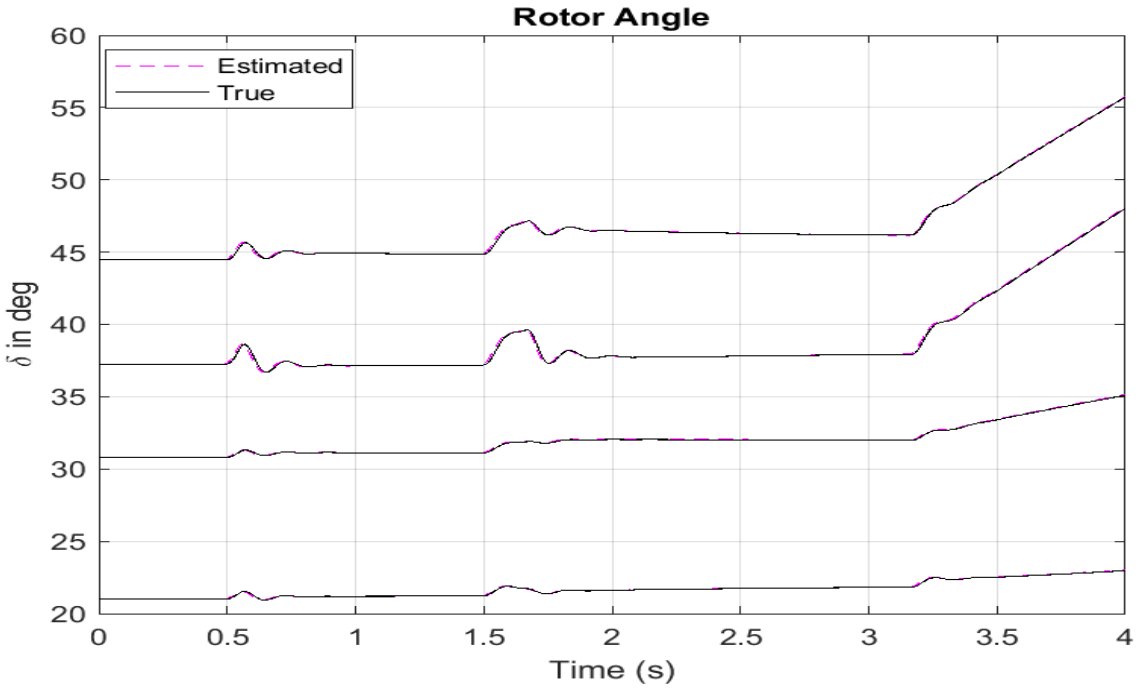

Figure 5.34: True vs. Estimated δ

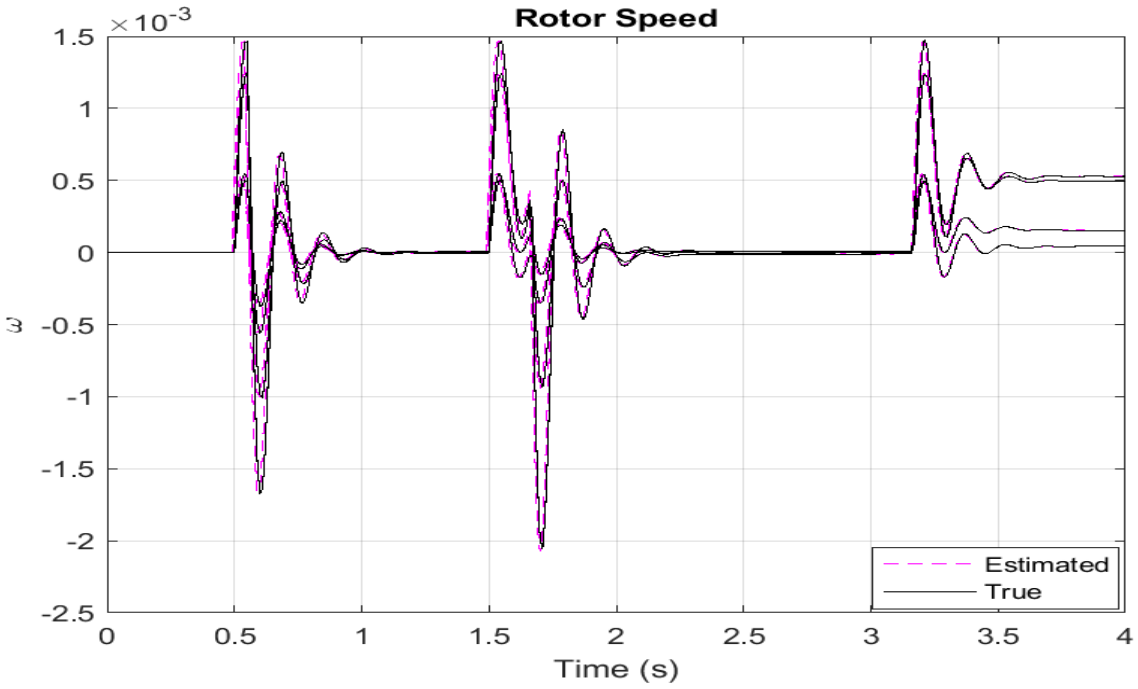

Figure 5.35: True vs. Estimated ω

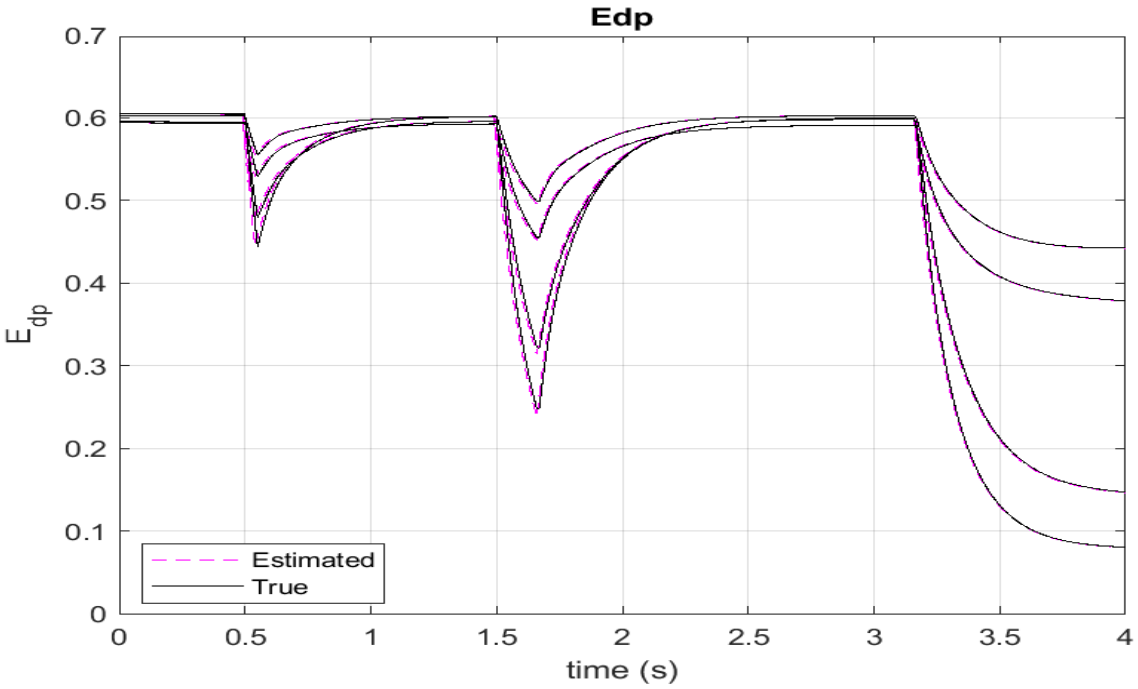

Figure 5.36: True vs. Estimated E_{dp}

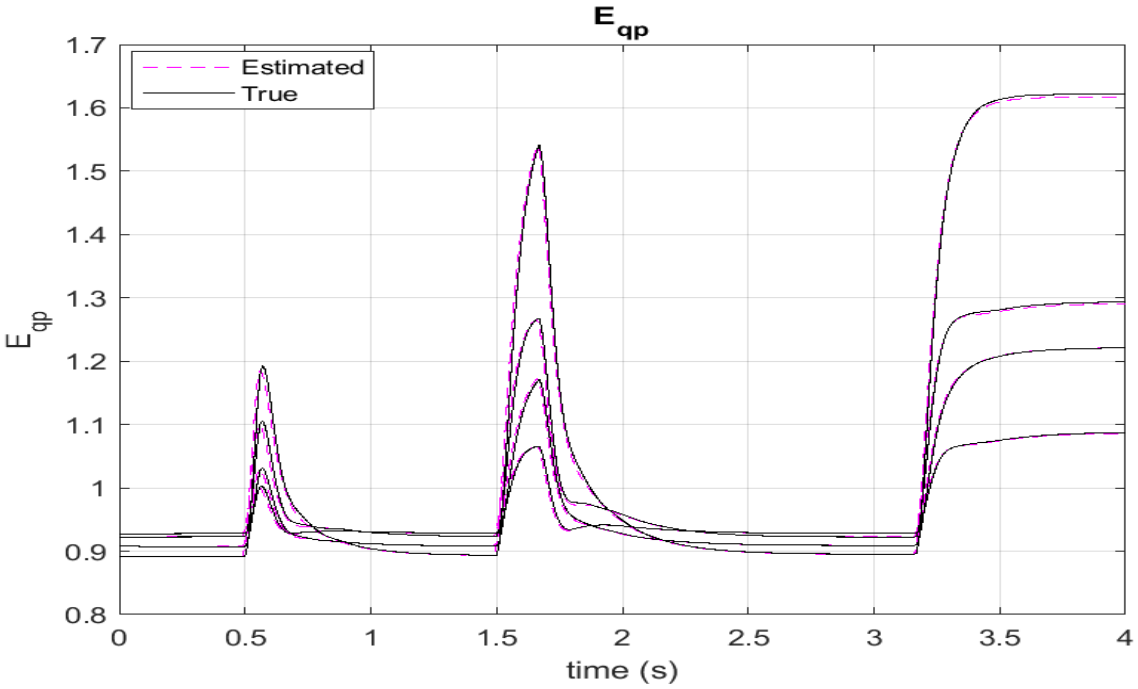

Figure 5.37: True vs. Estimated E_{qp}

Table 5.5: Case III Mean Squared Error

States	MSE
δ	$8.981e^{-06}$
ω	$6.739e^{-09}$
E_{qp}	$2.254e^{-5}$
E_{dp}	$5.858e^{-5}$

The plot illustrates that the rotor angles diverged from the steady state when the transmission line tripped and returned to the steady state when the fault cleared. The same process was repeated for the second fault event, the fault clears and returned to a normal state as indicated in the plot. At 3.2 seconds the rotor angles of the generators diverged without returning to a steady state because the line tripped and locked out. The MSE for all the generators' rotor angles were calculated and shown in Table 5.5.

The graph in Figure 5.35 displays the rotor speeds (ω) of the generators. The plot clearly illustrates that when the fault occurred at 0.5 and 1.5 seconds, the rotor speed deviation diverged from the steady state for a few cycles when the transmission line trips. The rotor speed returns to steady-state after the transmission line recloses. At 3.2 seconds the rotor speeds and other dynamic states of the generators diverged without returning to a steady state because the line

The MSE of the rotor speeds (ω) was also calculated as shown in Table 5.5. The d-axis transient voltage $E_d^{'}$ of the generator can be seen in Figure 5.31, while the q-axis transient voltage $E_q^{'}$ is illustrated in Figure 5.32. The MSE for E_{fd}, $E_d^{'}$, and $E_q^{'}$ were also calculated and shown in the table 5.5.

Chapter 6

Dynamic State Estimation: Unbalanced Faults

Similar to balanced faults, unbalanced fault simulation and analysis are very important to system protection engineering (SPE). SPE utilizes short-circuit software like ASPEN or CAPE to develop settings for generation, transmission, and distribution. Transmission lines trip or reclose due to balanced or unbalanced faults, hence, the need to study the effect of line reclosing on the generator states for unbalanced faults. Unbalanced faults may lead to critical heating of the machine due to negative sequence currents induced during these faults. The induced negative sequence current makes the machine field rotate at twice the rated frequency and could damage the rotor of the machine [52]. Hence, it is very important for SPE to develop settings that can protect the system from an unbalanced fault when it occurs in the system. Another effect of unbalanced fault is the saturation of the magnetic components of the machines [68]. With saturation, the elements or parameters of the machines vary and are not as expected and thus, affect the estimated states of the machines.

In this chapter, the dynamic state estimation simulation is developed for unbalanced faults, including: phase-to-ground (LG), phase-to-phase (LL), and double phase-to-ground (LLG) using the reduced UTK HTB WECC model to simulate

various fault events. The WECC model simulation was carried out using the electromagnetic transient (EMT) PSCAD model of the reduced WECC model from the UTK HTB. This chapter focuses on studying the effect of unbalanced faults and saturation of the machines on the rotor speed and the rotor angle of the synchronous generator. The estimated dynamic states are then compared with the true states with Gaussian noise added to the measurements as input noise.

6.1 UTK HTB Reduced WECC System

The UTK HTB Reduced WECC model is a transmission network that represents or emulates the large-scale WECC model with the help of converters that emulate generators and loads. Figure 6.1 shows the interconnections modeled on the HTB to simulate the large-scale models with integrated real-time protection, control, and communication. The HTB has the advantage of broad time scales from milliseconds to seconds. Figures 6.2 and 6.3 show the power flow of the reduced HTB WECC model in MW.

The summer model is selected and used for the dynamic state estimation. The parameter data for the HTB was used to develop a PSCAD model. An unbalanced fault applied to one of the transmission lines for a few cycles to trip the transmission line and then is reclosed after the fault was cleared. The true states from the HTB PSCAD model were exported and compared with the estimated states from the state estimator. Different cases were used to test the HTB model from using the HTB measurements to estimate the dynamic states to compare the states of the HTB with the dynamic state estimator using the robust unscented Kalman filter.

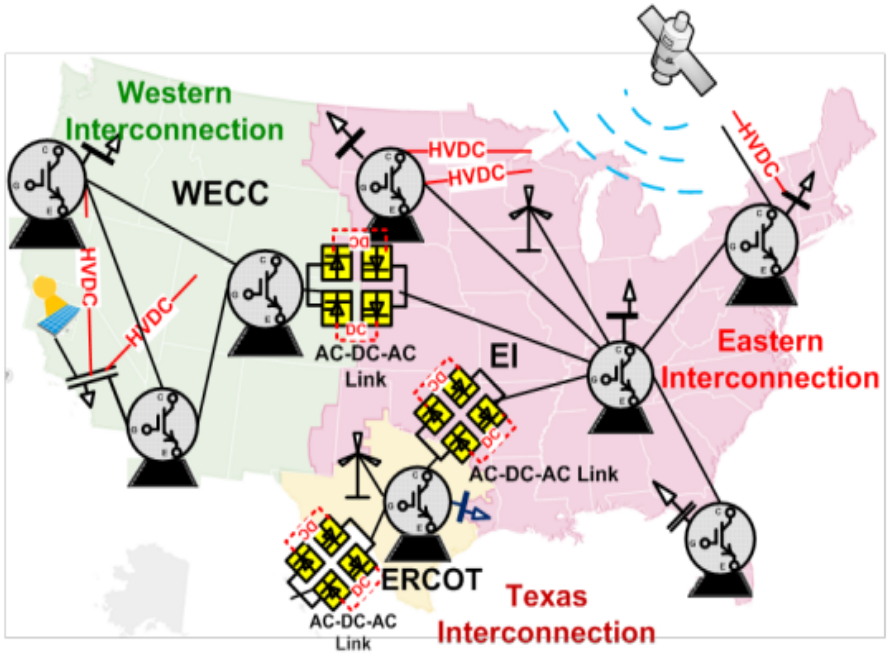

Figure 6.1: UTK HTB WECC Model

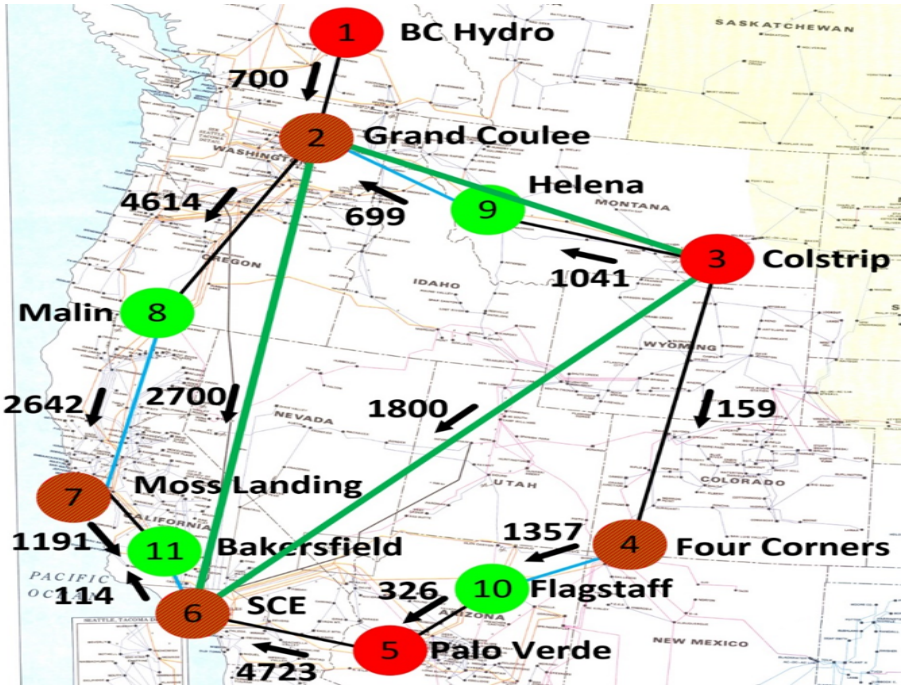

Figure 6.2: UTK HTB WECC Summer Model

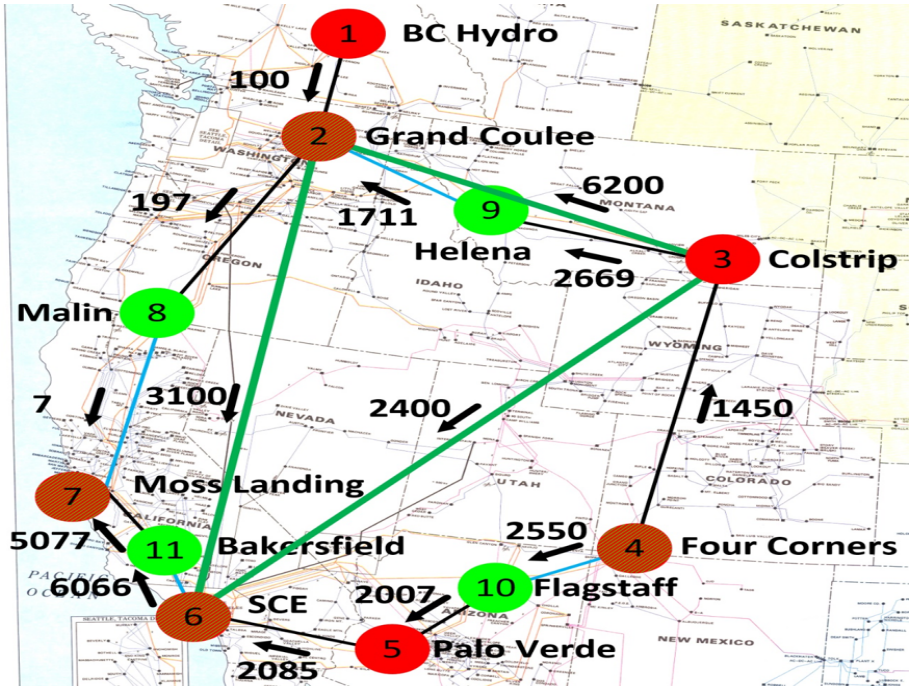

Figure 6.3: UTK HTB WECC Winter Model

6.1.1 PSCAD Model

The WECC EMT PSCAD model of the interconnection was developed to investigate the impact of line reclosing on the synchronous states. The PSCAD model of the WECC interconnection is shown in Figure 6.4. The reduced model includes seven generators and four areas, similar to the WECC model depicted in Figure 6.2. All model parameters are the same as those used in the HTB lab. Prior to applying an unbalanced phase-to-ground fault on transmission line L_{2-8}, the simulation was run for a few minutes in a steady state. The objective of developing the WECC EMT PSCAD model of the interconnection was to analyze and understand the effect of line reclosing on the states. The PSCAD model of the WECC interconnection is illustrated in Figure 6.4 similar to the WECC model displayed in Figure 6.2. The model parameters used in the simulation are identical to those utilized in the HTB lab, ensuring accuracy and reliability. Before simulating an unbalanced phase-to-ground fault on transmission line L_{2-8}, the simulation was run for a few minutes in a steady state. This approach allows for a comprehensive analysis of the effects of the fault on the system, providing insights into the behavior of the synchronous states under different scenarios. The generator's measurements, such as its active power (P_e), reactive power (Q_e), and terminal voltage (V_T), were exported from the simulation. These measurements were processed and used as inputs in the dynamic state estimator to effectively analyze the generator's behavior. is applied after running the simulation in a steady state for some seconds. The applied unbalanced fault cleared after a few cycles. As a result of the fault, the transmission line trips when the fault is applied and then recloses upon the fault being cleared.

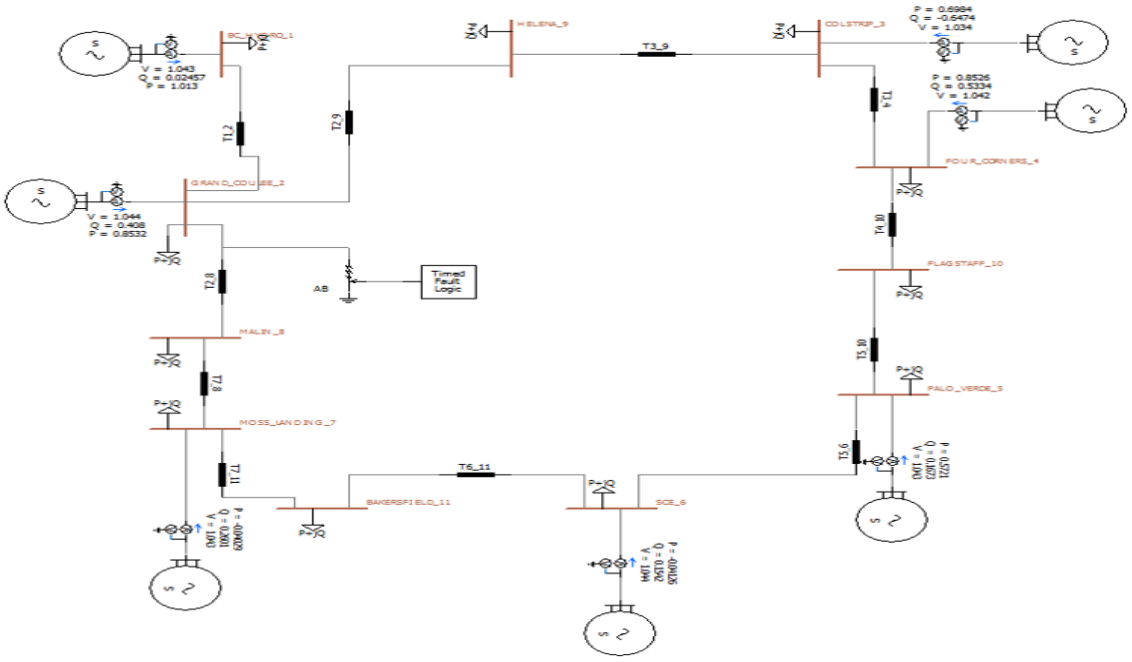

Figure 6.4: WECC PSCAD Model

6.1.2 Effect of Saturation on Synchronous Machine States

In the event of an unbalanced fault, such as a phase-to-ground fault, it may lead to a condition known as saturation in synchronous generators. Saturation can cause non-uniformity in the salient pole air gap of the machine, which can adversely affect the machine's dynamic states [68]. To mitigate this problem, an improved saturation modeling method was implemented in the synchronous machine using the GENTPF/GENTPJ model with multiplicative saturation [1]. The efficacy of this method is tested during simulation and found to improve the model's accuracy by better tracking between the true state and the estimated state [1]. The dynamic states of the machine were estimated using a robust iterated unscented Kalman filter that was specifically developed for this purpose [69]. The saturation was added to the q and d axes of the machine, this alters the differential equations with details shown in appendix A.

GENTPF/GENTPJ

This model is designed using the block diagram, as shown in Figure 6.5 from [1], and can be applied to both salient pole and round rotor machines. The model has a dynamic algorithm specifically modified for synchronous machines, which incorporates the GENTPF/GENTPJ model. Additionally, the model includes scaling between the d-axis and q-axis inputs of the saturation function, which allows for better tracking of dynamic states. Saturation is applied to all reactance terms in the dynamic two-axis model of synchronous machines, making use of multiplicative saturation.

As a result, the GENTPF/GENTPJ model provides a more accurate estimation of dynamic states, which closely tracks the true states of the WECC model. The model considers input parameters to be unsaturated, applying saturation to all equations. By using multiplicative saturation, the GENTPF/GENTPJ model provides a better match to the true machine states.

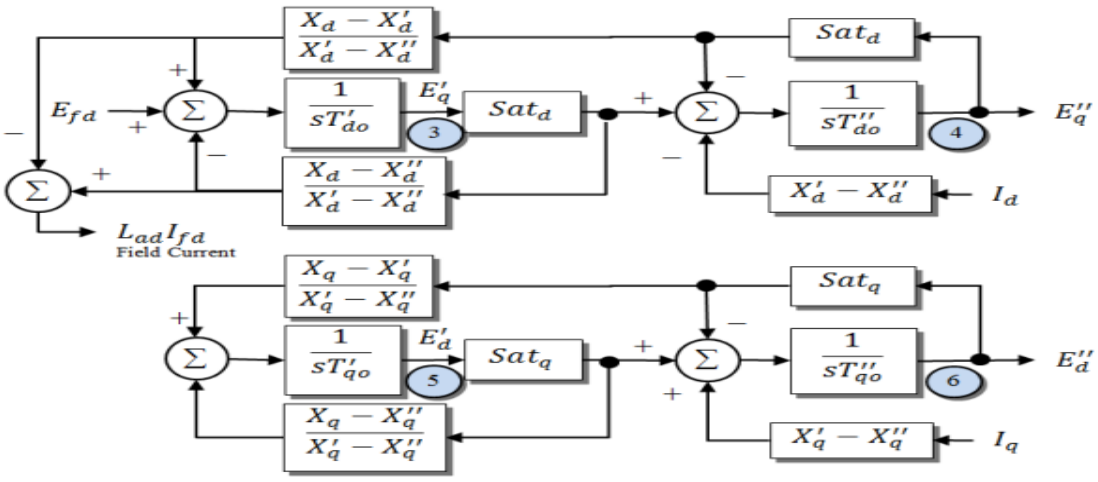

Figure 6.5: GENTPF/GENTPJ Block Diagram Excerpt from [1]

For this study, the rotor angle and the rotor speed of the machines are estimated. The remaining states (3-6) are pushed to future study with the saturation of the machines, as shown in Figure 6.5.

6.1.3 The Algorithm: Iterated Unscented Kalman Filter (IUKF)

In order to improve the performance of the dynamic state estimator, a more advanced estimator called the iterated unscented Kalman filter is developed. This estimator is better suited for tracking or estimating dynamic states when unbalanced faults occur in the system. The iterated UKF algorithm includes additional steps based on the UKF algorithm that was used in Chapter 5. Namely:

- Initialize the iteration to count the number of IUKF iteration For example if j=2, then $\hat{x}_{k,0} = \hat{x}_k^-$, $P_{k,0}^- = P_k^-$, $\hat{x}_{k,1} = \hat{x}_k^+$, $P_{k,1}^- = P_k^+$
- Compute new sigma point for IUKF

$$\begin{aligned} \hat{x}_{k,j}^i &= \hat{x}_{k,j-1}^+ + x_*^i \quad i = 1, ..., 2L \\ x_*^i &= (\sqrt{(LP_{k,j-1}^-)})_i^T \quad i = 1, ..., L \\ x_*^{n+i} &= -(\sqrt{(LP_{k,j-1}^-)})_i^T \quad i = 1, ..., L \end{aligned} \tag{6.1}$$

- Perform state correction for IUKF

$$\begin{aligned} \hat{x}_{k,j}^- &= \frac{1}{2L}\sum_{i=1}^{2L} \hat{x}_{k,j}^i \\ \hat{z}_{k,j} &= h(\hat{x}_{k,j}^i, k) \\ \hat{z}_{k,j} &= \frac{1}{2L}\sum_{i=1}^{2L} \hat{z}_{k,j}^i \\ P_{z,j} &= \frac{1}{2L}\sum_{i=1}^{2L} (\hat{z}_{k,j}^i - \hat{z}_{k,j})(\hat{z}_{k,j}^i - \hat{z}_{k,j})^T + R_k \end{aligned} \tag{6.2}$$

$$
\begin{aligned}
P_{xz,j} &= \frac{1}{2L}\sum_{i=1}^{2L}(\hat{x}^{i}_{k,j} - \hat{x}_{k,j})(\hat{z}^{i}_{k,j} - \hat{z}_{k,j})^{T} \\
K_{k,j} &= P_{xz,j}P^{-1}_{z,j} \\
\hat{x}^{+}_{k,j} &= \hat{x}^{-}_{k,j} + K_{k,j}(z_{k,j} - \hat{z}_{k,j}) \\
P_{k,j} &= P_{k,j-1} - K_{k,j}P_{z,j}K^{T}_{k,j}
\end{aligned}
\tag{6.3}
$$

6.1.4 Rotor Angle Results

A collection of measurements taken from the EMT simulation were processed. These measurements, which included the active power (P_e), reactive power (Q_e), and terminal voltage (V_T), were fed as input into the robust dynamic state estimator to estimate the dynamic states of the synchronous machines when an unbalanced fault was applied to a transmission line. A simulation time of 20 s and fault application time 6 s and a fault duration of 3 cycles was used. The fault is a single phase-to-ground the protection is a single short reclosing.

Gaussian noise using 10% of the standard deviation were used as added noise into the system. The MSE of the estimated states and true states is calculated using (6.4). The Table 6.1 shows the results of calculated MSE between the true and the estimated states. Figures 6.6 to 6.9 as shown above are the true and estimated states using the measurements from the generators as input into the estimator. The black solid line represents the true state, while the magenta broken line represents the estimated state.

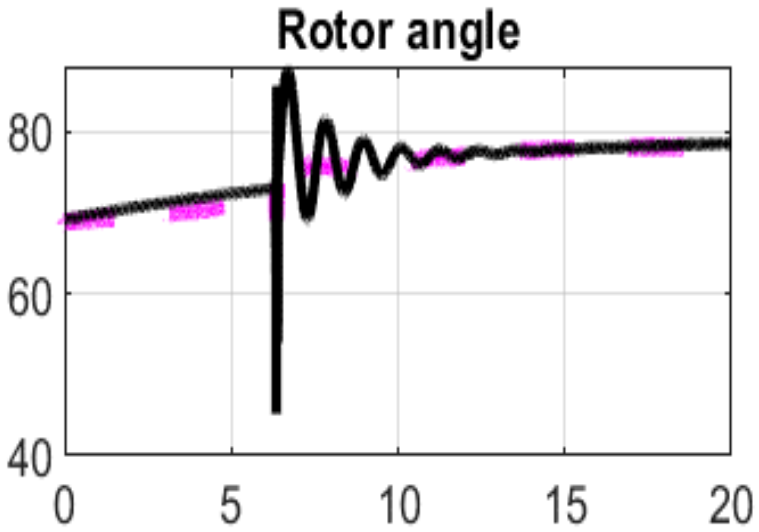

Figure 6.6: Relative Rotor Angle δ_{2-1}

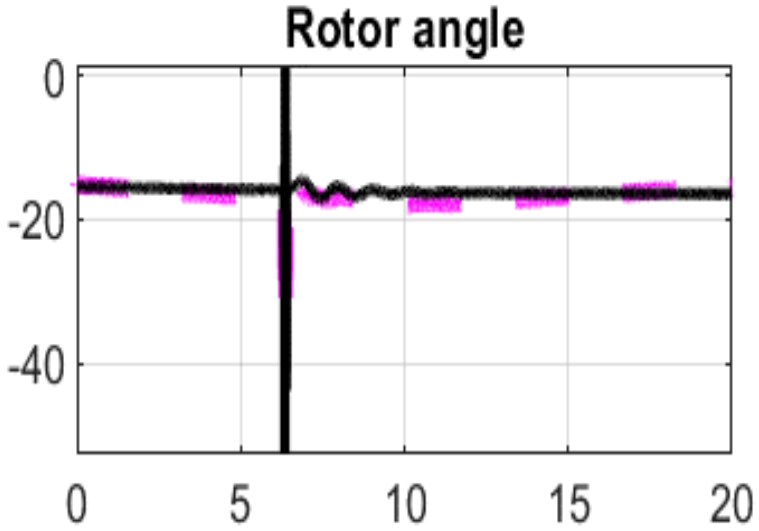

Figure 6.7: Relative Rotor Angle δ_{3-1}

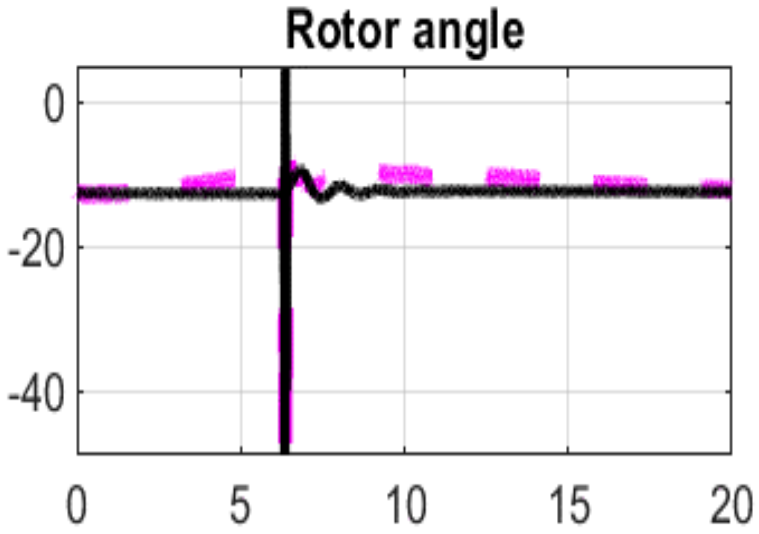

Figure 6.8: Relative Rotor Angle δ_{4-1}

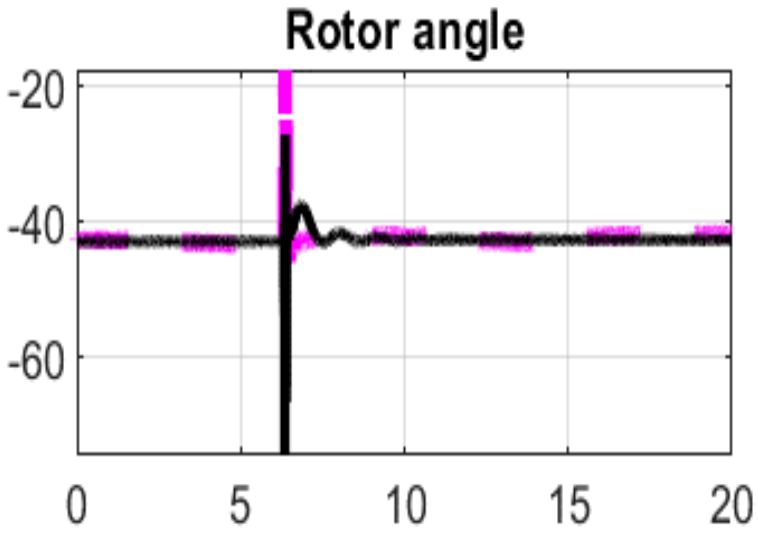

Figure 6.9: Relative Rotor Angle δ_{5-1}

6.1.5 Rotor Speed Results

The Table 6.1 shows the results of calculated MSE between the true and the estimated states. To estimate the rotor speed of the machines, the simulation was run for 20 seconds with an unbalanced fault applied for 5 cycles. The Figures displayed below, 6.10 through 6.13, present both the actual and estimated states obtained by utilizing data from the generators as inputs for the estimator. The true state is represented by the black color, while the magenta color illustrates the estimated state. Figure 6.10 shows the comparison between the true and the estimated rotor speed of generator number 1 of the WECC system. The simulation started in a steady state and unbalanced line-to-line fault (AB) was applied at 4s. The line trips and recloses when the fault is cleared after 5 cycles.

Similarly for generator 2 of the WECC system, Figure 6.11 shows the comparison between the true and the estimated rotor speed of generator one of the WECC system. The simulation starts in a steady state and unbalanced line-to-line fault (AB) is applied at 6s. The line trips and recloses when the fault cleared after 5 cycles. Generators 3 and 4 of the WECC system are simulated similarly to generator 1, Figures 6.12 and 6.13 show the comparison between the true and the estimated rotor speed of generator 1 of the WECC system.

The simulation starts in a steady state and unbalanced line-to-line fault (AB) applied at 6 s. The line trips and recloses when the fault clears after 5 cycles. To compare the accuracy of the estimated states with the true states, the mean squared error was computed to validate the results of the estimator and also compare the performance of the IUKF.

$$MSE = \sqrt{\frac{1}{N}\sum_{j=1}^{N}(x_j^i - \hat{x}_j^i)^2} \tag{6.4}$$

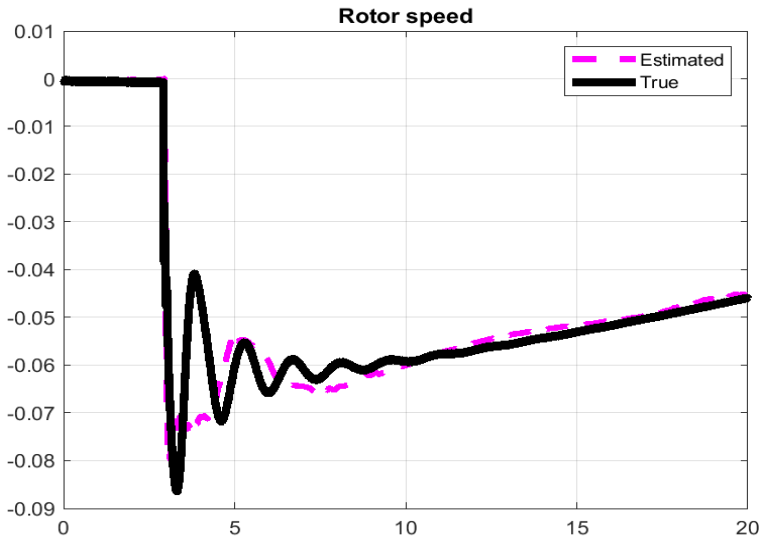

Figure 6.10: Rotor Speed ω_1

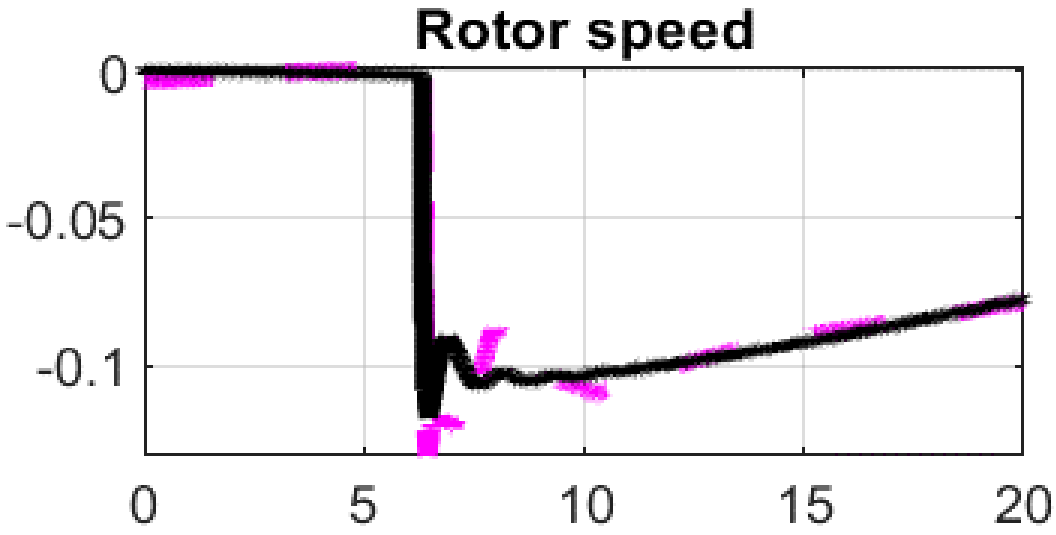

Figure 6.11: Rotor Speed ω_2

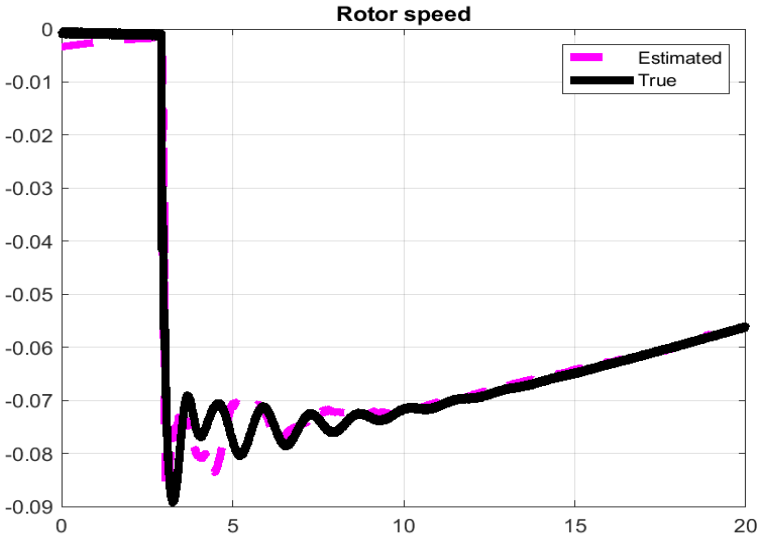

Figure 6.12: Rotor Speed ω_3

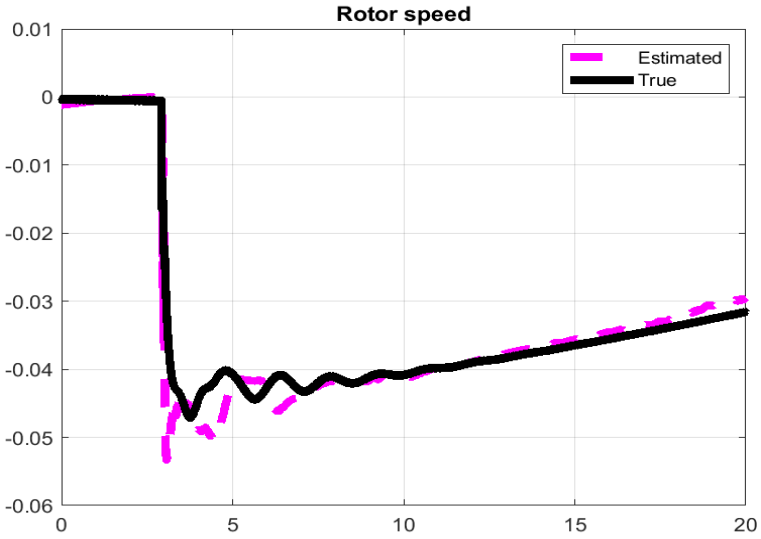

Figure 6.13: Rotor Speed ω_4

Table 6.1: WECC EMT Mean Squared Error

Generators	δ	ω
Generator 1	0.011	0.0051
Generator 2	0.0012	0.0061
Generator 3	0.00125	0.0034
Generator 4	0.0013	0.0019

where

x_j^i is the true state of the ith element of the associated state vector

$\hat{x}_j^i$ is the estimated state of the ith element of the associated state vector

N is the aggregate number of simulation steps.

Table 6.1 shows the performance of the GENTPF/J model with the effect of saturation. The IUKF performs better in estimating the dynamic states of the machines.

Chapter 7

Conclusion

In this dissertation, static and dynamic state estimation approaches have been developed for power systems. Using the Jacobian information with the projection statistics algorithm, a transmission line fault detection and identification virtual sensor was also developed to sense tripped transmission lines due to fault.

The static state estimation methods developed for the Western Electricity Coordinating Council (WECC) system at the CURENT HTB lab. The traditional weighted least square (WLS) method was developed with a robust state estimation method, namely, the least absolute value (LAV) and the quadratic methods were developed to estimate the state of the WECC system. The estimated states are computed with Gaussian noise added to the measurements of the system. All the state estimators developed performed very well, with the LAV performing better with bad data present.

In this research, the breaker status and the virtual sensor are used to detect and identify tripped transmission lines using the breaker node model and the projection statistics algorithm. The proposed solution serves as a backup option for control centers and fault analysis engineers. It utilizes a topology-less, node-breaker model that incorporates a power circuit breaker (PCB), zero impedance branches, and phasor measurement unit (PMU) measurements to detect transmission line faults.

To accomplish this, remote breaker status information is combined with a virtual sensor capable of detecting faults on the transmission line. This approach provides a dependable and effective means of pinpointing and resolving faults, which ultimately can enhance the power grid reliability.

To estimate the states of the system and the flow across the PCB, an augmented state was developed to account for both the states of the system and the PCB. The robust LAV state estimation method was applied with the objective of finding the minimum residuals of the resulting linear programming. A PCB incidence matrix was developed to capture the relationship and the flow states as detailed in Chapter 3. Also, the formulation of a virtual sensor in the form of a projection statistics approach was developed using the Jacobian information of the system to detect tripped or faulty transmission lines. This approach is precise for detecting anomalies in transmission line data, such as bad data, outliers, and leverage points. Through the integration of remote PCB status with virtual sensors, it becomes possible to accurately detect any faulty transmission lines within the system. This, in turn, saves valuable troubleshooting time for line engineers, resulting in improved overall efficiency and potentially significant cost savings for the company.

This dissertation examines the effect of balanced and unbalanced faults on the dynamic states of synchronous machines. When there is a temporary or permanent fault, the generator's dynamic states will be affected by the transmission line reclosing, which could impact the system's stability and reliability. The unscented Kalman filter (UKF) and optimal performance iterated unscented Kalman filter (IUKF) dynamic state estimation techniques were developed to estimate the dynamic states of the machines during balanced and unbalanced faults on the transmission line. However, during an unbalanced fault, the dynamic states of the machines are affected by the magnetic saturation of the machine. Hence, an approach was developed to account for the saturation of the machines using the GENTPJ model recommended by the North American Electric Reliability Corporation (NERC). The developed approach

for unbalanced fault and machine saturation helped in estimating the dynamic states of the machines.

The developed approaches were tested on the IEEE bus system, Kundur's two-area model, and the reduced WECC model of the UTK electrical engineering hardware test bed (HTB). This methodology offers a comprehensive solution to address the challenges posed by balanced and unbalanced faults on transmission lines. Furthermore, the study examined the response of synchronous generators to faults that arise during the reclosing cycles of transmission lines. The effectiveness of the solution was confirmed by monitoring the reaction of dynamic state variables during reclosing cycles due to temporary faults and transmission line lockout resulting from permanent faults.

Bibliography

[1] PowerWorld Corporation. Synchronous machine modeling: Gentpf and gentpj models. URL `https://www.powerworld.com/files/D02SynchronousMachines.pdf`. xv, 116, 117

[2] Ali Abur. Use of pmus in wls and lav based state estimation. In *2015 IEEE Power & Energy Society General Meeting*, pages 1–5, 2015. 1

[3] Cem Bila. Power system dynamic state estimation and load modeling. Master's thesis, Northeastern University ät Boston, Massachusetts, 2013. 1, 13, 14

[4] NR Shivakumar and Amit Jain. A review of power system dynamic state estimation techniques. In *Power System Technology and IEEE Power India Conference, 2008. POWERCON 2008. Joint International Conference on*, pages 1–6. IEEE, 2008. 1, 3, 6, 34, 73

[5] A Monticelli. Electric power system state estimation. *Proceedings of the IEEE*, 88(2):262–282, 2000. 1, 3

[6] Antonio Gomez-Exposito and Ali Abur. *Power system state estimation: theory and implementation*. CRC press, 2004. 1, 2, 5, 6

[7] Zhou Suquan, Gao Zhongwen, Liu Youbin, and Liu Zhuo. Electrical power system state forecasting and estimation. In *Proceedings of TENCON '93. IEEE Region 10 International Conference on Computers, Communications and*

Automation, volume 5, pages 426–429 vol.5, 1993. doi: 10.1109/TENCON.1993.320673. 1

[8] Adnan Anwar and Abdun Naser Mahmood. Stealthy and blind false injection attacks on scada ems in the presence of gross errors. In *Power and Energy Society General Meeting (PESGM), 2016*, pages 1–5. IEEE, 2016. 2

[9] Yu A Grishin, IN Kolosok, ES Korkina, and LV Em. State estimation of electric power system for new technological systems. In *Electric Power Engineering, 1999. PowerTech Budapest 99. International Conference on*, page 273. IEEE, 1999. 2

[10] Fred C Schweppe. Power system static-state estimation, part i: Implementation. *IEEE Transactions on Power Apparatus and systems*, (1):120–125, 1970. 2

[11] Fred C Schweppe and Douglas B Rom. Power system static-state estimation, part ii: Approximate model. *IEEE Transactions on Power Apparatus and Systems*, (1):125–130, 1970. 2

[12] Fred C Schweppe. Power system static-state estimation, part iii: Implementation. 2

[13] Milton Brown Do Coutto Filho and Julio Cesar Stacchini de Souza. Forecasting-aided state estimation—part i: Panorama. *IEEE Transactions on Power Systems*, 24(4):1667–1677, 2009. 2

[14] Hugh D Young, Roger A Freedman, and Lewis Ford. *University Physics Vol 2 (Chapters 21-37)*, volume 2. Pearson Education, 2007. 2, 11

[15] EA Blood, MD Ilic, and BH Krogh. A kalman filter approach to quasi-static state estimation in electric power systems. In *Power Symposium, 2006. NAPS 2006. 38th North American*, pages 417–422. IEEE, 2006. 2

[16] Devesh Shukla, Satyendra P Singh, and SP Singh. Pseudo pmu for quasi-static analysis of power system. In *India Conference (INDICON), 2016 IEEE Annual*, pages 1–6. IEEE, 2016. 3

[17] O Alsac, N Vempati, B Stott, and A Monticelli. Generalized state estimation [power systems]. In *Power Industry Computer Applications., 1997. 20th International Conference on*, pages 90–96. IEEE, 1997. 3, 6

[18] Fred C Schweppe and Edmund J Handschin. Static state estimation in electric power systems. *Proceedings of the IEEE*, 62(7):972–982, 1974. 3, 6

[19] Robert E Larson, William F Tinney, and John Peschon. State estimation in power systems part i: Theory and feasibility. *IEEE Transactions on Power Apparatus and Systems*, (3):345–352, 1970. 3

[20] A Monticelli and Felix F Wu. Network observability: Identification of observable islands and measurement placement. *IEEE Transactions on Power Apparatus and Systems*, (5):1035–1041, 1985. 5, 23

[21] Alireza Rouhani and Ali Abur. Observability analysis for dynamic state estimation of synchronous machines. *IEEE Transactions on Power Systems*, 32(4):3168–3175, 2017. 5

[22] Ali Abur. Observability and dynamic state estimation. In *Power & Energy Society General Meeting, 2015 IEEE*, pages 1–5. IEEE, 2015. 5, 36

[23] Allen J Wood and Bruce F Wollenberg. *Power generation, operation, and control*. John Wiley & Sons, 2012. 5, 6

[24] Richard O Duda, Peter E Hart, and David G Stork. *Pattern classification*. John Wiley & Sons, 2012. 6

[25] Miguel Yucra Ccahuana, Fabiano Schmidt, and Madson C de Almeida. Analysis of bad data detection in power system state estimators considering pmus. In *Power & Energy Society General Meeting, 2015 IEEE*, pages 1–5. IEEE, 2015. 6

[26] Gabriele D'Antona and Luca Perfetto. Bad data detection and identification in power system state estimation with network parameters uncertainty. In *Knowledge-Based Engineering and Innovation (KBEI), 2015 2nd International Conference on*, pages 26–31. IEEE, 2015. 6

[27] Frhat Aeiad, Wenzhong Gao, and James Momoh. Bad data detection for smart grid state estimation. In *North American Power Symposium (NAPS), 2016*, pages 1–6. IEEE, 2016. 6

[28] Kaveri Mahapatra, Nilanjan Ray Chaudhuri, and Rajesh Kavasseri. Bad data detection in pmu measurements using principal component analysis. In *North American Power Symposium (NAPS), 2016*, pages 1–6. IEEE, 2016. 6

[29] A Zakerian, A Maleki, Y Mohammadnian, and T Amraee. Bad data detection in state estimation using decision tree technique. In *Electrical Engineering (ICEE), 2017 Iranian Conference on*, pages 1037–1042. IEEE, 2017. 6

[30] Yiming Wu, Yong Xiao, Fabian Hohn, Lars Nordstrom, Jianping Wang, and Wei Zhao. Bad data detection using linear wls and sampled values in digital substations. *IEEE Transactions on Power Delivery*, 2017. 6

[31] Yuqi Zhou and Le Xie. Detection of bad data in multi-area state estimation. In *Power and Energy Conference (TPEC), IEEE Texas*, pages 1–6. IEEE, 2017. 6

[32] G Durgaprasad and SS Thakur. Robust dynamic state estimation of power systems based on m-estimation and realistic modeling of system dynamics. *IEEE Transactions on Power Systems*, 13(4):1331–1336, 1998. 6, 73

[33] Junbo Zhao. Power system dynamic state estimation considering measurement correlations. *IEEE Transactions on Energy Conversion*, 32(4):1630–1632, 2017. 6, 7, 37, 73

[34] Roque Filipe Mesquita Brandao, Jose Antonio Beleza Carvalho, and Fernando Maciel Barbosa. Gps synchronized measurements in power systems state estimation: An overview. In *Universities Power Engineering Conference, 2006. UPEC'06. Proceedings of the 41st International*, volume 2, pages 452–456. IEEE, 2006. 6, 73

[35] Prabhash Nanda, CK Panigrahi, and Abhijit Dasgupta. Phasor estimation and modelling techniques of pmu-a review. *Energy Procedia*, 109:64–77, 2017. 6, 73

[36] Damir Novosel, Khoi Vu, Virgilio Centeno, Srdjan Skok, and Miroslav Begovic. Benefits of synchronized-measurement technology for power-grid applications. In *System Sciences, 2007. HICSS 2007. 40th Annual Hawaii International Conference on*, pages 118–118. IEEE, 2007. 6, 73

[37] Patricia Rousseaux, Th Van Cutsem, and TE Dy Liacco. Whither dynamic state estimation? *International Journal of Electrical Power & Energy Systems*, 12(2): 104–116, 1990. 7, 34, 36

[38] Alireza Rouhani and Ali Abur. Measurement selection for observability in dynamic state estimation. In *Power Systems Computation Conference (PSCC), 2016*, pages 1–6. IEEE, 2016. 7

[39] Junbo Zhao, Antonio Gómez-Expósito, Marcos Netto, Lamine Mili, Ali Abur, Vladimir Terzija, Innocent Kamwa, Bikash Pal, Abhinav Kumar Singh, Junjian Qi, Zhenyu Huang, and A. P. Sakis Meliopoulos. Power system dynamic state estimation: Motivations, definitions, methodologies, and future work. *IEEE Transactions on Power Systems*, 34(4):3188–3198, 2019. doi: 10.1109/TPWRS.2019.2894769. 7

[40] Amin M Najafabadi and Ali T Alouani. Real time estimation of sensitive parameters of composite power system load model. In *Transmission and Distribution Conference and Exposition (T&D), 2012 IEEE PES*, pages 1–8. IEEE, 2012. 7

[41] Junbo Zhao, Marcos Netto, and Lamine Mili. A robust iterated extended kalman filter for power system dynamic state estimation. *IEEE Transactions on Power Systems*, 32(4):3205–3216, 2017. 7, 69

[42] Ali Abur and A Rouhani. Linear phasor estimator assisted dynamic state estimation. *IEEE Transactions on Smart Grid*, 2016. 7

[43] Hesam Khazraj, Filipe Miguel Faria da Silva, and Claus Leth Bak. A performance comparison between extended kalman filter and unscented kalman filter in power system dynamic state estimation. In *51st International Universities' Power Engineering Conference*. IEEE Press, 2016. 8, 37

[44] Happy Novanda, Pawel Regulski, Francisco M González-Longatt, and Vladimir Terzija. Unscented kalman filter for frequency and amplitude estimation. In *PowerTech, 2011 IEEE Trondheim*, pages 1–6. IEEE, 2011. 8, 37

[45] Rudolph Van Der Merwe. Sigma-point kalman filters for probabilistic inference in dynamic state-space models. 2004. 8, 37, 38

[46] Yih-Fang Huang, Stefan Werner, Jing Huang, Neelabh Kashyap, and Vijay Gupta. State estimation in electric power grids: Meeting new challenges presented by the requirements of the future grid. *IEEE Signal Processing Magazine*, 29(5):33–43, 2012. doi: 10.1109/MSP.2012.2187037. 8

[47] H. Saadat. *Power System Analysis*. PSA Pub., 2010. ISBN 9780984543809. 11, 13, 14, 16, 17, 21

[48] Prabha Kundur, Neal J Balu, and Mark G Lauby. *Power system stability and control*. McGraw-hill New York, 1994. 12, 14, 16, 21

[49] S. Krishna. *An Introduction to Modelling of Power System Components*. SpringerBriefs in Electrical and Computer Engineering. Springer India, 2014. ISBN 9788132218470. 12, 14

[50] J Duncan Glover, Mulukutla S Sarma, and Thomas Overbye. *Power system analysis & design, SI version*. Cengage Learning, 2012. 14

[51] Peter W Sauer, Mangalore A Pai, and Joe H Chow. *Power system dynamics and stability: with synchrophasor measurement and power system toolbox*. John Wiley & Sons, 2017. 14

[52] Westinghouse Electric & Manufacturing Company. Relay Department and Westinghouse Electric Corporation. Relay-Instrument Division. *Applied Protective Relaying*. A New "Silent sentinels" publication. Westinghouse Electric Corporation, Relay-Instrument Division, 1982. 16, 17, 20, 21, 110

[53] S.H. Horowitz and A.G. Phadke. *Power System Relaying*. RSP. Wiley, 2008. ISBN 9780470758793. 17, 21

[54] Jorge Santamaria. Analysis of power systems under fault conditions. Master's thesis, CALIFORNIA STATE UNIVERSITY ät , SACRAMENTO, CA, 2006. 20

[55] A.J.W.B. Wollenberg. *POWER GENERATION OPERATION & CONTROL, 2ND ED (With CD)*. Wiley India Pvt. Limited, 2006. ISBN 9788126508389. 23

[56] M. Göl and A. Abur. Lav based robust state estimation for systems measured by pmus. *IEEE Transactions on Smart Grid*, 5(4):1808–1814, 2014. doi: 10.1109/TSG.2014.2302213. 23

[57] A. Monticelli. *State Estimation in Electric Power Systems*. 3Island Press, 1999. ISBN 9781461550006. 23

[58] A Brameller and SH Karaki. Power-system state estimation using linear programming. In *Proceedings of the Institution of Electrical Engineers*, volume 126, pages 246–247. IET, 1979. 28, 31

[59] Murat Göl and Ali Abur. Lav based robust state estimation for systems measured by pmus. *IEEE Transactions on Smart Grid*, 5(4):1808–1814, 2014. 28, 32

[60] Ali Abur and Yuzhang Lin. Robust state estimation against measurement and network parameter errors. *IEEE Transactions on Power Systems*, 2018. 28, 32

[61] Dishang D Trivedi, Santosh C Vora, and Meera R Karamta. Analysis of extended kalman filter based dynamic state estimator's performance under anomalous measurement conditions for power system. In *Electrical Power and Energy Systems (ICEPES), International Conference on*, pages 557–563. IEEE, 2016. 34

[62] Steven X Ding. *Model-based fault diagnosis techniques: design schemes, algorithms, and tools*. Springer Science & Business Media, 2008. 68

[63] Francisco AA Souza, Rui Araújo, and Jérôme Mendes. Review of soft sensor methods for regression applications. *Chemometrics and Intelligent Laboratory Systems*, 152:69–79, 2016. 68

[64] Petr Kadlec, Bogdan Gabrys, and Sibylle Strandt. Data-driven soft sensors in the process industry. *Computers & chemical engineering*, 33(4):795–814, 2009. 68

[65] Jyrki Kullaa. Bayesian virtual sensing for full-field dynamic response estimation. *Procedia engineering*, 199:2126–2131, 2017. 68

[66] L. Mili, M. G. Cheniae, N. S. Vichare, and P. J. Rousseeuw. Robust state estimation based on projection statistics [of power systems]. *IEEE Transactions on Power Systems*, 11(2):1118–1127, 1996. doi: 10.1109/59.496203. 69

[67] S. L. Els, A. D. Els, J. A. Jordaan, and R. Zivanovic. Projection statistics for power system state estimation. In *1999 IEEE Africon. 5th Africon Conference in Africa (Cat. No.99CH36342)*, volume 2, pages 783–786 vol.2, 1999. doi: 10.1109/AFRCON.1999.821867. 69

[68] K.W. Louie and J.R. Marti. Saturation in synchronous generators during unbalanced faults. In *Canadian Conference on Electrical and Computer Engineering 2004 (IEEE Cat. No.04CH37513)*, volume 2, pages 819–822 Vol.2, 2004. doi: 10.1109/CCECE.2004.1345240. 110, 116

[69] Ronghui Zhan and Jianwei Wan. Iterated unscented kalman filter for passive target tracking. *IEEE Transactions on Aerospace and Electronic Systems*, 43(3): 1155–1163, 2007. 116

Appendix

Appendix A

Summary of Equations

A.1 GENTPF/GENTPJ Model

A.1.1 Reactance Values

$$\begin{aligned} X^{'}_{dsat} &= \frac{X^{'}_{d} - X_l}{Sat_d} + X_l \\ X_{dsat} &= \frac{X_d - X_l}{Sat_d} + X_l \\ X^{'}_{qsat} &= \frac{X^{'}_{q} - X_l}{Sat_q} + X_l \\ X_{qsat} &= \frac{X_q - X_l}{Sat_q} + X_l \end{aligned} \tag{A.1}$$

A.1.2 Time Constants

$$\begin{aligned} T^{'}_{dosat} &= \frac{T^{'}_{do}}{Sat_d} \\ T^{'}_{qosat} &= \frac{T^{'}_{qo}}{Sat_q} \end{aligned} \tag{A.2}$$

$$E^{'}_{fdsat} = \frac{E^{'}_{fd}}{Sat_d} \tag{A.3}$$

A.1.3 Exciter Interface Signal

$$E'_{fdsat} = \frac{E'_{fd}}{Sat_d} \tag{A.4}$$

$$\Psi_{ag} = \sqrt{(V_{qterm} + I_q R_a + I_d X_l)^2 + (V_{dterm} + I_d R_a + I_q X_l)^2} \tag{A.5}$$

$$\begin{aligned} Sat_d &= 1 + Sat(\Psi_{ag} + K_{is}\sqrt{I_d^2 + I_q^2}) \\ Sat_q &= 1 + \frac{X_q}{X_d} Sat(\Psi_{ag} + K_{is}\sqrt{I_d^2 + I_q^2}) \end{aligned} \tag{A.6}$$

where Ψ_{ag} is the air gap flux and K_{is} is the stator current multiplier multiplier for saturation calculation. The K_{is} values used in this dissertation range from 0.01 to 0.15.

Vita

Ibukunoluwa O. Korede is a PhD. candidate with the Department of Electrical Engineering and Computer Science at the University of Tennessee, Knoxville. He earned a B.S. degree in applied physics electronics from the University of Lagos, an M.S. degree in applied physics from Indiana University of Pennsylvania, and an M.S. degree in electrical engineering from the University of Tennessee, Knoxville. He is currently employed as an electric transmission operations engineering supervisor at Dominion Energy Virginia. Before this role, he held the position of a senior system protection engineer at the same company. His research interests primarily focus on the practical implementation of static and dynamic-state estimation modeling for power systems protection and control, smart grids, substation modeling, and virtual sensor modeling for identifying transmission line faults.